



2

MICHIGAN STATE UNIVERSITY LIBRARIES



3 1293 01572 1990



This is to certify that the

thesis entitled

USE OF GENETIC ALGORITHMS FOR  
OPTIMAL DESIGN OF LAMINATED  
COMPOSITE SANDWICH STRUCTURES WITH  
BENDING-TWISTING COUPLING

presented by

Bradley Arthur Malott

has been accepted towards fulfillment  
of the requirements for

Master of Science degree in Mechanics

Major professor

Date July 10, 1996

**PLACE IN RETURN BOX to remove this checkout from your record.  
TO AVOID FINES return on or before date due.**

DATE DUE	DATE DUE	DATE DUE
NOV 23 2000	_____	_____
_____	_____	_____
_____	_____	_____
_____	_____	_____
_____	_____	_____
_____	_____	_____
_____	_____	_____

**MSU is An Affirmative Action/Equal Opportunity Institution**

c:\cir\dateduea.pm3-p.1

**USE OF GENETIC ALGORITHMS FOR  
OPTIMAL DESIGN OF LAMINATED  
COMPOSITE SANDWICH STRUCTURES WITH  
BENDING-TWISTING COUPLING**

**By**

**Bradley Arthur Malott**

**A THESIS**

**Submitted to  
Michigan State University  
in partial fulfillment of the requirements  
for the degree of**

**MASTER OF SCIENCE**

**Department of Material Science and Mechanics**

**1996**

## **ABSTRACT**

# **USE OF GENETIC ALGORITHMS FOR OPTIMAL DESIGN OF LAMINATED COMPOSITE SANDWICH STRUCTURES WITH BENDING-TWISTING COUPLING**

By

Bradley Arthur Malott

The first section of this study compares different theories available for analyzing laminated composite plates. Symmetric and unsymmetric square sandwich panels subjected to sinusoidally varying transverse surface loadings were analyzed. The LZZHT model proved to be the most accurate followed by the ZZHT, HSDT, and FSDT theories, respectively. A genetic algorithm approach was applied to the optimum design of an idealized laminated sandwich composite aircraft wing using the ZZHT finite element model in conjunction with the genetic algorithm, GALOPPS v3.0. The optimum stacking sequence for the top and bottom face sheets was determined which produced the desired twisting response, minimized weight, and maximized in-plane stiffness while maintaining stress levels below the failure strength of the material in the fiber and matrix directions.

Four different GA architectures, single node, ring, injection, and hybrid structures were used and their results compared. The ring structure produced the design with highest fitness. The highest average fitness was achieved by both the ring and hybrid structures. The injection structure converged the fastest.

## **ACKNOWLEDGEMENTS**

I wish to express my gratitude to Dr. Erik Goodman and Dr. William F. Punch III for the support, insight, guidance and expertise offered throughout my research. I also would like to express my gratitude to the Genetic Algorithms Research Group for their patience, advice, and good humor. I also wish to thank Ying Ding for his diligence, hard work, and assistance during this research.

I also thank all members of the Computational Mechanics Research Group for their support and assistance. Finally, I extend my sincere gratitude to my advisor Dr. Ronald C. Averill for his guidance and support through the duration of my research.

## Table of Contents

List of Tables .....	vi
List of Figures .....	vii
<b>Chapter 1</b>	
<b>Introduction .....</b>	<b>1</b>
1.1 Introduction .....	1
1.2 Problem Definition .....	2
1.3 Genetic Algorithm Design .....	3
1.4 Literature Review .....	10
<b>Chapter 2</b>	
<b>Description of Laminated Plate Theories .....</b>	<b>37</b>
2.1 Introduction .....	37
2.2 Equivalent Single-Layer Theories .....	38
2.3. Zig Zag Theories .....	44
<b>Chapter 3</b>	
<b>Assessment of Laminated Plate Theories for Analysis of Composite</b>	
<b>Sandwich Panels .....</b>	<b>51</b>
3.1 Introduction .....	51
3.2 Description of Models .....	52
3.3 Results .....	57
3.4 Conclusions .....	62
<b>Chapter 4</b>	
<b>Optimal Design Laminated Composite Sandwich Structures Using</b>	
<b>Genetic Algorithms. ....</b>	<b>77</b>
4.1 Introduction .....	77
4.2 Previous Work .....	79

4.3 Model Description .....	82
4.4 Optimization Problem .....	86
4.5 Genetic Algorithm Topologies .....	93
4.6 Finite Element Model .....	99
4.7 Results and Discussion .....	101
4.8 Conclusions .....	109
4.9 Recommendations .....	111

## Chapter 5

Summary and Conclusions .....	130
-------------------------------	-----

References .....	134
------------------	-----

## **List of Tables**

<b>Table (3.1) Sandwich Panel Material Properties</b>	<b>54</b>
<b>Table (3.2) Layup 1.</b>	<b>55</b>
<b>Table (3.3) Layup 2.</b>	<b>56</b>
<b>Table (3.4) Convergence Data: Transverse center displacement.</b>	<b>56</b>
<b>Table (4.1) Sandwich Panel Material Properties.</b>	<b>86</b>
<b>Table (4.2) Weighting Coefficient Values.</b>	<b>89</b>
<b>Table (4.3) Mesh Convergence Data.</b>	<b>100</b>
<b>Table (4.4) Results for Best Design of Each GA Structure.</b>	<b>104</b>
<b>Table (4.5) Optimization Result From Various GA Structures.</b>	<b>113</b>
<b>Table (4.6) Layup Determined by Single Node Structure.</b>	<b>125</b>
<b>Table (4.7) Layup Determined by Ring Structure GA.</b>	<b>126</b>
<b>Table (4.8) Layup Determined by Injection Structure GA.</b>	<b>127</b>
<b>Table (4.9) Layup Determined by Hybrid Structure GA.</b>	<b>128</b>

## List of Figures

Figure (2.1) - (a) Plate and coordinate system. ....	39
Figure (2.1) - (b) Undeformed and deformed plate section for CLPT .....	39
Figure (2.2) - Undeformed and deformed plate section for FSDT. ....	42
Figure (3.1) - Sandwich plate geometry .....	52
Figure (3.2) - Quarter plate geometry and loading. ....	53
Figure (3.3) - Normalized transverse center deflection versus aspect ratio, ESL theories, layup 1 .....	64
Figure (3.4) - Normalized transverse center deflection versus aspect ratio, zig zag theories, layup 1. ....	64
Figure (3.5) - Normal stress vs. normalized thickness for ESL theories, $a/h=4$ layup 1. ....	65
Figure (3.6) - Normal stress vs. normalized thickness for zig-zag theories, $a/h=4$ layup 1. ....	65
Figure (3.7) - Normal stress vs. normalized thickness for ESL theories, $a/h=4$ , layup 1. ....	66
Figure (3.8) - Normal stress vs. normalized thickness for zig-zag theories, $a/h=4$ layup 1. ....	66
Figure (3.9) - Shear stress vs. normalized thickness for ESL theories, $a/h=4$ layup 1. ....	67
Figure (3.10) - Shear stress vs. normalized thickness for zig-zag theories, $a/h=4$ layup 1. ....	67
Figure (3.11) - Shear stress vs. normalized thickness for zig-zag theories, $a/h=4$ layup 1. ....	68

Figure (3.12) - Shear stress vs. normalized thickness for zig-zag theories, a/h=4 layup 1. ....	68
Figure (3.13) - Normal stress vs. normalized thickness for ESL theories, a/h=10, layup 1. ....	69
Figure (3.14) - Normal stress vs. normalized thickness for zig-zag theories, a/h=10 layup 1. ....	69
Figure (3.15) - Normal stress vs. normalized thickness for ESL theories, a/h=10, layup 1. ....	70
Figure (3.16) - Normal stress vs. normalized thickness for zig-zag theories, a/h=10, layup 1. ....	70
Figure (3.17) - Shear stress vs. normalized thickness for ESL theories, a/h=10, layup 1. ....	71
Figure (3.18) - Shear stress vs. normalized thickness for zig-zag theories, a/h=10, layup 1. ....	71
Figure (3.19) - Shear stress vs. normalized thickness for zig-zag theories, a/h=10, layup 1. ....	72
Figure (3.20) - Shear stress vs. normalized thickness for zig-zag theories, a/h=10, layup 1. ....	72
Figure (3.21) - Normal stress vs. normalized thickness for ESL theories, a/h=10, layup 2. ....	73
Figure (3.22) - Normal stress vs. normalized thickness for zig-zag theories, a/h=10, layup 2. ....	73
Figure (3.23) - Normal stress vs. normalized thickness for ESL theories, a/h=10, layup 2. ....	74
Figure (3.24) - Normal stress vs. normalized thickness for zig-zag theories, a/h=10, layup 2. ....	74
Figure (3.25) - Shear stress vs. normalized thickness for ESL theories, a/h=10, layup 2. ....	75
Figure (3.26) - Shear stress vs. normalized thickness for zig-zag theories, a/h=10, layup 2. ....	75
Figure (3.27) - Shear stress vs. normalized thickness for zig-zag theories,	

<b>a/h=10, layup 2.</b> .....	76
<b>Figure (3.28) - Shear stress vs. normalized thickness for zig-zag theories,</b> <b>a/h=10, layup 2.</b> .....	76
<b>Figure (4.1) - (a) Elliptical spanwise load distribution approximation.</b> .....	84
<b>Figure (4.1) - (b) Linear chordwise load distribution approximation.</b> .....	84
<b>Figure (4.1) - (c) Elliptical spanwise load distribution approximation.</b> .....	84
<b>Figure (4.2) - Sandwich panel dimensions in meters.</b> .....	85
<b>Figure (4.3) - Schematic of Optimization Process.</b> .....	87
<b>Figure (4.4) - Chromosome structure.</b> .....	92
<b>Figure (4.5) - Ring GA Architecture.</b> .....	94
<b>Figure (4.6) - Injection GA Architecture, 7 subpopulations.</b> .....	96
<b>Figure (4.7) - Hybrid GA Architecture.</b> .....	99
<b>Figure (4.8) - Fitness versus generation number for single node GA structure.</b> .....	114
<b>Figure (4.9) - Fitness versus generation number for ring GA structure.</b> .....	115
<b>Figure (4.10) - Fitness versus generation number for injection GA structure.</b> .....	116
<b>Figure (4.11) - Fitness versus generation number for hybrid GA structure.</b> .....	117
<b>Figure (4.12) - Fitness function terms vs. generation number for single node</b> <b>topology GA.</b> .....	118
<b>Figure (4.13) - Fitness function terms vs. generation number for ring structure GA.</b> ...	119
<b>Figure (4.14) - Fitness function terms vs. generation number for Injection</b> <b>structure GA.</b> .....	120
<b>Figure (4.15) - Fitness function terms vs. generation number for hybrid</b> <b>structure GA.</b> .....	121
<b>Figure (4.16) - Extensional stiffness matrix versus generation number.</b> .....	122
<b>Figure (4.17) - Coupling stiffness matrix versus generation number.</b> .....	123

Figure (4.18) - Flexural stiffness matrix versus generation number. ....124

## **Chapter 1**

# **Introduction**

### **1.1 Introduction**

Optimization problems are present all disciplines and thus a wide range of goals exist. For example, the goals of manufacturing optimization problems could be to maximize product output, minimize material waste, minimize cycle time, maximize equipment use, etc., These goals, of course, coincide with the ultimate goal of business-related optimization problems which is to maximize profit. In the engineering field uncountable optimization problems exist. Of these, structural optimization is the concern of the current study. In structural optimization problems goals are similar to other optimization problems. Minimum weight, minimum cost, maximum performance, and maximum manufacturability are a few common goals. In many aerospace optimization problems are concerned with determining the design which minimizes weight while maintaining structural integrity and function. Various techniques are used to solve design optimization problems. Traditional techniques use gradient based approaches which have numerous limitations. Random search techniques are also used, which also have limitations. Guided random search methods using genetic algorithms are very effective for solving many optimization problems. This technique is used to solve the structural optimization problem in

the current research.

## **1.2 Problem Definition**

During flight an aircraft wing experiences bending and twisting loads which can be detrimental to the aircraft's performance. During flight the pressure differential across the airfoil causes the wing to twist up and back. To compensate for this deflection washout is built into the wing, providing the best compromise of the lift distribution through a range of flight speeds. When a wing encounters wind gusts the wing's lift distribution is adversely affected. This situation is the motivating factor for the current research. To compensate for such gust loads the wing needs to twist in the opposite direction from which the load normally causes the wing twist. This type of response can be accomplished using laminated composite sandwich panels by tailoring the lamination sequence accordingly to utilize the inherent bending-twisting coupling of such materials.

The goal of the current research is to determine the design of a laminated composite sandwich panel which achieves the above mentioned "opposite" twisting response while minimizing weight and maximizing in-plane stiffness (to maximize buckling strength). To do this the optimum lamination sequence (i.e. number of plies, fiber orientations, and core thicknesses) must be determined. Sandwich panel dimensions, loading, and geometry are representative of an idealized aircraft wing. The desired twisting response was for the wing to twist -1.5 degrees from the horizontal in the direction opposite the loading. This is four times the amount of twist, but in the opposite direction, exhibited by a specially isotropic baseline sandwich panel with the same loading.

This optimization problem is solved using the genetic algorithm GALOPPS v.3.0. All details of the optimization problem are discussed in Chapter 4. To determine the twisting response and stresses in the wing a finite element plate code was used. The theory used is discussed in Chapters 2 and 3.

### **1.3 Genetic Algorithm Design**

Laminated composite structure design lends itself quite openly to optimization techniques. Ply thickness and stacking sequence are two common design variables for laminate design. Numerous optimization techniques are available, one category of which is calculus-based or gradient-based methods. Gradient-based methods can be classified as either direct or indirect [16]. Both approaches rely on the gradient of the objective function providing the necessary information to locate a local optima. One obvious drawback of this method is the gradient of the function must exist and be obtainable. Determination of the gradient may be impracticably difficult. Also, these methods seek out local optima, which may or may not be the global optimum. Gradient based methods are not well suited to find singular optima common in optimization of laminated composite structures. The apparent lack of robustness of calculus-based optimization techniques rules out this method for many applications.

Various algorithms exist which search finite design spaces, evaluating an objective function at all points in a given domain. This approach is obviously inefficient and impractical for large domains. Random search techniques perform a random search of the design space for optima, but are also inefficient. Guided random search techniques are a more

effective means of searching a design space. Genetic algorithms (GA) are guided random searches which utilize information obtained during the search for direction. This method mimics nature in the search for an optimum state. This technique is relatively efficient and quite robust in comparison to other methods. Genetic algorithms are used in this study and are explained more thoroughly next.

### 1.3.1 Genetic Operations

Natures means of dealing with existence and reproduction of all species is described as “survival of the fittest”. Genetic algorithms draw from this phenomena, employing a similar philosophy when searching a design space for global optima. GAs perform operations of selection, reproduction, crossover, mutation, and permutation of the coded design variables.

### 1.3.2 Design Coding

In an optimization problem one must first define the problem. Design constraints and design space must be identified and the objective function determined. Next, a necessary operation is coding of the design variables to produce a string of finite length. These strings are devised in a way as to represent a particular design. Strings are analogous to chromosomes in natural systems. Strings are usually coded in either binary or integer form depending on the situation. As an example, each digit of a string could represent the fiber orientation of a particular ply in a laminate comprised of five plies:

$$[0 \ 1 \ 2 \ 2 \ 1] \quad (1.1)$$

where 0 represents a ply oriented at 0 degrees in some reference coordinate system, 1 represents 45 degrees, and 2 denotes 90 degrees. This string describes an individual design. Each digit in a string has a representative counterpart in natural systems which are genes.

Binary coding is useful in creating new design options but does have limitations. Furuta and Haftka [13] provide an explanation of three disadvantages of using binary coding versus integer coding. First binary coding is complex, which is further intensified by design solutions which are not a power of two. Another disadvantage is certain designs are relatively inaccessible since it is not always easy to mutate one design into another similar design. The third disadvantage is the child string may not resemble the parent.

### 1.3.3 Initial Population Generation

Creation of “life” is next. With a coding scheme decided upon, an initial population must be generated. This is usually done stochastically. The number of individual strings comprising the initial population is somewhat variable.

### 1.3.4 Reproduction/Selection

The first operation performed by the genetic algorithm in the reproduction process is selection. In the selection process individual strings are selected based on their objective function value, or fitness. Reproduction is essentially a synthetic version of natural selection. The objective function of each string is evaluated thus assigning a “fitness” to each. Fitness values aid in determining a string’s probability of being “mated”; the more fit an individual, the greater the probability it will survive and reproduce.

The most common method of determining which strings will be selected for

mating is called roulette wheel selection (see Goldberg [16]). In roulette wheel selection each string, or design, is allotted a portion of a roulette wheel, the size of which corresponds to the relative fitness (or objection function value) of the design. Strings with relatively high fitness values are assigned a larger portion of the wheel and thus have a greater probability of being chosen as parents for reproduction once the wheel is spun. As is the case in nature, the “fittest” survive, and mating the most fit strings should provide fit “offspring”. Other selection techniques are also used. In addition to roulette wheel selection, Johnson [19] investigates and compares stochastic remainder selection, binary tournament selection, and binary tournament with continuously updated sharing selection techniques.

### 1.3.5 Crossover

The next genetic operation performed by the GA is crossover. The parent strings selected for reproduction are mated and characteristics of each are combined in their offspring. Different levels of crossover are used. In two-point crossover two digits (genes) of each string (chromosome) are exchanged. For example, given the two parents:

$$[0\ 1\ \underline{1}\ \underline{1}\ 1] \quad (1.2)$$

$$[1\ 1\ \underline{0}\ \underline{1}\ 1] \quad (1.3)$$

two offspring are formed by two-point crossover of the underlined two digits to give:

$$[0\ 1\ 0\ 1\ 1] \quad (1.4)$$

$$[1\ 1\ 1\ 1\ 1] \quad (1.5)$$

The number of points and location(s) where crossover occurs varies. Variations of averaging, random selection, and uniform crossover methods were compared by Furuya and Haftka [13]. The probability assigned to the occurrence of crossover is generally quite high, often near 1.0. Negendra et al. [35] assign the probability of crossover to be 0.95 which means crossover will occur with a probability of 95% for each generation.

### 1.3.6 Mutation

Following the crossover operation is mutation. The mutation operator is applied to introduce new genetic data into a population which helps prevent premature convergence of the algorithm by maintaining population diversity. In other words, mutation protects against genetic data being lost. As an example, the following occurs during mutation:

before mutation [0 1 1 1 1] (1.6)

after mutation [0 1 1 0 1] (1.7)

where the digit underlined is replaced by 0 upon mutation.

Mutation is applied with very low probability. LeRiche and Haftka [27] apply mutation to a string with a probability of 0.01. Variations of the mutation operator were investigated by Riche and Haftka in efforts to improve the GA. Minor improvements were achieved by using new variations of the mutation operator.

### 1.3.7 Permutation

Permutation is another operator. Permutation is actually a type of mutation. This

stochastic operator typically inverts a substring of digits within a string:

$$\text{before permutation } [0 \underline{110} 1] \quad (1.8)$$

$$\text{after permutation } [0 0 1 1 1] \quad (1.9)$$

The three underlined digits are inverted. LeRiche and Haftka [27] also investigate variations of the permutation operator and show a decrease in computational cost from using a new form of the permutation operator.

### 1.3.8 Penalty Method

Genetic algorithms are unable to directly deal with constraints. Consequently a constrained optimization problem must be transformed into an unconstrained problem. This can be accomplished via penalty methods. In such methods penalty parameters are incorporated into the objective function which penalize the fitness for violation of the constraints. Penalty methods also serve to drive the optimization process toward optimum designs. Since many design configurations may satisfy the given constraints, the desired choices are those closest to or at the global optimum.

### 1.3.9 Comparison of Genetic Algorithms to Traditional Methods

Genetic algorithms differ intrinsically from traditional search and optimization techniques. As previously stated, traditional methods utilize derivatives whereas GAs make use of objective function data. GAs work with a coded set of variables and not the actual variables as do traditional methods. Another important distinction between GAs

and traditional methods is GAs simultaneously search from numerous points in the design space and traditional methods search from a single point. To that end, it is apparent traditional methods may locate a local optima and not a global optima depending on the initiation point of the search. The final fundamental difference is GAs are governed by stochastic rules, and traditional methods are governed by deterministic rules.

#### 1.3.10 Advantages and Disadvantages of GAs

In the current study GAs are utilized for optimization of a cantilever sandwich panel. Genetic algorithms are ideas for this type of problem because of the highly non-linear behavior of the fitness with respect to the design variables. Linearization is not necessary with GAs, while other methods place such requirements in the optimization problem. Also derivatives need not be continuous and do not even need to exist when using the GA approach. GAs are very good to use for large design spaces, however they are relatively inefficient for small domains.

A unique advantage of GAs is their fostering of innovative and creative designs. Designs can be categorized as either routine, innovative, or creative. Routine designs are quite common, being based on existing, well established ideas and constraints. Innovative and creative designs are much more difficult to achieve. These designs require new constraints and goals. GAs can be considered a design search technique which is influenced only by the design representation and performance which allows existing design paradigms to be ignored.

## 1.4 Literature Review

Next a summary of literature reviewed and utilized in the current research is presented. The articles reviewed are categorized according to the content. First a section on optimization is given followed by a section containing articles pertaining to GA design of laminated composite plates. Other examples of optimization problems using GAs is listed next. This section helped to open my mind to new methods for problem representation in the GA. The next section contains optimization problems solved by other methods, which served to enforce the use of GAs for solution to the current problem. Various plate theories for analysis of finite element methods are presented in the next section of this literature review followed by a section containing articles reviewed pertinent to the aircraft wing design characteristics.

### 1.4.1 Optimization

Olhoff and Taylor [37] present the basic concepts of structural optimization emphasizing the fundamentals. They discuss the features and elements involved optimization of both discrete and continuum structures, and they discuss the mathematical formulation of such problems.

According to Olhoff and Taylor [37], fundamental structural optimization problems were of interest to the likes of Galileo (1638), J. Bernoulli (1687), Newton (1687), Lagrange (1770), and later to Saint-Venant (1864), Maxwell (1869), and Levy (1873).

Olhoff and Taylor [37] group design variables into six categories. *Cross-sectional design variables* are the first group. These variables refer to the properties of the structural

elements such as plate thickness and second moment of area, etc., which are typically assumed to be continuous but may also be discreet. *Topological and configurational design variables* describe the structural layout by specifying such things as the number and location of structural members and joints in a design. *Shape design variables* are variables which are usually continuous and describe the structures shape. *Material design variables* describe material properties and are generally discreet. The final category is the *support or loading design variables* which describe the loading and boundary conditions on the structure. This type of variable can be either discreet or continuous.

An optimal design problem can be termed discreet or continuous depending on the dependence of the design variables on the spatial coordinates of the problem. Design problems such as truss structures are discreet where as plates and beams which are often continuous.

In design problems certain constraints are imposed on all designs to help identify feasible designs. Olhoff and Taylor [37] divide constraints into two categories; behavioral and geometric constraints.

Behavioral constraints are, in general, non-linear constraints which can further be classified as equality or inequality. Equality constraints are, for example, equations of state and compatibility which govern the structural response. Inequality constraints place restrictions on the quantities governing the structures response by placing limits on stress or deflection for example.

Geometric constraints can also be classified as equality or inequality. Geometric constraints place restrictions on the design variables due to for example manufacturing limitations or required appearance of the design.

To determine the “fitness” or “goodness” of a design an objective function is used. The objective function is an expression given in terms of the design variables which has a value for each design or each point in the design space. In an optimization problem the objective is either maximized or minimized. In single-criteria optimization problems the objective function represents a single property where as in multi-criteria optimization problems the objective function contains a weighted sum of two or more properties.

While single-criteria optimization problems have been thoroughly studied, there are few realistic problems which contain merely a single objective to optimize. Multi-criteria optimization (MCO) problems involve the simultaneous optimization of several criteria and consequently are more difficult to solve. Olhoff and Taylor [37] mention three of the better known methods for solving MCO problems: weighted sum method, goal attainment or bound method, and the constraint method. A brief discussion of these methods will be given next. For explanation purposes  $c_i(D)$  will represent the criteria for design  $D$ , and the intent is to minimize with respect to  $D$  the vector  $\{c_1, c_2, c_3, \dots, c_n\}$ .

For the weighted sum method the problem is posed as:

$$\min_D \left( \sum_i w_i c_i \right) \quad (1.10)$$

where  $w_i \geq 0$  are weights specified by the designer based on the experience and judgement of the designer. This method determines  $D$  which minimizes the weighted sum of all criteria.

In the constraint method the problem is given as:

$$\min_D(c_k) \quad \text{subject to } c_i - b_i \leq 0 \quad (i=1,2, \dots, n, i \neq k) \quad (1.11)$$

where the constraint bounds  $b_i \geq 0$  are again specified by the designer.

The goal attainment or bound method gives the problem as:

$$\min_D(\xi) \quad \text{subject to } w_i c_i - \xi \leq 0 \quad (i=1,2, \dots, n) \quad (1.12)$$

This method can be used to solve a min-max problem where for example the criteria  $c_i$  are identified with a maximum such as when the problem is stated as:

$$\min_D \left[ \max_i (w_i c_i) \right] \quad (1.13)$$

In this situation the weighted sum and constraint methods cannot be used.

Stadler and Dauer [47] first present a brief historical review of the field of multicriteria optimization, tracing it's origins to the area of economics where it was discussed by Adam Smith in his book *The Wealth of Nations* (1776) in dealing with economics in a competitive environment. Stadler and Dauer discuss optimization as finding Edgeworth Pareto optimal points (EP-points), which are named after the two economists Francis

Ysidro Edgeworth and Vilfredo Pareto. EP-points are optimal or compromise points in a multicriteria optimization problem.

Stadler and Dauer [47] outlined four steps involved in the solution of a multicriteria optimization problem. First an appropriate mathematical model must be chosen, second a design set must be selected, third preferences are determined to allow the best design be chosen, and finally the optimality concept or condition must be selected.

Stadler and Dauer [47] state the method of constraints approach is a good choice for solving multicriteria objective problems. This approach is good since nearly any mathematical programming code can be used. Many standard approaches for analyzing multi-objective linear problems are based on the simplex algorithm which generates a set of acceptable points from which the best design is chosen.

Finally Stadler and Dauer [47] outline examples of multicriteria optimization problems from a survey they conducted. Two simple examples mentioned were the design of a simple arch structure, and of an elastic truss structure. More difficult and interesting optimization problems analyzed by Professor R. Statnikov of the Research Institute for Mechanical Engineering of the Russian Academy of Sciences in Moscow were also briefly mentioned. Statnikov applied his optimization methods to air-frame and body design of the Russian space shuttle Buran. In this problem mass, structural rigidity, rib spacing, and cross-section shape were the design variables. This optimization effort gained a 300kg reduction in the tail section of the shuttle alone. Other work by Statnikov included design of the Russian truck ZIL. This problem contained 12 criteria.

Another example mentioned by the authors was conducted by H. Eschenauer, a professor in the Laboratory for Structural Optimization at the University of Siegen,

Germany. In his work Eschenauer solves the general optimal design problem for laminated conical shells with weight and deformations design criteria.

#### 1.4.2 Application of GAs to laminate design

Design of composite laminates with design variables of ply thickness and fiber orientation is a common continuous optimization problem. With only these two design variables present, the optimization is an integer problem which can be linearized. Branch and bound algorithms have been used to solve this type of problem once it has been linearized. Genetic algorithms can optimize nonlinear problems without the need for linearization. Inclusion of frequency and strength constraints, such as in buckling load optimization problems, leads to a nonlinear problem.

Haftka et al. [24, 25, 27, 33] have used GAs for determining an optimum laminate stacking sequence which minimizes laminate thickness or weight subject to strength, buckling, and ply contiguity constraints. The ply contiguity constraint is included to avoid matrix cracking by limiting the number of contiguous plies having the same fiber orientation. In these investigations the maximum allowable number of contiguous plies without penalty to the objective functions four. Another penalty parameter is used which penalizes the objective function for violation of the critical buckling load constraint. Performance and accuracy depend on tuning of penalty values which is undesirable.

In these studies the laminates analyzed consisted of a simply supported plates with compressive loads in longitudinal and lateral directions. The balanced, symmetric, laminates were comprised of 0, +/-45, and 90 degree plies of equal thickness. To simplify

calculations and maintain balanced conditions, stacks of two 0 degree plies ( $0_2$ ), two 90 degree plies ( $90_2$ ), and a combination of one +45 and one -45 degree ply (+/-45) were used in combination. Flexural stiffnesses were expressed in terms of only two lamination sequence parameters and material constraints.

An integer coding scheme is used in these investigations. Combinations of stacks of plies containing 0, +/-45, and 90 degree fiber orientation were used to represent the balanced, symmetric, laminate. Design strings consisted of the above mentioned stacks of plies with the  $0_2$  stack of plies represented by the integer 1, the +/-45 stack represented by 2, and the  $90_2$  stack represented by 3. Empty stacks were represented by 0 in the string. Empty stacks were packed to the outside of the string.

In studies [24] and [25] Haftka et al. utilized genetic algorithms with memory, storing useful information about past designs in a *binary tree*. Data stored in the binary tree consisted of the coded design string, objective function value, laminate thickness, in-plane lamination parameters, bending lamination parameters, normalized strain failure load, and normalized buckling load. Since during the evolution process designs are duplicated, the binary tree can be searched to supply necessary data pertaining to a design being evaluated, thus avoiding expensive duplicate calculations. The use of binary tree storage was shown to reduce the number of analyses required by 30-40% for the design problems considered.

A local improvement procedure utilized information stored in the binary tree. Studies [24] and [25] used local improvement. Local improvement searches for improved design in the neighborhood of a design generated by the genetic operations. For example, if two stacks are interchanged, the resulting laminate is not explicitly evaluated but its

fitness is estimated based on neighboring designs stored in the binary tree. Neighborhoods are defined based on relative distance between designs in the binary tree. In [25] one load case showed an increase in performance by a factor of three from use of local improvement. However, the average performance of three load cases implementing local improvement was lower than without local improvement due to load case three which has a singular optima.

As noted by Haftka et al. [24, 25, 27], one possible difficulty encountered in laminate design is that of singular optima. In these studies, strain constraints in plies of one certain orientation can be satisfied by either adding more plies of this particular orientation or removing these plies completely. As plies of this orientation are gradually removed strain constraints become more violated until these plies are no longer present and the corresponding strain constraint vanishes. The optimum solution contains no plies of the particular orientation mentioned and thus is termed singular. For certain load cases this situation typically occurs in plies with a fiber orientation aligned with the loading direction, usually zero-degree plies.

The genetic algorithms used in these studies difficulty removing these 0-degree plies from the design because critical strain constraints are violated. To assist the algorithm in doing so the initial population is seeded with designs containing no zero-degree plies (NZP). This is called NZP seeding and is used in [24, 25, and 27].

Comparison of the basic GA with and without the permutation genetic operator were made in [27]. In this computational cost was reduced by a factor of two by using permutation. For a nominal increase in price of the search, permutation greatly improved the practical reliability when compared to mutation. The authors define practical reliability as

the probability of reaching a practical optimum. Practical optima were defined as those designs whose fitness values were within 10% of the “best so far” design. As a means of evaluating performance, the normalized price is used which is defined as the number of evaluations of the objective function divided by the practical reliability. Considering only buckling constraints reveals the need for very high probabilities of permutation (300%) where as by including strain constraints probabilities of only 100% are necessary [27].

Kogiso et al. [24] utilize GAs for stacking sequence optimization of a laminated composite plate for buckling load maximization. Local improvement and a binary tree were used to improve performance and efficiency of the optimization process. This study uses an “elitist plan” version of the GA which carries the best design from each generation into the subsequent generation. Here again, singularities exist in the solution since the optimum contains no 0 degree plies. This is remedied by NZP seeding.

Nagendra et al. [33] investigated the stacking sequence optimization of a rectangular, balanced, symmetric, plate with simply supported boundary conditions subjected to buckling and strain constraints. The buckling constraint was linear in the ply identity design variables but strain functions were nonlinear. The strain functions were linearized to allow solution of the problem via sequential linearization using the branch and bound algorithm. To predict failure due to in-plane compressive loading, a maximum strain criterion (Jones [20]) was used. Results from the branch and bound algorithm were compared with global optimum designs found using genetic algorithms. The branch and bound procedure results were within 0.5 percent of the global optima.

LeRiche and Haftka [27] sought to minimize the thickness of a composite laminate plate subject to in-plane biaxial loading and buckling, strength, and ply contiguity

constraints. Here again, a rectangular, symmetric, balanced laminate is used. In this optimization, the use of new selection, mutation, and permutation operators are investigated. A constant penalty is applied, penalizing the objective function for violation of strength and buckling constraints. The need for large values of the penalty parameter was alleviated by doing this. The penalty parameter may need to be very large for some load cases to allow an objective function of a feasible optimum design to be smaller than the objective function of better feasible optimum designs.

New selection procedures explored the use of various crossover schemes. A thick crossover technique was used which confines crossover to the “full” portion of thinner parent laminate being mated, where full means the portion of the string where plies are present and not empty. Another crossover technique used restricts crossover to the full portion of the thickest parent and is called thick crossover. Averaging crossover was also investigated. These three crossover techniques were applied with different orders (number of points where crossover occurs). Uniform crossover produced the best results and one point crossover the worst. Each digit or gene of the offspring has equal probability of coming from each parent in uniform crossover.

A new mutation technique was also employed. This new mutation differs from the traditional mutation technique because of its ability to add plies anywhere in the laminate and not merely on the outside where empty plies are found. The new permutation technique employed randomly selects and swaps two stacks from the full part of the string. It was thought old permutation causes too much change in the string. This new permutation provided a 56% reduction in search price. Scaling mutation was introduced which provided a 10% decrease in search price. The scaling mutation operation biases mutation

toward adding rather than deleting a stack (of plies) in infeasible designs, and toward deleting a stack in a feasible design.

The study by Punch et al. [39] sought to maximize the capacity of a laminated composite beam to absorb mechanical energy without fracture using a GA with a new course-grain parallel structure called island injection. This structure allows different levels of refinement in the representation of the design. The best designs of each level are “injected” into a node with higher resolution where it is further refined. This method gives rise to “algorithmic” super linear speedup. A new finite element model developed by the authors is used for evaluation of each design. This model assumes a piecewise continuous through-the-thickness in-plane displacement distribution which accurately accounts for the layerwise variations of stress and displacement in a laminate.

In this study a 24-layer beam made of graphite-epoxy composite layers with clamped-clamped end conditions and an applied point load at midspan is designed. A thin layer (about 5.5% of the nominal ply thickness) is placed at the top of each composite layer, so there are actually 48 layers in the model. Each thin layer may be assigned the same material properties as the layer immediately below it, or it may be assumed that the thin layer is compliant, with stiffness properties three orders of magnitude less than the composite layers. The length-to-thickness ratio of the beam is 50. The length of the beam is divided into 20 divisions (finite elements), so there are  $20 \times 48 = 960$  design elements. The GA must decide whether to place a 0 degree ply (henceforth called material 1) or a 90 degree ply (henceforth called material 2) in each of the 480 structural ply design elements, and whether or not to place a compliant material in each of the 480 thin layer design elements.

In this application, we used a number of representations but focused on a 480-bit-string version which fully represents one half of the beam, and which was then mirrored across the vertical centerline to create a full beam. Thus the search space examined by the GA was  $2^{480}$ , representing all possible combinations of material and compliant material. The results of this work were quite promising. The GA generated a number of unique designs, including designs with “cantilever” beams of compliant layers.

In another application of GAs Nagendra et al. [34] present a study designing stiffened composite laminate panel with a hole for minimum weight. As in all other studies mentioned thus far, the rectangular panel is balanced and symmetric and is subjected to in-plane biaxial loading. Four equally spaced stiffeners with identical laminates were considered. Both the panel and stiffeners consisted of stacks of 0, +/-45, and 90 degree plies. The panel and stiffeners possess buckling, strength, and ply contiguity constraints. Also, the panel must not fail near the hole due to buckling or fail due to stress concentrations near the hole. A finite element code and a stiffened plate code was used simultaneously with a sequential approximate optimization procedure, which is a continuous optimization. Designs based on eigenvalue separation were evaluated. Designs found using the GA approach were superior to those found by the continuous approach, however, the computational cost of the GA approach were much higher.

In [35] Nagendra et al. modify the basic GA to reduce computational cost and improve reliability. The particular subject of this study is the design of stiffened composite laminates. Designs found by this modified GA were approximately 4 percent lighter than those found using the unmodified GA. The panel considered was rectangular, balanced, symmetric, and contained four equal spaced stiffeners. In plane loading was applied in the

form of normal and a small shear load which was applied to reduce sensitivity of off-design conditions. A penalty parameter was employed to enforce ply contiguity constraints. Buckling and strength were also constrained. Crossover was modified to improve performance of the GA. Substring crossover was used which effectively acted as an eight point crossover compared to the four point traditional crossover. New mutation operators called stack deletion, stack addition, and orientation mutation improved reliability, performing better than the old mutation.

Arbate [2] examines various aspects of optimal design of laminated plates and shells subjected to stiffness, strength, buckling load, and natural frequency constraints.

#### 1.4.3 Other GA applications

Johnson [19] implements continuously updated sharing in the simple genetic algorithm to determine the optimal placement of elastic supports on a simply supported plate. This paper illustrates application of a tournament selection routine with continuously updated sharing for optimization of elastic support locations on a square plate to maximize the first system eigenvalues. Sharing serves to aid a GA in possession of multiple optima. A sharing function is generally a power law function dependent upon the distance between two individuals. It was found in this study that certain sharing algorithms caused chaotic behavior when used in tournament selection, but the continuously updated sharing method was successful. Selection methods investigated included the traditional roulette wheel selection, stochastic remainder, binary tournament selection, and as discussed, binary tournament selection with continuously updated sharing. The computational cost of the GA approach was determined to be much higher than traditional optimization methods for

this set of parameters.

Another application of GAs which is unrelated to laminate plates is presented by Leung and Nevill [28]. In this study GAs are used to generate a stable, light weight, simple truss structure capable of supporting given forces. In this case, unlike in optimization of laminated plates, a binary coding of the design variables is used in a two dimensional format. Consistent results were obtained for the design problem at hand. This was a very basic study as it was intended to produce preliminary design possibilities.

Sandgren et al. [46] provide an example of GA use in the automotive industry. A genetic algorithm was used to both optimize the cross-section and minimize weight of an automobile bumper subject to simple bending and to minimize the weight of a body panel with stress and deflection constraints. Both cases involved a two dimensional chromosome structure, where in most of the previously presented cases of laminate design a one dimensional string of design variables was used. Penalty functions served the purpose of driving material properties closer to their optimum values. Using the GA approach to design such structures is feasible however the efficiency is questionable.

In [13] Furuta and Haftka determine optimum placement of actuators on large space structures using GAs. Averaging, uniform, random selection, and multiple-point crossover were compared. Mutation appeared to be a more effective operator than crossover. The comparison of several variations of integer coded and binary coded GAs revealed integer coding to produce highest performance and lowest cost.

In another application of GAs, Punch et al. [38] use a genetic algorithm with a K nearest neighbor (Knn) algorithm to classify soil samples from three environments found in agricultural experiments. The actual experiment was conducted by researchers at the

Center for Microbial Ecology. A large design space of  $3 \times 100 \times 96$  was necessary for this experiment which ruled out use of traditional approaches. The Genesis genetic algorithm program was used with a Knn program which was written by the authors. On test cases weighted Knn showed improved performance over the standard and normalized Knn. It was also shown for large data sets the 0/1 weighting did not perform adequately. Parallel processing was used to reduce run time. A nearly linear speed up was observed by the use of parallel processing which reduced run time by 40% over the case using a single processor. The nearly linear speed up was achieved by using multiple processors to calculate fitness which requires more time than all other GA operations.

#### 1.4.4 Design optimization via other techniques

The following articles provide examples of design optimization problems solved by other techniques.

Graesser et al. [14] present a design methodology for a stiffened laminated composite panel subject to in-plane loads and bending moments. Design variables included ply orientation angles of both the panel and stiffeners and stiffener geometry. Maximum strain and minimum strength constraints were imposed in the minimization of structure weight. The optimization software UWCODA (University of Washington Composite Optimization Design Algorithm) was used in this study. This software, originally developed as a design tool for laminated plates, utilizes classical lamination theory combined with the global optimization algorithm called "improving hit and run". This code deals with maximum strain failure criteria, buckling, and damage tolerance requirements. Effects of fiber orientation on the objective function (structure weight) is illustrated. One case considered

only increments of 15 degrees as possible fiber orientations. The weight of structures with this constraint imposed were found to be 30% higher than those with no restriction on fiber orientation angle.

Wang and Costin [50] present an optimum design study of composite structures including manufacturing constraints. They mathematically define the manufacturing constraints which control ply thickness variation, interleaving of plies, and ply orientation percentage. These constraints were applied simultaneously in the design of a simple wing structure for minimum weight using ASTROS optimization software. Ply thickness was treated as a continuous design variable. Ply dropoff rate constraints controlled the rate of thickness change between zones. Imposition of the ply interleaving constraint had the smallest affect, increasing structure weight by 2.2%. The largest effect was seen by applying the ply percentage constraint which increased structure weight by 17.3%. Ply dropoff rate constraint increased weight by 6.3%. Applying all three constraints produced an increase of 35.3% in structure weight.

In [32] Miki and Sugiyama present an optimal design method for obtaining symmetric, orthotropic, laminated composite plate designs with required in-plane stiffness, buckling strength, maximum bending stiffness, and natural frequency symmetric, orthotropic, laminated composite plates. By minimization of strain energy, maximum stiffness is determined. Optimum laminate configuration for maximization of buckling stress is an angle ply laminate. Likewise for maximization of stiffness angle ply laminates are the optimum configuration.

The multi-start global optimization technique is utilized by Miki and Sugiyama [32] determination of optimal laminate configuration in multi-layer, symmetric, laminated

plates which maximizes stiffness. This study notes the great amount of work already done in this area but identifies a need for more effective and efficient techniques in optimization of laminated plates. The multi-start technique is shown to be very efficient for such optimization problems. To obtain maximum stiffness, strain energy is minimized. The strain energy and its gradient are used to search for the optimum. In the multi-start technique trajectories are initialized at numerous random starting points in the design space. Each trajectory converges to a local minimum (since strain energy is being minimized), and is compared to others. If a local minimum corresponds to the lowest value to date, the probability of it being a global minimum is calculated. The constraints are then evaluated for this case. Optimum ply orientations of centrally loaded plates, uniformly loaded plates, and plates subject to combined loading were determined. Analysis of the uniformly loaded case produced multiple global optima as the number of plies increased. Reductions of 9.4-42.5% in deflection of both centrally and uniformly loaded cases were predicted for 16-ply lay-ups when considering optimum configurations.

Fukunaga and Vanderplaats [11] use a mathematical programming method for strength optimization of laminated composites subject to in-plane loading in a study optimizing strength of a laminated composite plate with respect to layer thickness. The modified direction method of the ADS (Automated Design Synthesis) program was utilized. Design variables were ply thickness and orientation angle. Strength constraints for zero thickness plies were deleted to improve efficiency and reliability of the approach. Since optimization with respect to orientation produces nonlinear constraints, the authors transformed the design variables to reduce the nonlinearity of the in-plane stiffness. Results show a strong dependence on initial points of search in finding the global optimum instead

of local optimum.

Fukunaga and Vanderplaats [12] present a stiffness optimization approach using lamination parameters by using the example of buckling optimization of orthotropic symmetric balanced laminated cylindrical shells under combined loadings. The feasible direction method in the ADS (automated design synthesis) program determined optimal laminate configurations. Since stiffness components of laminated composites are expressed as linear functions of lamination parameters, their use as design variables is an efficient method for such optimization problems. Also, expression of buckling load as a linear function of lamination parameters is simpler than expressing in terms of ply orientation angle. When considering the case of compressive axial loading for homogenous laminates, the optimal configuration was shown to be an isotropic laminate with respect to in-plane and out of plane stiffnesses. This was also stated as the case by other studies. For heterogeneous laminates (heterogeneous through the thickness) optimal configurations for the same loading case were shown to achieve 27% higher maximum buckling stress.

Kam and Lai [21] present an optimal design study of optimization of a four ply symmetric laminated plate and of a sandwich plate. The four ply laminate was simply supported on all edges and subjected to a transverse, central point load. The cantilever sandwich plate was loaded by uniform pressure. The purpose of the optimization was to determine optimal fiber orientation and ply thicknesses which minimized structure weight subject to strength and vibration constraints. A two level approach was used to do so. The first level of the optimization procedure determined the optimum fiber orientations which maximized stiffness and the natural frequency of the first vibration mode. The second level optimized ply thicknesses. A finite element model containing five degrees of

freedom per node was utilized to determine strains. Transverse shear effects were included and results obtained were shown to differ significantly from those obtained from classical laminate theory. A recursive linear programming method was used as the optimization algorithm. The main purpose of this paper was to illustrate performing such an optimization problem and no mention was made of convergence rate or efficiency of the algorithm.

a method for design of laminated composite plates for required flexural stiffness is presented by Miki [31]. The laminates considered were multiple balanced angle-ply symmetric laminates. All plies are of the same material. A design region was determined in terms of two flexural lamination parameter thus creating a two dimensional parabolic shaped region. From this region the lamination point is determined for a given stacking sequence. The lamination point is where all flexural stiffness values are determined. The converse is also possible, that is, for a given lamination point the stacking sequence can be found from this method. For the given laminate type it was shown that only two angles are necessary and sufficient in designing a laminate with required flexural stiffness.

Avalle and Belingardi [3] present a theoretical study of optimization of laminated plates. The model consisted of simply supported, rectangular, plates subjected to a symmetric transverse pressure loading. The laminate was restricted to be symmetric. The problem was that of determining the optimal fiber orientation and ply thicknesses which maximized flexural stiffness. The proposed analytical approach was validated by comparison to results from the ANSYS finite element code. Avalle and Belingardi showed that for a orthotropic laminate (without bending-twisting coupling) the number of different fiber orientations necessary to achieve maximum stiffness is restricted to two. The values of these orientations are a dependent on ply thickness, stacking sequence, and

material properties. The layer thicknesses need to maintain global orthotropy of the laminate.

Chattopadhyay *et al.* [8] present a multidisciplinary optimization of helicopter rotor blades which they decomposed into three levels. Baseline performance for the rotors is compared with a reference rotor. In the first level the total power coefficient is taken as the objective function with the rotor thrust coefficient constrained to insure at least the same lift characteristics as the reference rotor. In level two vibratory and static stresses in the blade and the dynamic and aeroelastic characteristics of the rotor are optimized. Spar design is determined in level three by using the optimal structural stiffness obtained in level two. In level three the objective function is the total blade weight.

The nonlinear optimization algorithm used is based on the method of feasible directions. A two-point exponential approximation technique was used for objective function evaluation in lieu of exact evaluation of the objective function which is much more computationally expensive. Chattopadhyay *et al.* [8] claim that since gradient information is retained by this technique it is better than using Taylor series expansions for this purpose. Significant improvements over the reference configuration resulted from this study. A reduction of 19.8% in the coefficient of total power was obtained, vertical shear was reduced by 45.8%, and total blade weight was reduced by 3.7%. Also, the optimum configuration contained a significant reduction in total rotor twist with only approximately 6 degrees of twist from root to tip which is a great improvement over the reference rotor.

The object of a study by Lake *et al.* [26] was to provide a basis for understanding elastic coupling in composite rotor blade structures and to develop a finite element modeling method capable of accurately predicting dynamic response of the rotor blades.

Experimental results were compared with analytical results for tubular spars of three types of cross-sectional geometries. These three geometries were square, D-shaped, and elliptical. Since these geometries are not circular they experience warping. Each spar was comprised of four plies of T-650/42 graphite fiber with ERLX 1925-2 epoxy resin plane weave cloth pre-preg. Five global modes were identified for each span type in the range of 0 to 2000Hz. These modes were (in no particular order) first and second lateral bending, first and second vertical bending, and first torsion mode. Agreement between experimental and analytical results ranged from 1.6% difference in the best of the elliptical spars to 13.8% in the worst case of the D-shaped spars.

Kam and Lai [23] use a constrained multi-start optimization approach to determine the optimal design of a laminated composite plate for maximum stiffness. The problem is converted into an unconstrained minimization problem and an unconstrained global optimization method is used. Ply thickness and fiber orientation are treated as design variables. In the optimization process a shear-deformable laminated composite finite element is used in the finite element analysis. Only symmetric laminates are considered. Results from cases with simply supported or with fixed edges subjected to a center point load were used for comparison with two other optimization routines, one of which was used by the authors in a previous study and the other was the BCONF minimization routine from the IMSL mathematical package. The optimization algorithm used was shown to be more efficient and it provided laminates with higher stiffnesses than the other two optimization methods. Kam and Lai [23] illustrated the affects of aspect ratio, length to thickness ratio, and number of ply groups on the results.

Adali et al. [1] present two optimization problems. One of which is a lamination

scheme optimization for maximum buckling load and the other is for material cost minimization. In both cases, discrete fiber orientations were considered with fixed ply thicknesses. The effects bending-twisting stiffnesses  $D_{16}$  and  $D_{26}$  are considered negligible provided two dimensionless ratios involving these stiffnesses are within a certain range. To reduce material costs hybrid construction was considered which uses high stiffness, expensive graphite/epoxy outer plies and low stiffness glass/epoxy inner plies. Results showed buckling loads of the optimal hybrid laminates to be only about 10-15% less than for laminates using all graphite/epoxy plies. The critical buckling load was shown to quickly decrease as the number of glass/epoxy plies exceeded 1/2 of the total number of plies. In some cases increasing the total number of plies was shown to increase critical buckling load. Results also show for the case of uniaxial loading, laminates with aspect ratios less than 0.6 consist of all 0 degree plies where as for aspect ratios ranging from 0.8 to 2.0 optimal layups consist of all +/- 45 degree ply orientations.

#### 1.4.5 Plate theories and finite element models

In [29] Livine presents an equivalent plate structural model for wing shape optimization which includes transverse shear effects. Many of the codes available for multidisciplinary structural aerodynamic optimization of wing configurations, such as ELAPS, LS-CLASS, and ELFINI, are based on the kinematic assumptions of classical plate theory (CPT). In this study, the author shows use of these assumptions leads to models which are too stiff and do not accurately capture coupling between chordwise bending, spanwise bending, and torsion. Natural frequencies of higher mode shapes are overpredicted by these codes. In this paper a new plate wing modeling theory, which utilizes a first order

shear deformation plate theory (FSDT), is compared to CPT, finite element methods (FEM), and actual measured results.

The model consisted of an all aluminum cantilever wing containing spars and ribs. The wing was swept back by 30 degrees. A 1lb vertical force was applied to the tip of the trailing edge. CPT results were 17% too stiff and natural frequencies were too high, especially in torsional modes [29]. The FSDT and FEM results correlated nicely with each other and agree fairly well with measured results. Both plate techniques converged faster than the FEM technique which is due to the smaller mass and stiffness matrices of the plate theories. Since the plate theories are based on a Ritz approximation the order of the polynomial can be varied. When the order was varied from 5 to 8 a change of less than 2% was achieved for determination of the natural frequency and displacement. The author feels using FSDT method improves reliability and generality of equivalent plate structural wing modeling techniques.

Averill and Yip [6] present a high-order zig-zag finite element model for use with thick laminated and sandwich beams. This element has the nodal topology of a four noded planar element with beam type kinematics and an interpolation scheme which eliminates locking. The number of sublaminates is variable for the linear zig-zag theory (LZZT) element with increasing accuracy as the number of sublaminates increases. Results are provided for simply supported thick laminated beams with sinusoidally varying loading. The LZZT results were compared with first order shear deformation theory (FSDT) and elasticity solutions and were shown to accurately predict in-plane stresses and displacements with use of only one sublaminate through the thickness. It was also noted that LZZT results converge to the elasticity solution as the number of sublaminates is increased.

Burton and Noor [7] present analytic thermoelasticity solutions for sandwich panels and cylindrical shells. These elasticity solutions are used for comparison with the models analyzed in the current research. Burton and Noor considered cases of simply supported, doubly curved, sandwich panels with uniform pressure applied to one side. The core was treated as a homogenous orthotropic continuum. The affect of variations of material parameters of the face sheets and the core was studied by evaluating first-order sensitivity coefficients. The procedure used by Burton and Noor [7] was shown to be very efficient compared to other methods for obtaining converged normalized transverse displacement. Also, the strain energy for different stress components was calculated and compared. One set of results showed that for thick face sheets the strain energy in sandwich cylinders and panels was very sensitive to changes in  $E_1$  and  $G_{1t}$  of the face sheets and of  $G_{13}$  of the core. Geometric parameters such as the ratios of axial length to radius, total thickness to radius, and face sheet thickness to total thickness were varied to determine their affect on strain energy components.

In [36] Noor summarizes various aspects of the mechanics of anisotropic plates and shells. Computational models and deformation types were briefly discussed. A short discussion on the predictor-corrector approach for analysis of thick anisotropic plates and shells was also included.

In [10] Cho *et al.* present a finite element formulation which accounts for both material and geometric nonlinearities in laminated composite structural components. An isoparametric degenerated shell element containing independent rotational and displacement degrees of freedom was used. To maintain continuity of shear deformation between the layers the first shear deformation theory was used and a shear correction factor was

included to help approximate transverse shear energy. For treatment of the progressive failure due to matrix degradation the Newton-Raphson method was used and for geometric nonlinearities the Lagrange method was used. For filament wound cylinders and laminated plates numerical results were compared with experimental results. Numerical results appeared to be in good agreement with experimental results however, it was mentioned that the experimental results accuracy could be improved.

Averill and Reddy [4] present a four noded plate element based on the general third order theory of Reddy. This theory is employed in the current research. This theory assumes a cubic expansion of the in-plane displacement field in the thickness coordinate:

$$u = u_0 - z \frac{\partial w_0}{\partial x} + z \left[ 1 - \frac{4}{3} \left( \frac{z}{h} \right)^2 \right] \hat{\phi}_x \quad (1.14)$$

$$v = v_0 - z \frac{\partial w_0}{\partial y} + z \left[ 1 - \frac{4}{3} \left( \frac{z}{h} \right)^2 \right] \hat{\phi}_y \quad (1.15)$$

$$w = w_0 \quad (1.16)$$

where  $u_0$ ,  $v_0$ , and  $w_0$  are displacements in the  $x$ ,  $y$ , and  $z$  directions, respectively, of a point on the midsurface of the plate,  $(x,y,0)$ . Traction free boundary conditions on the top and bottom surfaces of the element are satisfied.

#### 1.4.6 Aircraft design literature

Raymer [41] presents a conceptual approach to aircraft design, and in doing so he provides general and historical data for various design parameters. This data proved useful

as a guide for selection of geometric and loading parameters used in the current study. Wing aspect ratios typically are 7.5 for jet transport aircraft, 7.6 for single engine aircraft, 7.8 for twin engine aircraft, and as high as 9.2 for twin turboprop aircraft. Tail aspect ratios range from 6-10 for sail planes, 3-4 for fighter aircraft, and 3-5 for other aircraft.

Airfoil thickness ratio,  $t/c$  (thickness/chord) is another parameter of interest. Raymer [41] provided a graph containing historical data which he suggests as a good method for initial selection of thickness ratio when designing an aircraft. For mach numbers slightly less than 1.0 this graph shows thickness ratios historically range from 0.06 to 0.14. Also a graph of test data for a NACA 65(216)-415 airfoil section with a chord of 24 inches has a thickness ratio of approximately 0.14. An interesting note is that supercritical airfoils are approximately 10% thicker than subsonic airfoils. Quite often airfoil thickness can be 20-60% thicker at the root than at the tip without substantially affecting the drag due to fuselage effects. Raymer [41] also mentions the thicker root airfoil should not extend more than approximately 30% of the total span.

To estimate wing loading some idea of typical aircraft weight must be attained. Raymer[41] says the take-off weight of a Lockheed S-3A is approximately 52,500 lbs and that of a C-5 is approximately 764,000 lbs. While an aircraft is at cruise speeds, i.e. level unaccelerated flight, lift equals aircraft weight and thrust equals drag. The highest cruise weight occurs at the beginning of cruise since at this time the most fuel is present. The aircraft weight at the beginning of cruise is the take-off weight minus the fuel consumed to reach cruise. Typical wing loading ratios,  $W/S = \text{weight/wing lift area}$ , are listed in table 5.5, pp. 84, which shows  $W/S$  ranging from 17 for single engine planes, to 26 for twin engine planes, to as much as 120 for jet transports. As a safety measure a load limit of 5

g's was first considered by the Wright brothers for design purposes. Depending on the type of aircraft and application different load factors are assumed. Aerodynamic loading in the chord-wise direction of typical airfoils can be crudely approximated by a constant load for the first 15% of chord length then by a linearly decreasing load which is zero at the trailing edge. In the spanwise direction a good approximation is an elliptic load distribution with the least load at the wing tips.

Twist is often built into a wing to both prevent tip stall and modify the lift distribution to approximate an ellipse at some desired velocity. Two different types of twist are aerodynamic and geometric twist. Geometric twist is the change in airfoil incidence angle with respect to the root airfoil and aerodynamic twist is the angle between the zero-lift angle of the airfoil and root zero-lift angle. Raymer[41] recommends not exceeding a twist of 5 degrees with 3 degrees being typical. Home built aircraft and general aviation type planes usually have a twist of 2 degrees where transport aircraft use 1 degrees and military aircraft 0 degrees.

## **Chapter 2**

# **Description of Laminated Plate Theories.**

### **2.1 Introduction**

Composite materials are a good choice for structural materials in many applications due to their favorable properties of high strength-to-weight and high stiffness-to-weight ratios. The use of thick-section laminated composites is particularly prevalent in many military and industrial, aerospace and marine applications. Accompanying the use of such materials is the structural designer's need for an accurate means of analyzing structures composed of these materials. To satisfy this need many different theories have been developed. Certainly a fully three dimensional analysis is one method capable of handling the problem. However, this method quickly becomes computationally infeasible for even simple structures. Equivalent single-layer (ESL) and layerwise theories are two other approaches to modeling laminated plates. These approaches can furnish adequate results, depending on the design problem, while also providing a good balance of computational efficiency and accuracy.

This chapter discusses different plate theories and the associated finite element models available for analysis of laminated composite plates. Five theories are discussed: CLPT, FSDT, HSDT, ZZHT, and LZZHT. In the current research FSDT, HSDT, ZZHT,

and LZZHT are used for analysis of different laminates.

## 2.2 Equivalent Single-Layer Theories

### 2.2.1 Classical Laminated Plate Theory (CLPT)

Equivalent single-layer laminate theories reduce a three dimensional continuum problem to a two dimensional problem. To achieve this reduction non-homogeneous laminated plates are treated as a statically equivalent single layer having certain constitutive behavior [44]. Classical laminated plate theory (CLPT), based on the kinematic assumptions of Kirchhoff plate theory, is the simplest in the hierarchy of ESL theories. This theory is intended for use with thin laminates. CLPT is based on the Kirchhoff assumptions requiring a straight line normal to the plane of the plate to be inextensible and remain straight and normal to the plane after deformation [9, 20, 43], see Figure (2.1). Thus transverse shear and normal effects are neglected. This is specified by the following conditions

$$\epsilon_z = 0 \quad \epsilon_{xz} = 0 \quad \epsilon_{yz} = 0 \quad (2.1)$$

The in-plane displacements are represented as linear functions of the thickness coordinate.

The displacement field for CLPT is given in Equation (2.2) as follows:

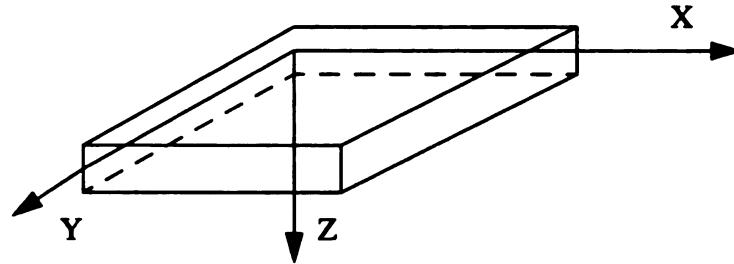


Figure (2.1) - (a) Plate and coordinate system.

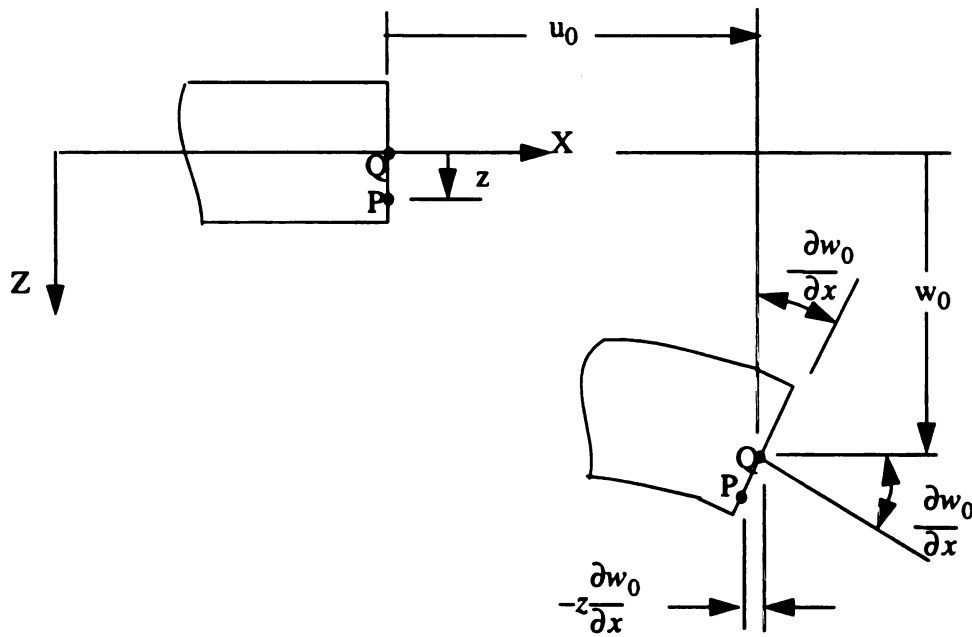


Figure (2.1) - (b) Undeformed and deformed plate section for CLPT.

$$\begin{aligned}
u(x, y, z) &= u_0(x, y, t) - z \frac{\partial}{\partial x} w_0(x, y) \\
v(x, y, z) &= v_0(x, y, t) - z \frac{\partial}{\partial y} w_0(x, y) \\
w(x, y, z) &= w_0(x, y)
\end{aligned} \tag{2.2}$$

Where  $u$ ,  $v$ , and  $w$  are the respective displacements in the  $x$ ,  $y$ , and  $z$  directions, of a point  $(x, y, z)$ , and  $u_0$ ,  $v_0$ , and  $w_0$  are displacements in the  $x$ ,  $y$ , and  $z$  directions of a point on the midplane of the plate,  $(x, y, 0)$ , as shown in Figure (2.1).

Since laminated composites have low transverse shear stiffness compared to in-plane stiffnesses, the transverse shear and normal deformations, and thus stresses, are significant and cannot be ignored. Classical plate theory neglects these transverse effects and therefore cannot accurately predict the plate response to complex loads. Consequently, this theory is often not a good choice for modeling thick laminated composites unless the loading is predominantly in-plane.

### 2.2.2 First Order Shear Deformation Theory (FSDT)

The next higher order equivalent single-layer theory is first order shear deformation theory (FSDT) [48]. This is also called Hencky-Mindlin plate theory [43]. FSDT is intended for use in analyzing thin to moderately thick plates. A finite element code employing this FSDT theory is evaluated and compared to other theories in the current research. FSDT extends the kinematics of CLPT by allowing a line initially straight and normal to the laminate mid-plane to remain straight but no longer normal to the plane after deformation. This allows a constant state of transverse shear with respect to the thickness coordinate. Transverse normal strains are assumed to be zero. These

conditions are represented as [43]

$$\varepsilon_z = 0 \quad \varepsilon_{yz} = \varepsilon_{yz}(x, y) \quad \varepsilon_{xz} = \varepsilon_{xz}(x, y) \quad (2.3)$$

FSDT assumes the following displacement field [42-44]

$$\begin{aligned} u(x, y, z) &= u_0(x, y) - z\hat{\phi}_x \\ v(x, y, z) &= v_0(x, y) - z\hat{\phi}_y \\ w(x, y, z) &= w_0(x, y) \end{aligned} \quad (2.4)$$

where, again,  $u_0$ ,  $v_0$ , and  $w_0$  are displacements in the  $x$ ,  $y$ , and  $z$  directions of a point on the mid-plane of the plate  $z = 0$ , and  $\hat{\phi}_x$  and  $\hat{\phi}_y$  are rotations of the transverse normal about the  $y$  and  $x$  axes, respectively [42-44]. FSDT requires shear correction factors to correct the overpredicted shear strain energy. The finite element code based on FSDT used in this research calculates the shear correction factors using the approach of Whitney [51]. As can be seen from Figure (2.2), when  $\hat{\phi}_x = \frac{\partial w_0}{\partial x}$ , FSDT reduces to CLPT.

The finite element model used in the current research which is based on FSDT contains the “usual” engineering nodal degrees of freedom: displacements  $u$ ,  $v$ ,  $w$ , and rotations  $\hat{\phi}_x$ ,  $\hat{\phi}_y$ . This model uses a 9-noded plate element topology.

Finite element models based on FSDT assume the displacement field is  $C^0$  continuous which requires the displacement field to be continuous through-the-thickness. This is an improvement over use of CLPT which requires  $C^1$  continuity, in which case the



interpretation is usually not meaningful. With third-order or higher theories the gain in accuracy is often minimal for laminated composites and is not worth the increased complexity. In the current research a finite element model based on a general third-order theory, developed by Averill and Reddy [4], is evaluated and compared with other theories.

In this HSDT theory the displacement field is of the form:

$$\begin{aligned}
 u(x, y, z) &= u_0 - z \frac{\partial w_0}{\partial x} + z \left[ 1 - \frac{4}{3} \left( \frac{z}{h} \right)^2 \right] \hat{\phi}_x \\
 v(x, y, z) &= v_0 - z \frac{\partial w_0}{\partial y} + z \left[ 1 - \frac{4}{3} \left( \frac{z}{h} \right)^2 \right] \hat{\phi}_y \\
 w(x, y, z) &= w_0
 \end{aligned} \tag{2.5}$$

where here again,  $u_0$ ,  $v_0$ , and  $w_0$  are displacements in the  $x$ ,  $y$ , and  $z$  directions of a point on the midplane  $(x, y, 0)$ , and  $\hat{\phi}_x$  and  $\hat{\phi}_y$  are rotations of the transverse normal about the  $y$  and  $x$  axes, respectively. The nodal degrees of freedom in this theory are  $u$ ,  $v$ ,  $w$ ,  $\frac{\partial w_0}{\partial x}$ ,  $\frac{\partial w_0}{\partial y}$ ,  $\hat{\phi}_x$ , and  $\hat{\phi}_y$ . The element developed employing this theory uses a four noded plate topology.

Although equivalent single layer theories provide a good compromise between computational efficiency and accuracy for determination of global response of thin laminates, there are a few drawbacks of ESL theories. First, accuracy of the global response decreases as laminate thickness increases. Second, such models are unable to accurately predict strain and stress at layer interfaces and near geometric discontinuities. Finally,

transverse stresses cannot be accurately predicted by these theories [44].

## **2.3 Zig Zag Theories**

Layerwise theories were developed to overcome the deficiencies of ESL theories. The assumed displacement field of these theories provides a more correct kinematic representation for thick laminates. Layerwise theories assume a unique displacement field for each layer. The number of degrees of freedom in the problem may or may not be coupled to the number of layers in the laminate. If the number of degrees of freedom does depend on the number of layers, the analysis is similar in computational cost to a full three-dimensional analysis which is the case in full layerwise theories. The number of layers and number of degrees of freedom can also be uncoupled which is the case with the zig-zag theories. To achieve this the transverse stresses at ply interfaces are required to be continuous.

Two finite element models based on the zig-zag theory are used in the current research. The finite element codes employing these finite element models are called LZZHT, developed by Yip and Averill [52], and ZZHT. The LZZHT theory uses an eight-noded brick finite element which allows a laminate to be represented by one or more layers (or sublaminates) by “stacking” elements through-the-thickness. A four-noded plate element topology is used in the ZZHT theory. This element cannot be “stacked” in the thickness direction and thus the sublaminate approach cannot be used.

### 2.3.1 LZZHT Theory

The element based on the LZZHT theory of Yip and Averill [52] can be stacked in the thickness direction. This is called a sublaminar approach. In the sublaminar approach each sublaminar (or layer of elements) may contain several physical layers. Within each sublaminar an independent displacement field is assumed in which the through-the-thickness variation of in-plane displacements is represented by a piecewise linear (or zig-zag) function superimposed upon a cubic polynomial in the local thickness coordinate [6, 52]. The transverse deflection is assumed to vary quadratically with the thickness coordinate. The displacement field for the  $n$ th layer of the  $m$ th sublaminar is [52]:

$$\begin{aligned}
 u_x^{(m,n)}(x, y, z) &= \sum_{k=0}^3 z^k \hat{u}_k^{(m)} + \sum_{i=1}^{n-1} (z - z_i) \hat{\xi}_i^{(m)} \\
 u_y^{(m,n)}(x, y, z) &= \sum_{k=0}^3 z^k \hat{v}_k^{(m)} + \sum_{i=1}^{n-1} (z - z_i) \hat{\eta}_i^{(m)} \\
 u_z^{(m,n)}(x, y, z) &= w_b^{(m)} \left(1 - \frac{z}{h}\right) + w_t^{(m)} \left(\frac{z}{h}\right) + \hat{w}_3^{(m)} \left(\frac{z}{h}\right) \left(1 - \frac{z}{h}\right)
 \end{aligned} \tag{2.6}$$

where subscripts t and b refer to the top and bottom surfaces of the sublaminar, n is the layer number, h the sublaminar thickness,  $\hat{\xi}_i$  and  $\hat{\eta}_i$  are the zig-zag functions, and  $u_x$ ,  $u_y$ , and  $u_z$  are displacements in the x, y, and z directions, respectively. The displacement field variable  $u_z$  contains the non-conforming bubble function to eliminate the Poisson's ratio stiffening effect which occurs in continuum elements when only one layer of elements is

used through the thickness of a region [52]. This stiffening effect arises from bending energy terms due to the approximation function's inability to linearly interpolate the transverse normal strain through the thickness of the plate [52]. In the computation of transverse shear strain  $\hat{w}_3$  is ignored since the purpose of this term is only to eliminate Poisson's stiffening effects. This term is regarded as a nodeless variable degree of freedom which is condensed out at the element level.

The linear elastic constitutive relations for the  $j$ th layer of a laminate are:

$$\begin{bmatrix} \sigma_{xx} \\ \sigma_{yy} \\ \sigma_{zz} \\ \tau_{yz} \\ \tau_{xz} \\ \tau_{xy} \end{bmatrix}^{(j)} = \begin{bmatrix} C_{11} & C_{12} & C_{13} & 0 & 0 & C_{16} \\ & C_{22} & C_{23} & 0 & 0 & C_{26} \\ & & C_{33} & 0 & 0 & C_{36} \\ & & & C_{44} & C_{45} & 0 \\ & \text{symmetric} & & & C_{55} & 0 \\ & & & & & C_{66} \end{bmatrix}^{(j)} \begin{bmatrix} \epsilon_{xx} \\ \epsilon_{yy} \\ \epsilon_{zz} \\ \gamma_{yz} \\ \gamma_{xz} \\ \gamma_{xy} \end{bmatrix}^{(j)} \quad (2.7)$$

Using the small strain assumption, the infinitesimal strain-displacement relations are [30]:

$$\epsilon_{xx} = \frac{\partial u}{\partial x}, \quad \epsilon_{yy} = \frac{\partial v}{\partial y}, \quad \epsilon_{zz} = \frac{\partial w}{\partial z}, \quad (2.8)$$

$$\gamma_{yz} = \frac{\partial w}{\partial y} + \frac{\partial v}{\partial z}, \quad \gamma_{xz} = \frac{\partial w}{\partial x} + \frac{\partial u}{\partial z}, \quad \gamma_{xy} = \frac{\partial v}{\partial x} + \frac{\partial u}{\partial y}$$

The  $\hat{\xi}_i$  and  $\hat{\eta}_i$  degrees of freedom in Equation (2.6) can be eliminated by

enforcing transverse shear stress continuity at each layer interface. The conditions for shear stress continuity between layers (j) and (j+1) are:

$$\begin{aligned}\tau_{xz}^{(j)} &= \tau_{xz}^{(j+1)} \\ \tau_{yz}^{(j)} &= \tau_{yz}^{(j+1)}\end{aligned}\tag{2.9}$$

Using the strain displacement relations of Equations (2.8) along with the linear elastic constitutive equations in Equation (2.7), Equation (2.9) can be solved giving expressions for  $\hat{\xi}_i$  and  $\hat{\eta}_i$  in terms of the remaining degrees of freedom (see [52]).

Further simplification is possible by satisfying the applied transverse shear traction conditions on the top and bottom surface of the sublaminates as follows:

$$\begin{aligned}\tau_{xz}^{(1)}\Big|_{z=0} &= \tau_{xb} & \tau_{yz}^{(1)}\Big|_{z=0} &= \tau_{yb} \\ \tau_{xz}^{(N)}\Big|_{z=h} &= \tau_{xt} & \tau_{yz}^{(N)}\Big|_{z=h} &= \tau_{yt}\end{aligned}\tag{2.10}$$

where  $z = 0$  is the bottom surface and  $z = h$  is the top surface of the sublaminates,  $N$  is the number of layers in the sublaminates, and  $\tau_{xb}$ ,  $\tau_{yb}$ ,  $\tau_{xt}$ , and  $\tau_{yt}$  are applied shear tractions (or interlaminar shear stresses when more than one sublaminates is used) at the bottom and top surfaces of the sublaminates, respectively.

The final form of the displacement field is obtained by introducing the surface variables:

$$\begin{aligned}
u_b &= u_x^{(1)} \Big|_{z=0} = \hat{u}_0 & u_t &= u_x^{(N)} \Big|_{z=h} \\
v_b &= u_y^{(1)} \Big|_{z=0} = \hat{v}_0 & v_t &= u_y^{(N)} \Big|_{z=h}
\end{aligned} \tag{2.11}$$

$$\begin{aligned}
\theta_{xb} &= \frac{\partial w_b}{\partial x} & \theta_{yb} &= \frac{\partial w_b}{\partial y} \\
\theta_{xt} &= \frac{\partial w_t}{\partial x} & \theta_{yt} &= \frac{\partial w_t}{\partial y}
\end{aligned} \tag{2.12}$$

The rotational degrees of freedom are expressed in the above form to allow the assumed displacement field to remain  $C^0$  continuous. The constraints in Equation (2.12) were enforced by penalty methods in the element formulation [52]. The displacement field for each sublaminar is expressed in final form in terms of the operative degrees of freedom at the top and bottom surfaces of the sublaminar:

$$u_b, u_t, v_b, v_t, w_b, w_t, \theta_{xb}, \theta_{xt}, \theta_{yb}, \theta_{yt}, \tau_{xb}, \tau_{xt}, \tau_{yb}, \tau_{yt} \tag{2.13}$$

As mentioned previously, the number of degrees of freedom is not coupled to the number of layers in each sublaminar. In the finite element model using this theory each node contains seven degrees of freedom  $u$ ,  $v$ ,  $w$ ,  $\theta$  and  $\tau$ . The  $\tau$  degrees of freedom are easily dealt with when one sublaminar is used by setting them equal to the applied shear traction on the top and bottom surfaces of the laminate. When more than one sublaminar is used  $\tau$  is not specified at the internal nodes but is still specified on the top and bottom surfaces of the laminate in the same manner as when one sublaminar is used.

The finite element model based on this theory contains the above mentioned seven degrees of freedom per node. The element topology is an eight-noded brick, and thus the total number of degrees of freedom per element is 56.

### 2.3.2 ZZHT Theory

Another third-order zig-zag theory used in the current research is called ZZHT. The element developed from this theory contains seven degrees of freedom and a four noded plate element topology for a total of 28 degrees of freedom per element. This element is computationally more efficient than the code employing the LZZHT element due to the number of degrees of freedom per element for ZZHT being one-half that of the LZZHT element. The ZZHT theory is more accurate than any of the ESL theories. Good accuracy coupled with acceptable efficiency makes the ZZHT theory a likely choice for use in the optimization portion of this research.

The displacement field for this theory uses a cubic polynomial superimposed onto piecewise linear zig zag functions for the in-plane displacements, as done in the LZZHT theory, however the transverse displacement is assumed constant:

$$u_z = w_0 \quad (2.14)$$

Interlaminar transverse shear stress continuity at ply interfaces is enforced to eliminate the associated zig zag degrees of freedom as was done in the LZZHT theory (see Equation (2.9)). The displacement field is cast in final form in terms of the following degrees of freedom:

$$u_0, v_0, w_0, \theta_x, \theta_y, \phi_x, \phi_y \quad (2.15)$$

where  $u_0$ ,  $v_0$ , and  $w_0$  are displacements as defined previously,  $\theta_x$  and  $\theta_y$  are the same as in the LZZHT theory, and  $\phi_x$  and  $\phi_y$  are the generalized rotations as used by Averill and Reddy [4].

## Chapter 3

# Assessment of Laminated Plate Theories for Analysis of Composite Sandwich Panels.

### 3.1 Introduction

The first portion of this research compares different theories for the analysis of laminated composite plates. Various thick sandwich panels are analyzed using finite element models based on four different laminated plate theories. Results are compared with the elasticity solution of Burton and Noor [7]. The four theories compared are those previously discussed in Chapter 2. Two equivalent single layer (ESL) theories are used. One is based on first order shear deformation theory (FSDT) [48] using shear correction factors of Whitney [51] and a the second based on a modified version of Reddy's general third order theory (HSDT). The remaining two theories used for this comparison are third - order zig zag theories (ZZHT and LZZHT). This comparison of theories also aided in the selection of a theory for use in the optimization portion of this research. An appropriate theory is selected based on solution accuracy and computational efficiency which is extremely important in optimization processes where large numbers of calculations are performed.

### 3.2 Description of Models

The above mentioned four theories were compared for square sandwich panels with simply supported edges and subjected to a sinusoidal surface loading as shown in Figures (3.1) and (3.2). The simply supported boundary conditions were in the form:

$$u = w = 0; \sigma_y = 0 \quad \text{on} \quad y = 0, b \quad 0 < x < a \quad 0 < \zeta < h \quad (3.1)$$

$$v = w = 0; \sigma_x = 0 \quad \text{on} \quad x = 0, a \quad 0 < y < b \quad 0 < \zeta < h \quad (3.2)$$

where  $u$ ,  $v$ , and  $w$  are displacements in the  $x$ ,  $y$  and  $z$  direction, respectively, and  $\zeta$  is a

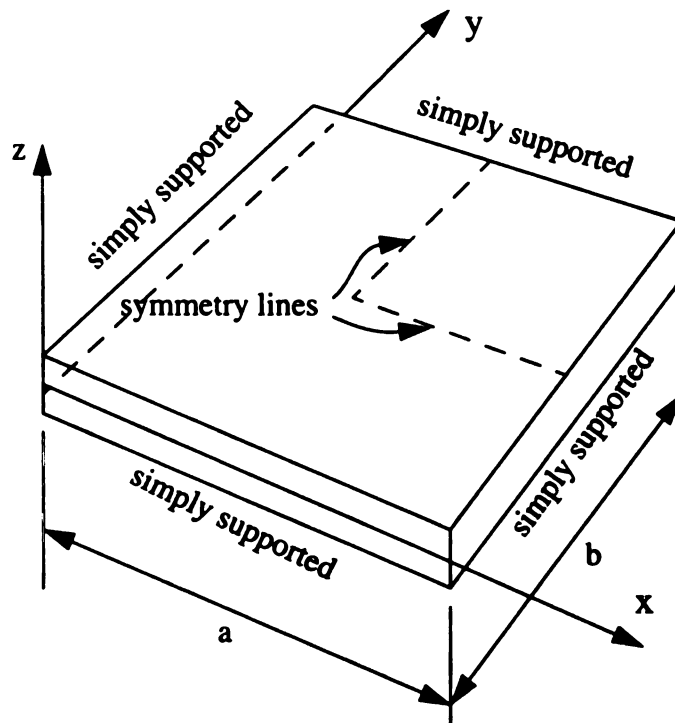


Figure (3.1) - Sandwich plate geometry

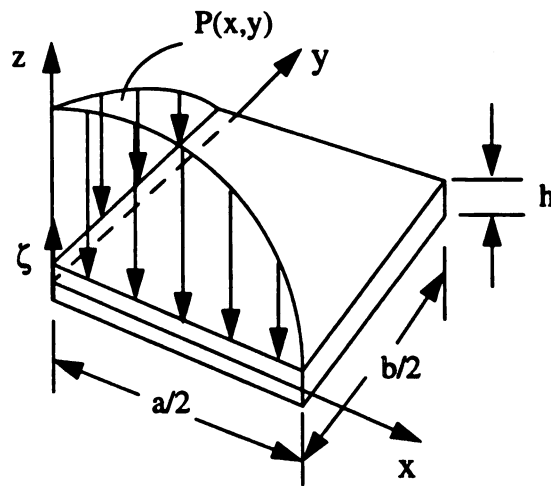


Figure (3.2) - Quarter plate geometry and loading.

thickness coordinate which is zero at the bottom surface of the laminate and 1 at the top. Due to the symmetry of the problem it was only necessary to model one quarter of the plate (see Figure 3.2).

Two lamination schemes were used in the present investigation. Material properties used for both cases are given in Table 3.1. The first case analyzed consisted of a symmetric sandwich panel having 5 layers top and bottom surrounding a thicker core layer. The lamination scheme for this case, called layup 1, is given in Table 3.2. For this lamination sequence two different aspect ratios were analyzed,  $a/h=4$  and  $a/h=10$ , where  $a$  is the length dimension of one side of the full plate and  $h$  is the thickness. The lamination sequence for the second case analyzed, layup 2, is given in Table 3.3. In this case the sandwich panel has a non-symmetric layup with 5 layers top and bottom surrounding a thick core.

**Table (3.1) Sandwich Panel Material Properties.**

Property	Material 1	Material 2	Material 3	Material 4
$E_{11}$	1.0e6	3.3e7	2.5e7	5.0e4
$E_{22}$	2.5e7	2.1e7	1.0e6	1.5e5
$E_{33}$	1.0e6	2.1e7	1.0e6	5.0e4
$\nu_{12}$	0.01	0.25	0.25	0.01
$\nu_{23}$	0.25	0.25	0.25	0.15
$\nu_{13}$	0.25	0.159	0.10	0.15
$G_{12}$	0.5e6	8.0e6	0.5e6	2.17e4
$G_{23}$	0.5e6	4.0e6	0.2e6	4.2e4
$G_{13}$	0.2e6	8.0e6	0.5e6	2.17e4

**Table (3.2) Layup 1.**

Layer No.	Material	Thickness	Orientation
1	1	0.01	0
2	2	0.025	0
3	3	0.015	0
4	1	0.020	0
5	3	0.030	0
6	4 (core)	0.800	0
7	3	0.030	0
8	1	0.020	0
9	3	0.015	0
10	2	0.025	0
11	1	0.010	0

**Table (3.3) Layup 2.**

Layer No.	Material	Thickness	Orientation
1	2	0.02500	0
2	3	0.01500	90
3	1	0.02000	90
4	3	0.03000	0
5	1	0.01000	0
6	4	0.40000	0
7	4	0.40000	90
8	3	0.03000	0
9	1	0.02000	0
10	2	0.02500	90
11	1	0.01000	90
12	3	0.01500	90

**Table (3.4) Convergence Data: Transverse center displacement.**

Mesh Density	FSDT	HSDT	ZZHT	LZZHT
4	-0.3550E-3	-0.1552E-3	-0.2242E-3	-0.2014E-3
16	-0.3529E-3	-0.1659E-3	-0.2144E-3	-0.2065E-3
64	-0.3518E-3	-0.1700E-3	-0.2118E-3	-0.2071E-3

### 3.3 Results

In all cases the square domain was discretized into a mesh containing 8 elements in the x-direction and 8 elements in the y-direction. This mesh was chosen based on a convergence study of four meshes with mesh densities of 4, 16, and 64 elements (see Table (3.4)). Mesh density is defined as the number of elements per layer in the mesh. The mesh for the FSDT theory contains 9-noded plate elements, while the HSDT and ZZHT theories uses a mesh of 4-noded plate elements, and the LZZHT theories uses a mesh of 8-noded brick elements.

Results produced by the finite element model based on first order shear deformation theory are denoted FSDT [53] in the following discussion. Results from the third order, equivalent single theory of Reddy [46] are labeled HSDT, and those from the third order zig zag theories are labeled ZZHT and LZZHT. Two different meshes are used with the LZZHT finite element code, denoted as LZZHT-1, which contains one layer of elements (or one sublaminates) through the thickness of the plate, and LZZHT-3 which contains 3 layers of elements (or sublaminates) through the thickness. LZZHT-3 uses one layer of elements for each of the top and bottom face panels and one for the core.

#### 3.3.1 Layup 1:

A laminate having the lamination scheme defined in Table (3.2) was first analyzed. Figures (3.3) and (3.4) display results for center deflection normalized with respect to the elasticity solution of Burton and Noor [7] versus plate aspect ratio. Large errors are present when the plate is thick. For the equivalent single layer theories, the predicted

center deflections are accurate for aspect ratios greater than 100. FSDT results are within 4% of the elasticity solution for an aspect ratio of 100 and within 1% at  $a/h=500$  and  $a/h=1000$ . HSDT results are within 2.1% of the elasticity solution for an aspect ratio of 50 and within 1% for aspect ratios of 100 and greater. At an aspect ratio of 4, ZZHT and LZZHT-1 results are within 3.8% and LZZHT-3 results are within 2.9% of the elasticity solution. For aspect ratios greater than 4 the center deflections predicted by all three zig-zag theories are within 1% of the elasticity solution.

Figures (3.5) through (3.10) contain results from the four different theories for in-plane stresses for an aspect ratio of  $a/h=4$ . Since the core experiences very little in-plane stress, results are presented for the top face sheet only. As can be deduced from these graphs, FSDT results are the least accurate and only slight improvement is gained using the third-order HSDT theory. Both zig-zag theories predict in-plane stresses very well. LZZHT-1 and ZZHT results are comparable in accuracy to each other and are very close to the results obtained from the elasticity solution. LZZHT-3 results are the most accurate, virtually identical to the elasticity results. These results illustrate the improvement in accuracy as the mesh is refined from 1 element through the thickness in the LZZHT-1 model to 3 elements through the thickness using the LZZHT-3 model. The elements from ZZHT theory cannot be refined through the thickness.

The maximum error in  $\sigma_{xx}$  of the FSDT theory is 118% and the maximum error from the HSDT theory is 71%, (see Figure (3.5)). Both zig-zag theories predict  $\sigma_{xx}$  very well as shown in Figure (3.6). The ZZHT theory error is the largest of the zig-zag theories with a maximum of 18.5%. Maximum error of the LZZHT-1 model is 13.9%, and an error of 4.3% was found for the LZZHT-3 model.

Results for  $\sigma_{yy}$  in Figures (3.7) and (3.8) are similar to the results of  $\sigma_{xx}$ . The FSDT theory produced the least accurate results with a maximum error of 1651%. The HSDT theory maximum error was 27%. In the top ply of the face sheet the error from the LZZHT-1 model was the largest of the zig-zag theories at 9.7% followed by 7.4% error by the ZZHT theory and finally 2.3% from the LZZHT-3 model.

Figures (3.9) and (3.10) give in-plane shear stress results. The maximum error of the FSDT theory was 43%, 19% for the HSDT theory, 10% for the LZZHT-1 model, 2.5% for the ZZHT theory, and 1.4% for the LZZHT-3 model.

Transverse shear stresses are compared in Figures (3.11) and (3.12) for the case  $a/h=4$ . Only results from the zig-zag theories are compared since the ESL theories do not sufficiently model transverse stresses. As before, results from the ZZHT and LZZHT-1 models are nearly identical in accuracy. It is important for a laminate theory to provide accurate results in the core region of sandwich panels. Core layers are typically much softer than the face sheets and failure due to transverse shear effects can be predicted if accurate transverse shear stresses can be determined. Both the ZZHT and LZZHT theories provide good results in the core region of the plate with errors of 4% for the ZZHT and LZZHT-1 models and 1% for the LZZHT-3 model for  $\tau_{yz}$ . Results for  $\tau_{xz}$  in the core region are better yet with errors of 1% for the ZZHT and LZZHT-1 models and 0.3% for the LZZHT-3 model.

The maximum transverse shear occurs in the face sheets and not in the core. The maximum error in  $\tau_{yz}$  in the top face sheet was 7.1% for the LZZHT-1 model, 6.9% for the ZZHT model, and 0.2% for the LZZHT-3 model. The maximum error in  $\tau_{xz}$  for the ZZHT and LZZHT-1 models was 42% and for the LZZHT-3 model it was 12%.

Figure (3.13) through (3.20) contain in-plane stress results for the plate with an aspect ratio of  $a/h=10$ . Accuracy of the results from all models show improvement over the case with  $a/h=4$  as expected, however, results are still quite poor for the two ESL theories. The maximum error in the prediction of  $\sigma_{xx}$  for the FSDT theory was 279%, and for the HSDT theory it was 313% (see Figure (3.13)). All zigzag theories predicted  $\sigma_{xx}$  very well with a 3% error from the LZZHT-1 model, a 0.8% error from the LZZHT-3 model, and a 0.7% error from the ZZHT theory, (see Figure (3.18))

Results for  $\sigma_{yy}$ , given in Figures (3.15) and (3.16), are similar to the results of  $\sigma_{xx}$ . The maximum error in the predictions of  $\sigma_{yy}$  by the FSDT theory was 23% and for the HSDT theory it was 13%. Here again, the zigzag theories did an excellent job predicting  $\sigma_{yy}$  with a maximum error of 3% from the ZZHT and LZZHT-1 models and a maximum error of 0.7% for the LZZHT-3 model.

In-plane shear stress predictions by the FSDT model contained a maximum error of 15%, and the HSDT model's maximum error was 2.9% (see Figure (3.17)). The zigzag theories again did an excellent job predicting  $\sigma_{xy}$ . Predictions from the ZZHT model, given in Figures (3.18), contained a maximum error of 2.8%. The maximum error of the LZZHT-1 model is 0.6%, and for the LZZHT-3 model the maximum error is 0.1%.

Figures (3.19) and (3.20) contain results for transverse shear stresses  $\tau_{yz}$  and  $\tau_{xz}$  as predicted by the zigzag theories. For both stresses the maximum error occurred in the face sheets. The maximum error in the predictions of  $\tau_{yz}$  by the ZZHT model was 18%, maximum error from the LZZHT-1 model was 17%, and maximum error from the LZZHT-3 model was 4.8%. Maximum errors in  $\tau_{xz}$  are as follows: 21% for the ZZHT model, 20%

for

3.3

of

lay

sch

tha

wi

LZ

pl

w

Z

in

m

m

R

fa

ti

tra

bot

for the LZZHT-1 model, and 11% for the LZZHT-3 model.

### 3.3.2 Layup 2:

A laminate having the lamination scheme defined in Table (3.3) and an aspect ratio of  $a/h=10$  was analyzed next. Layup 2 is a non-symmetric, random layup compared to layup 1 which has fiber orientation angles of zero degrees and a symmetric lamination scheme. Figures (3.21) - (3.28) contain the results comparing stresses from the different theories for this case. The same conclusions were arrived at as were for the case of layup 1 with aspect ratio  $a/h=10$ . Results from FSDT and HSDT codes are the least accurate and LZZHT-3 the most accurate. Transverse shear stresses are very accurate through the entire plate thickness for the LZZHT-3 model. Results from the LZZHT-1 and ZZHT models were again comparable, with a maximum error of 7% for LZZHT-1 model and 6% for ZZHT compared to the elasticity solution, in the core region at the core/bottom face sheet interface for  $\tau_{yz}$ . At the top face sheet/core interface results for  $\tau_{xz}$  from the LZZHT-1 model are a maximum of 6.5% less than the elasticity solution with results from the ZZHT model being under predicted by 5.6%. This is the maximum error in the core region. Results for  $\tau_{yz}$  are very good in both face sheets. In the bottom face sheet  $\tau_{xz}$  at the interface between the bottom two plies is predicted to be 36% greater than the elasticity solution by the LZZHT-1 model and 33% greater by the ZZHT model. The maximum transverse shear stress in the core region of all cases analyzed is predicted very well by both LZZHT-1 and ZZHT theories.

### 3.3.3 Computational Efficiency

Computational efficiency of the finite element codes employing the ZZHT and LZZHT-1 models were compared since both use the same mesh and produce similar results. All theories are programmed in FORTRAN77. Both the ZZHT and LZZHT-1 models used the same mesh size (64 elements) but the ZZHT model contains only 4 nodes per element giving 28 degrees of freedom per element whereas the LZZHT models contain 8 nodes per element and 56 degrees of freedom. The mesh used with the LZZHT-3 model contained three layers of 64 elements or a total of 192 elements.

The average system time required for one run of the code employing ZZHT finite element model was 0.21 seconds while one run required 0.68 seconds using the LZZHT model. This is 224% longer than the ZZHT model. User time for the ZZHT model was 8.58 seconds but for the LZZHT-1 model user time was 383 seconds, 4,364% longer than ZZHT. The LZZHT-3 model takes slightly longer than LZZHT-1. Based on these results the most efficient of the zig zag code is the ZZHT. This code is also very accurate for in-plane stresses and transverse shear stresses in the core region. This code was used for the optimization portion of this research.

## 3.4 Conclusions

The LZZHT-3 model is the most accurate in predicting stresses in sandwich panels and FSDT is the least accurate. HSDT shows a slight improvement in accuracy over FSDT for predicting in-plane stresses, however, neither theory can predict transverse stresses. An improvement in accuracy results from these models as the aspect ratio increases. For the

cases examined the ZZHT and LZZHT-1 models produced comparable results which were also in close agreement with the elasticity solution for in-plane stresses. For transverse stresses both the ZZHT and LZZHT-1 models predicted the maximum shear stress in the core very well but were not as accurate in the face sheets. The results illustrated an increase in accuracy is obtained by increasing the number of sublaminates used through the thickness. This is possible with the LZZHT theory. Also the results obtained from analysis of layup 2 indicate the zigzag theories perform very well for unsymmetric and symmetric layups.

The ZZHT model is superior to the LZZHT-1 model in computational efficiency. The best compromise of solution accuracy and computation efficiency is given by the ZZHT finite element model, thus it will be used in the optimization portion of this research.

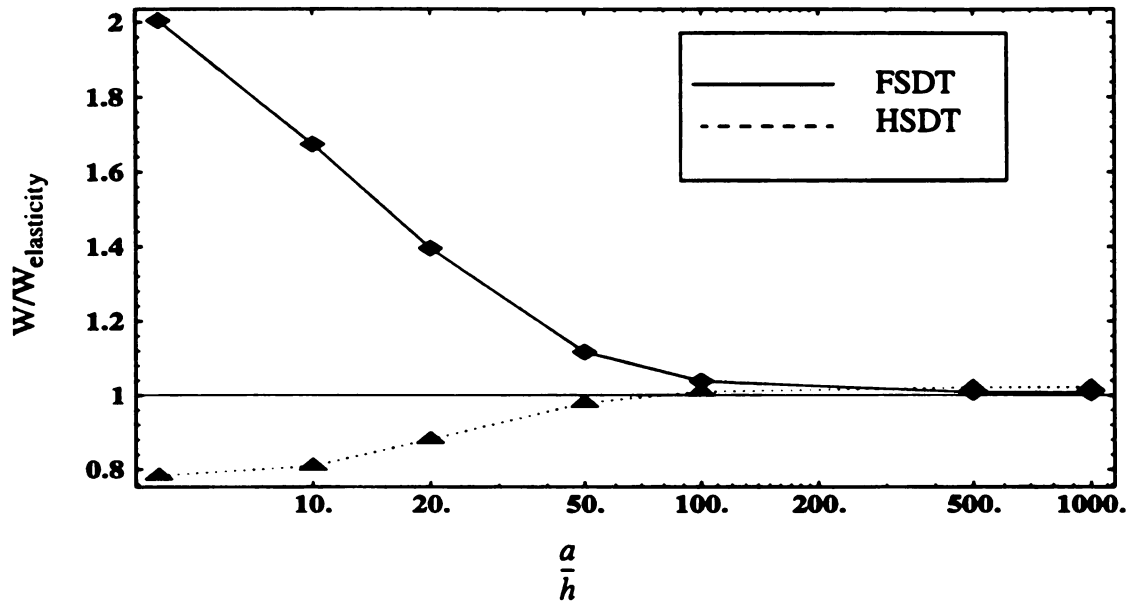


Figure (3.3) - Normalized transverse center deflection versus aspect ratio, ESL theories, layup 1.

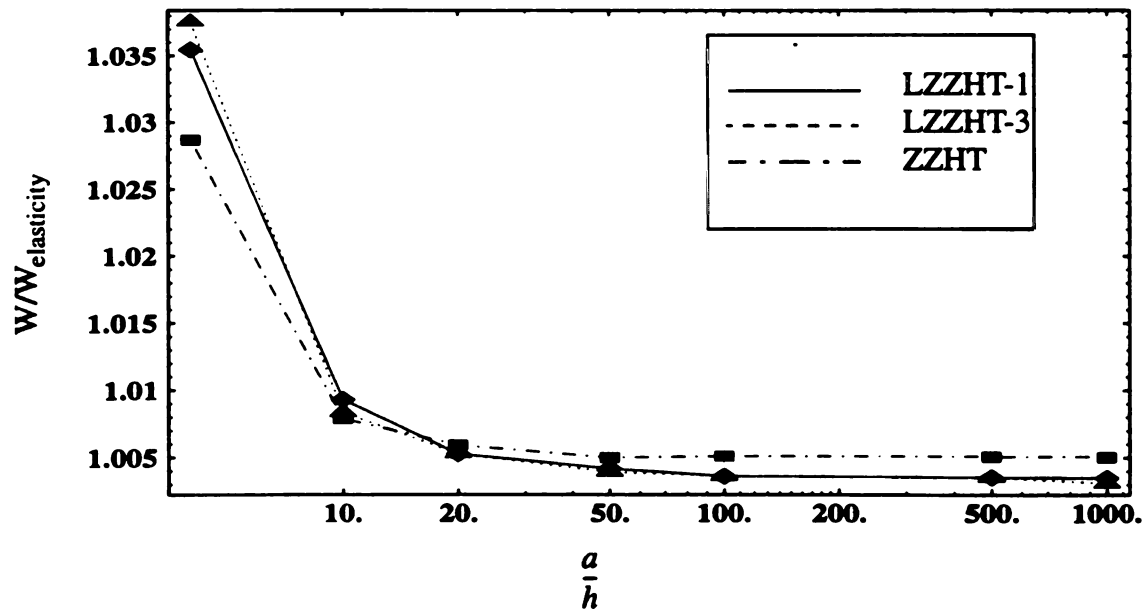


Figure (3.4) - Normalized transverse center deflection versus aspect ratio, zig zag theories, layup 1.

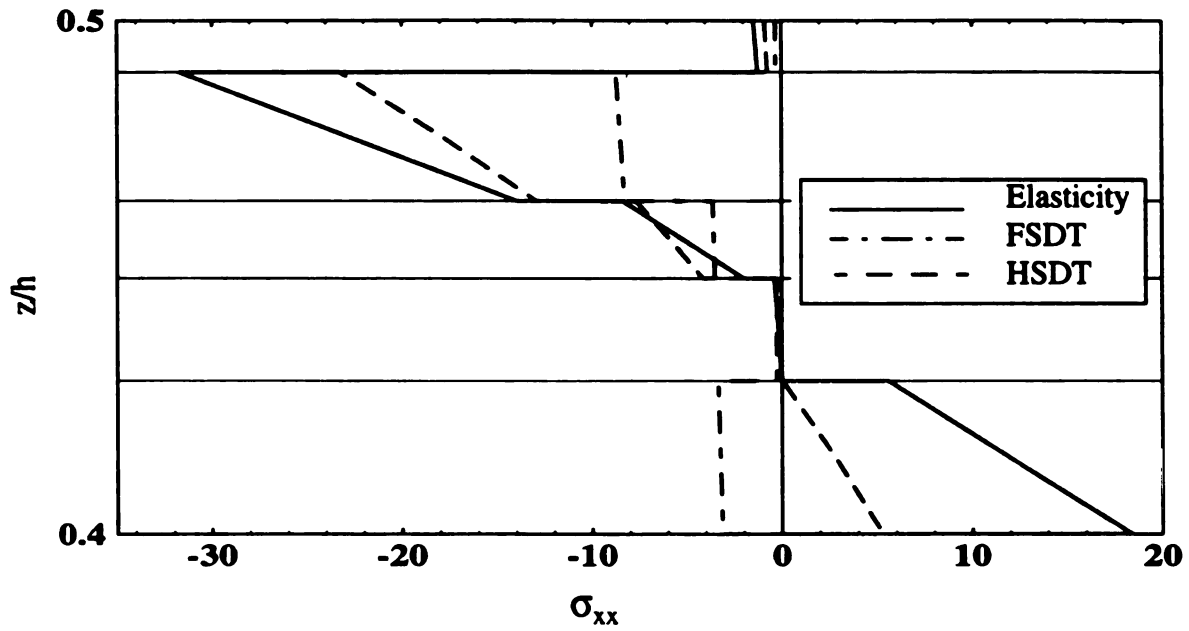


Figure (3.5) - Normal stress vs. normalized thickness for ESL theories,  $a/h=4$  layup 1.

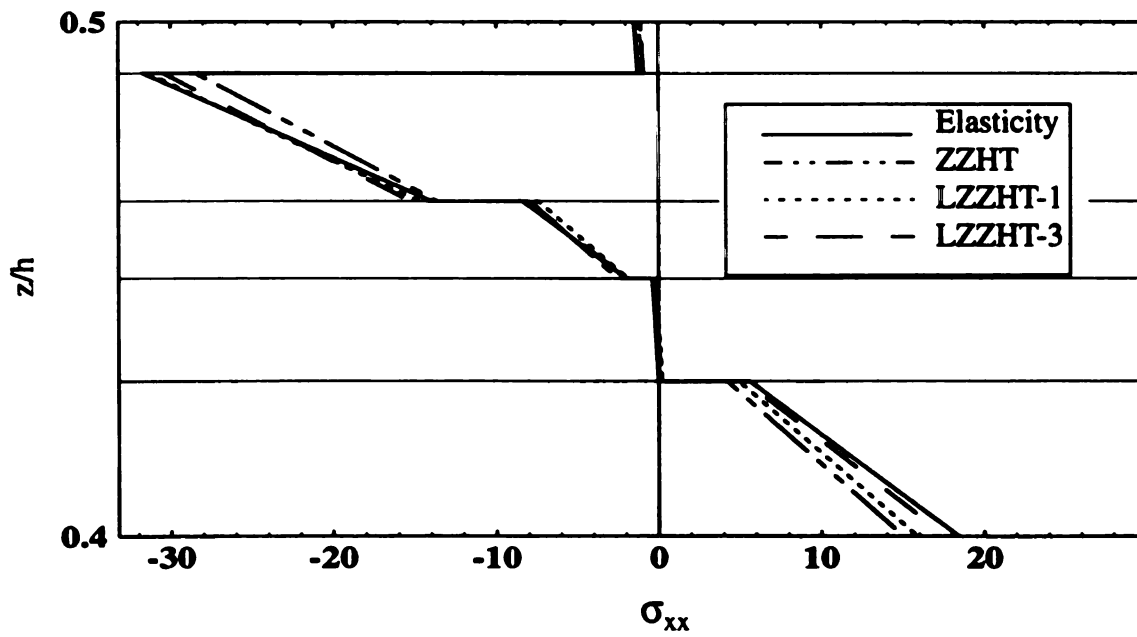


Figure (3.6) - Normal stress vs. normalized thickness for zig-zag theories,  $a/h=4$  layup 1.

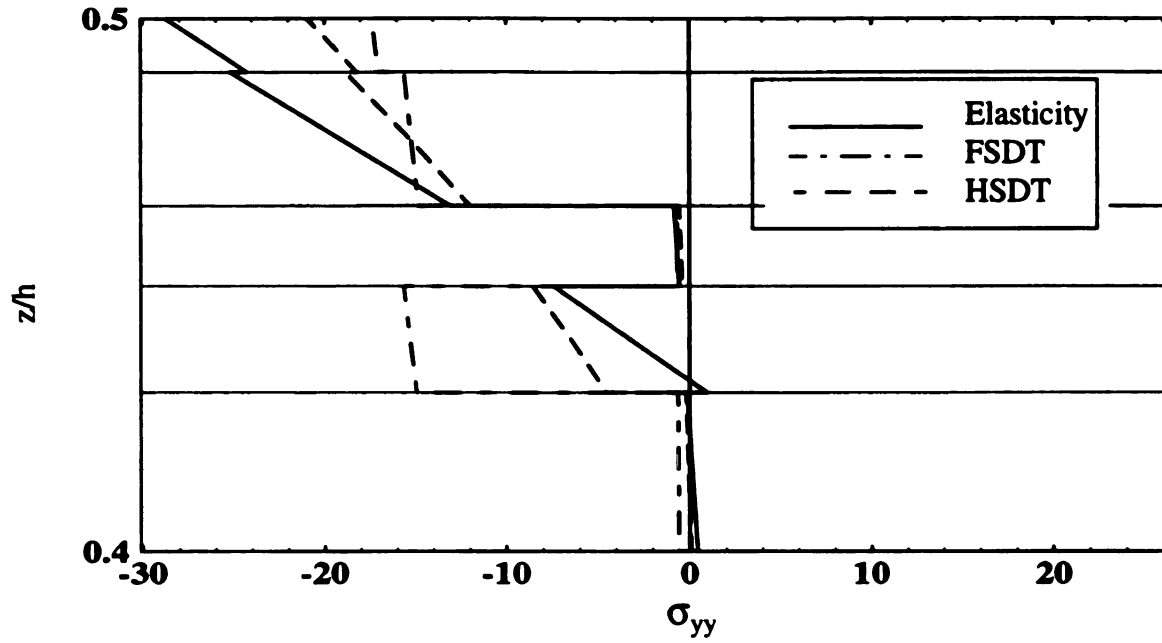


Figure (3.7) - Normal stress vs. normalized thickness for ESL theories,  $a/h=4$ , layup 1.

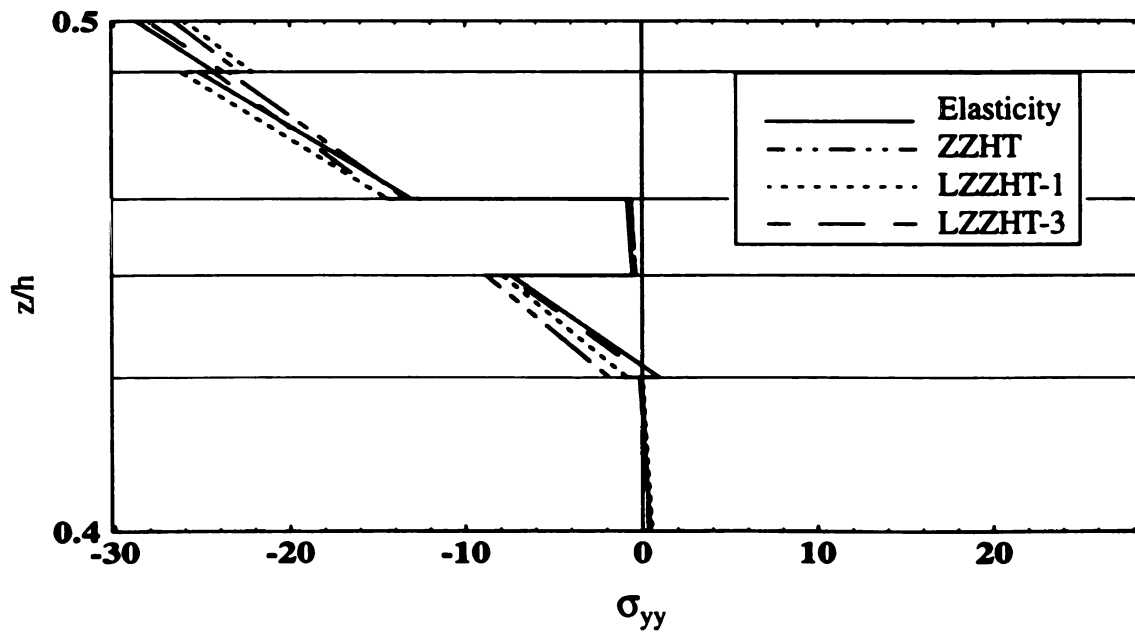


Figure (3.8) - Normal stress vs. normalized thickness for zig-zag theories,  $a/h=4$ , layup 1.

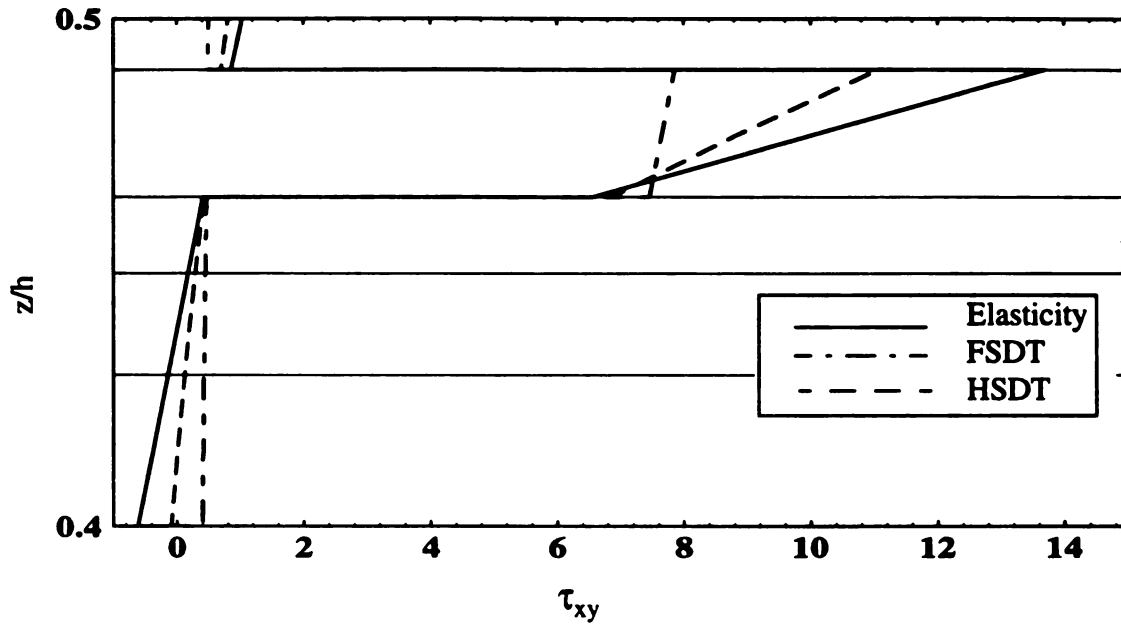


Figure (3.9) - Shear stress vs. normalized thickness for ESL theories,  $a/h=4$  layup 1.

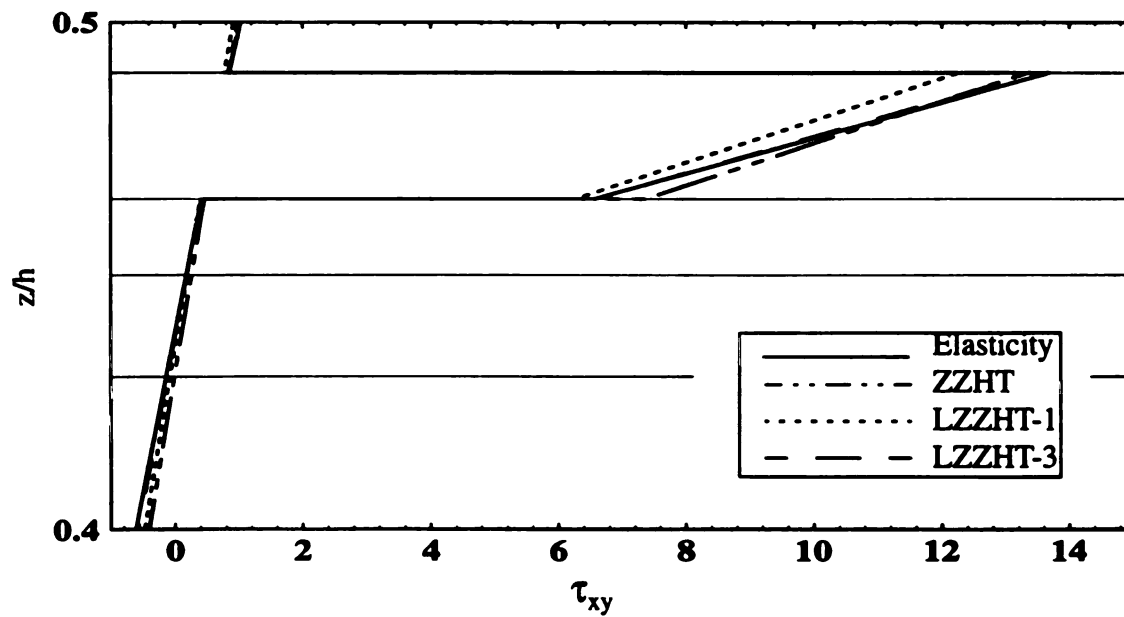


Figure (3.10) - Shear stress vs. normalized thickness for zig-zag theories,  $a/h=4$  layup 1.

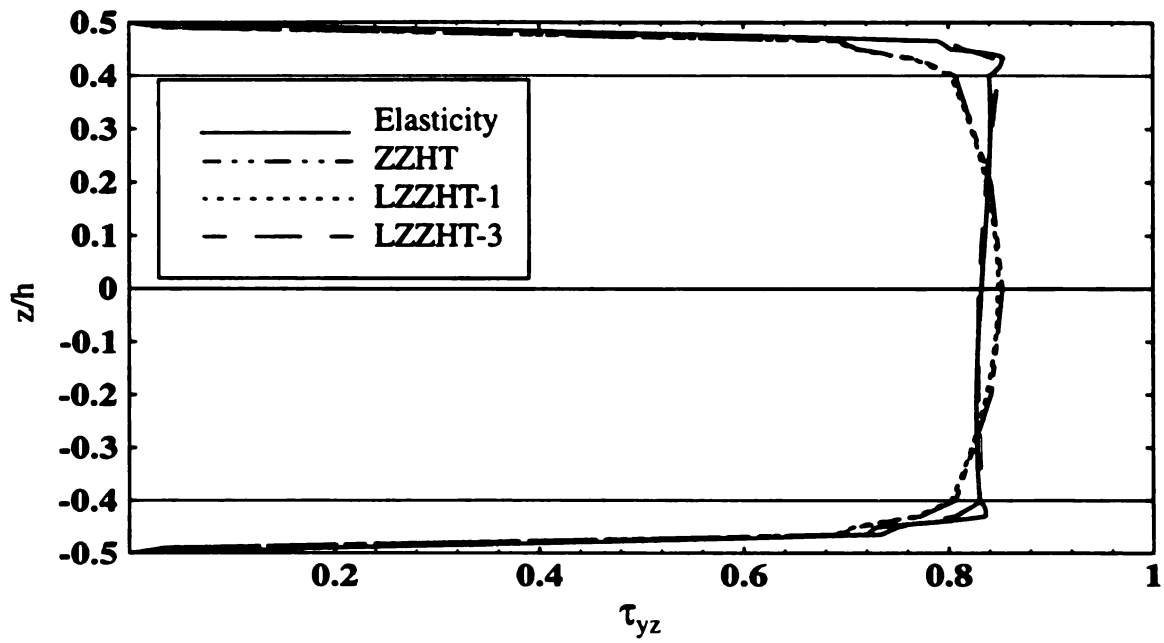


Figure (3.11) - Shear stress vs. normalized thickness for zig-zag theories,  $a/h=4$  layup 1.

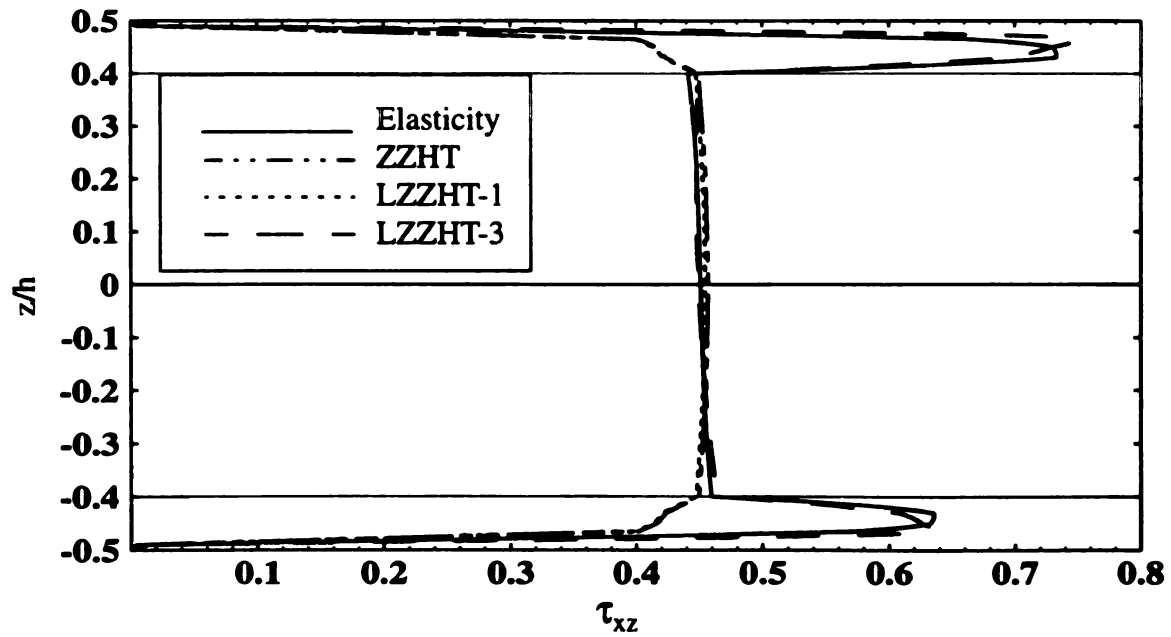


Figure (3.12) - Shear stress vs. normalized thickness for zig-zag theories,  $a/h=4$  layup 1.

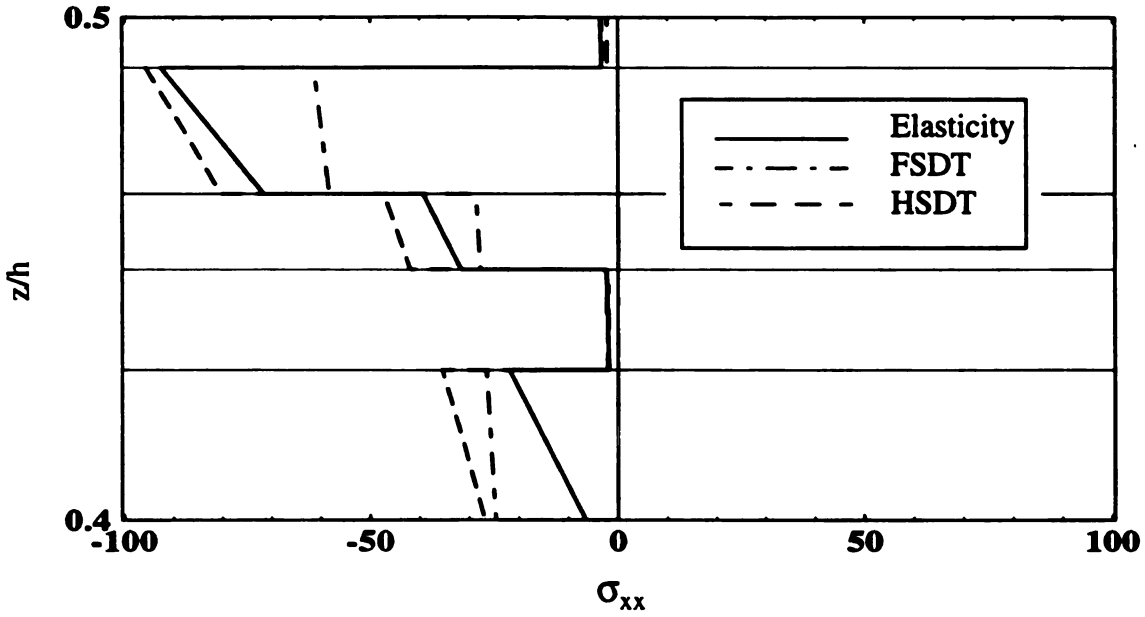


Figure (3.13) - Normal stress vs. normalized thickness for ESL theories,  $a/h=10$ , layup 1.

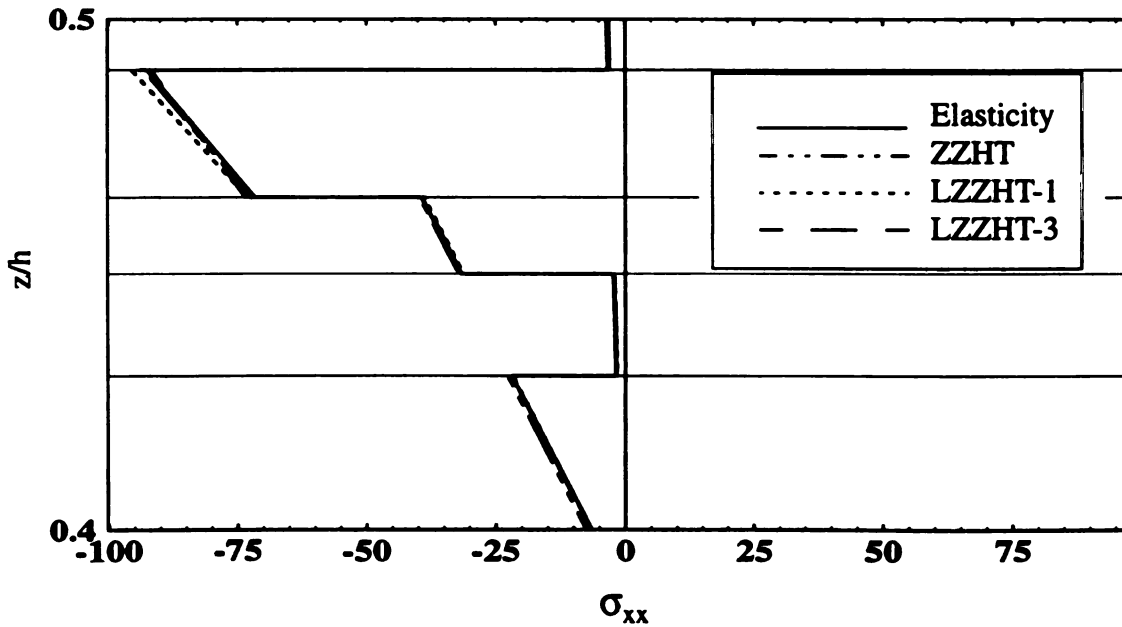


Figure (3.14) - Normal stress vs. normalized thickness for zig-zag theories,  $a/h=10$  layup 1.

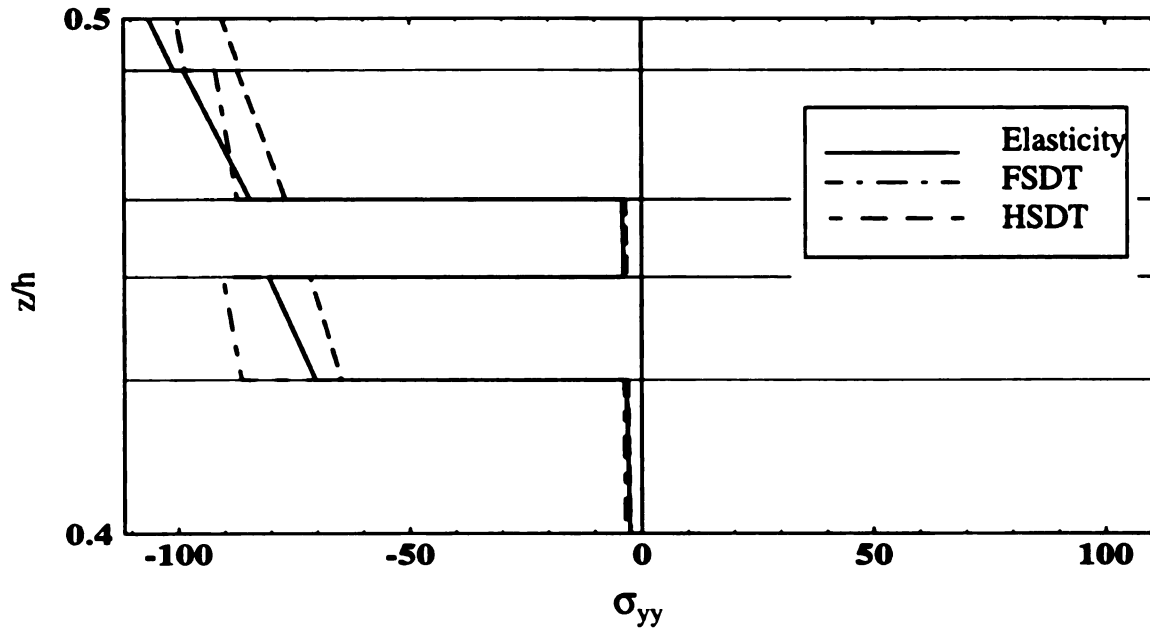


Figure (3.15) - Normal stress vs. normalized thickness for ESL theories,  $a/h=10$ , layup 1.

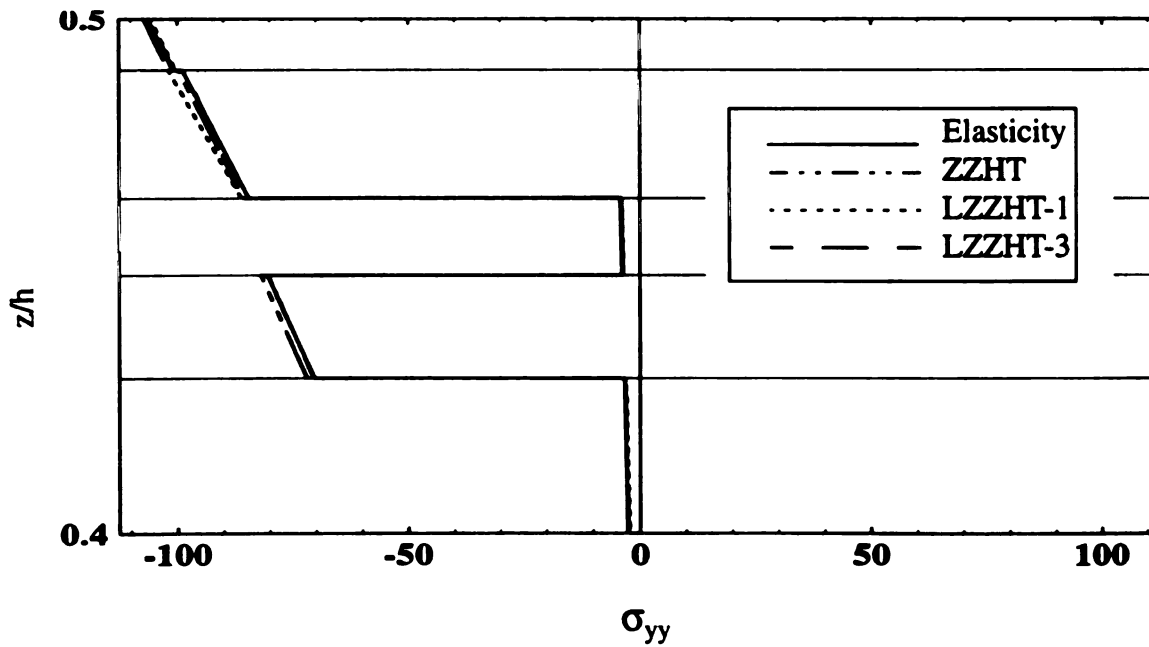


Figure (3.16) - Normal stress vs. normalized thickness for zig-zag theories,  $a/h=10$  layup 1.

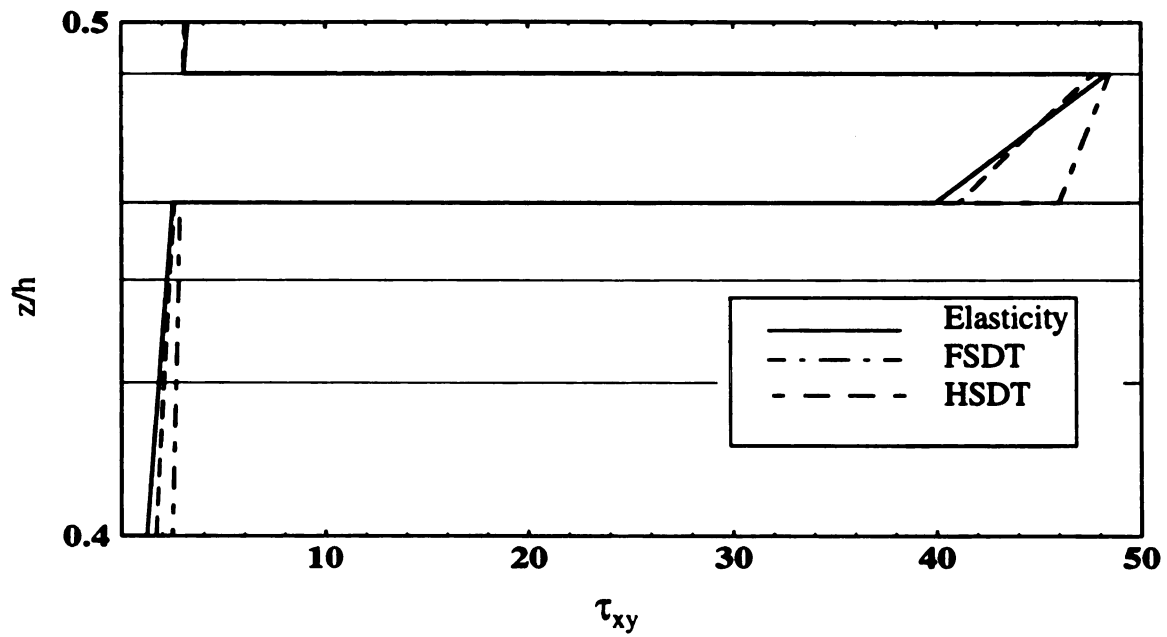


Figure (3.17) - Shear stress vs. normalized thickness for ESL theories,  $a/h=10$  layup 1.

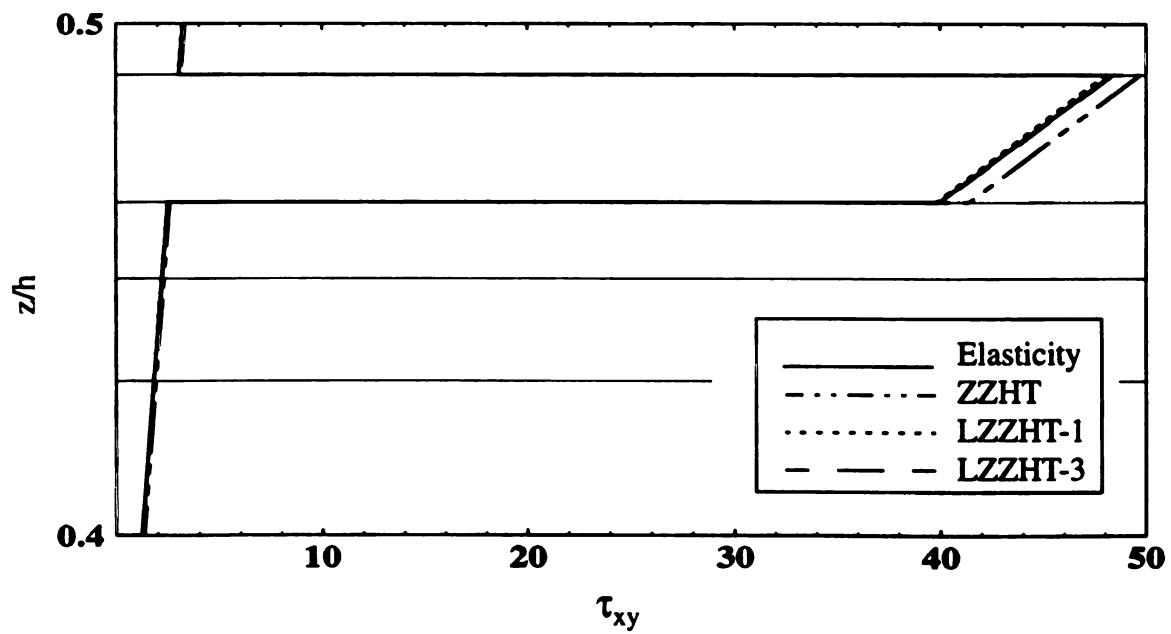


Figure (3.18) - Shear stress vs. normalized thickness for zig-zag theories,  $a/h=10$  layup 1.

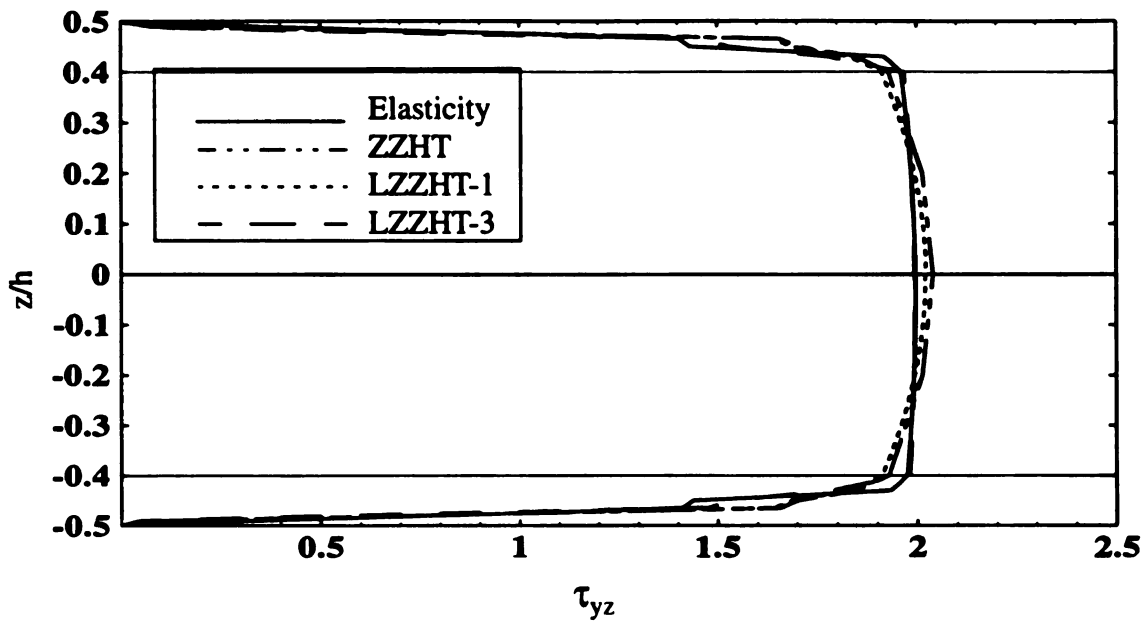


Figure (3.19) - Shear stress vs. normalized thickness for zig-zag theories,  $a/h=10$  layup 1.

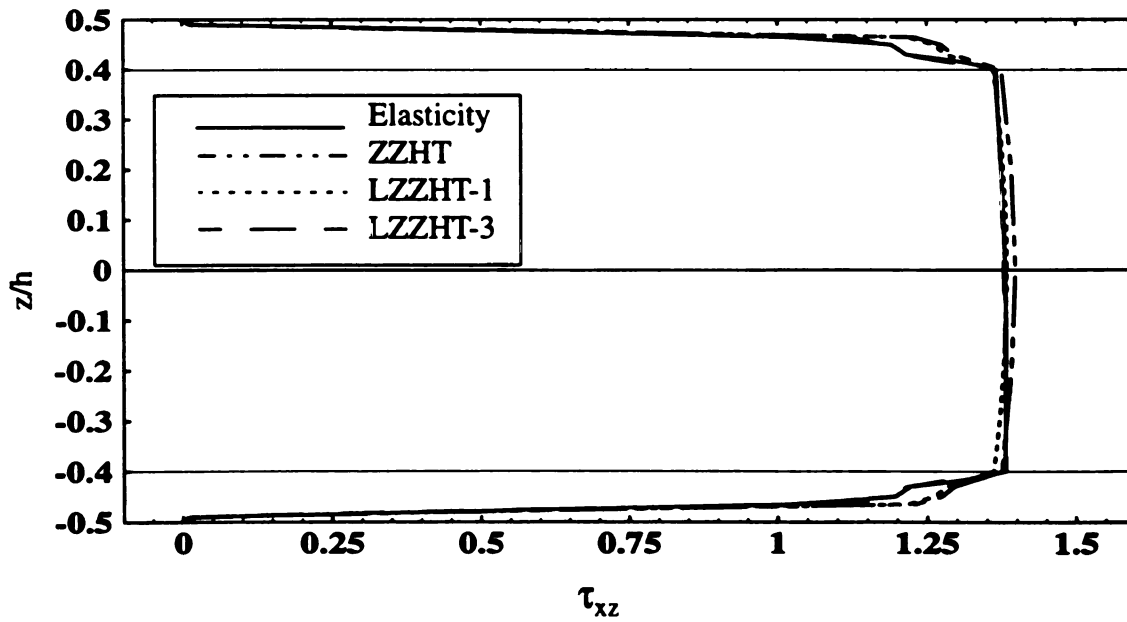


Figure (3.20) - Shear stress vs. normalized thickness for zig-zag theories,  $a/h=10$  layup 1.

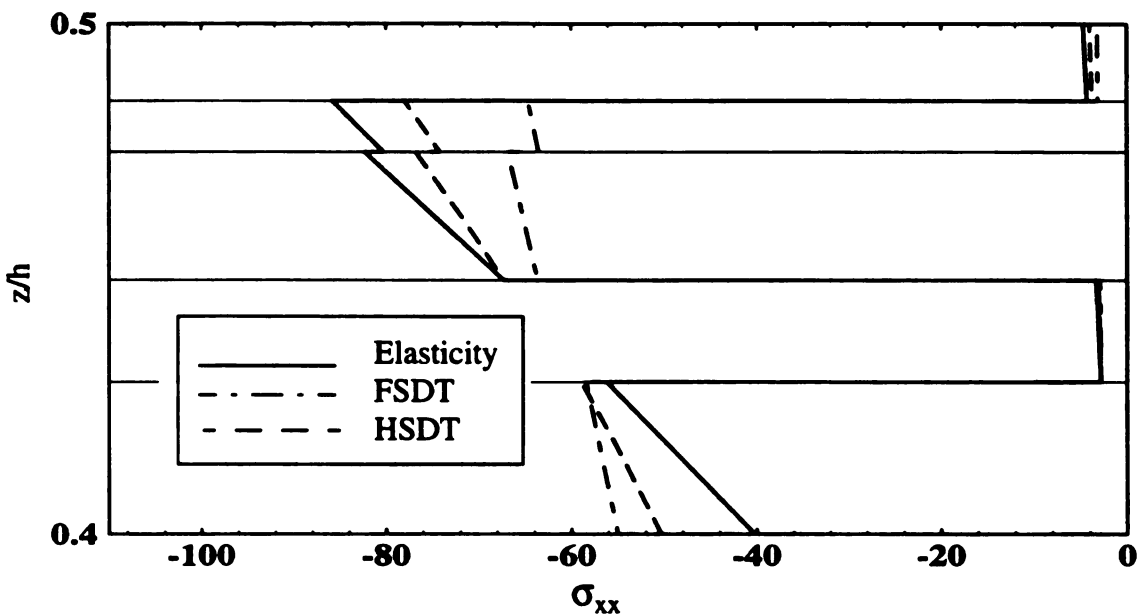


Figure (3.21) - Normal stress vs. normalized thickness for ESL theories,  $a/h=10$  layup 2.

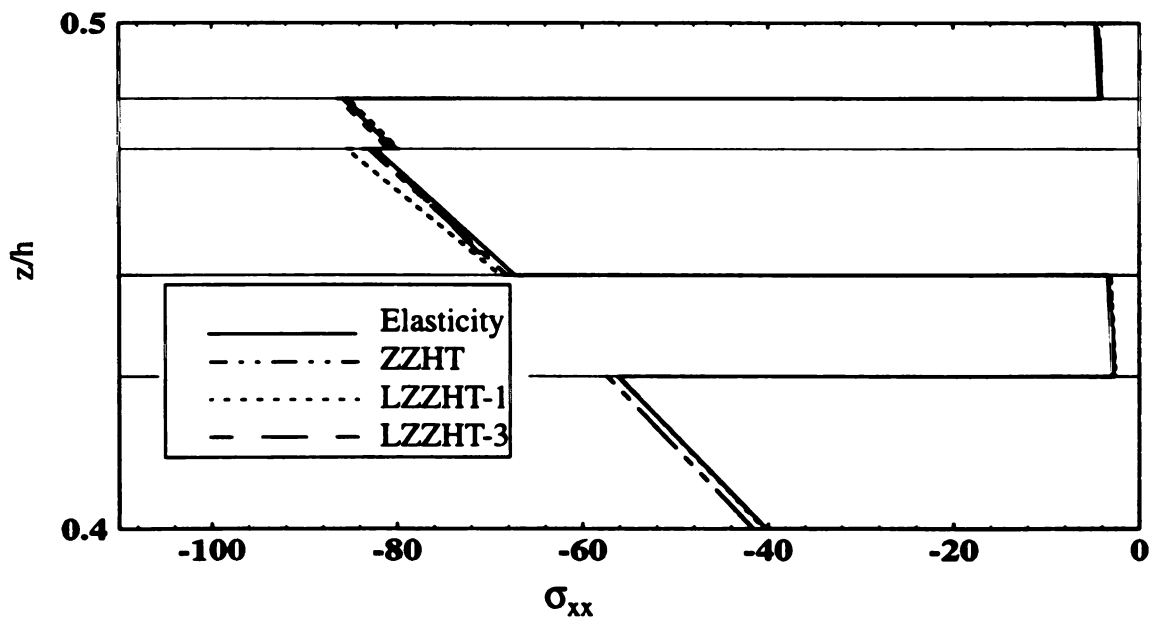


Figure (3.22) - Normal stress vs. normalized thickness for zig-zag theories,  $a/h=10$  layup 2.

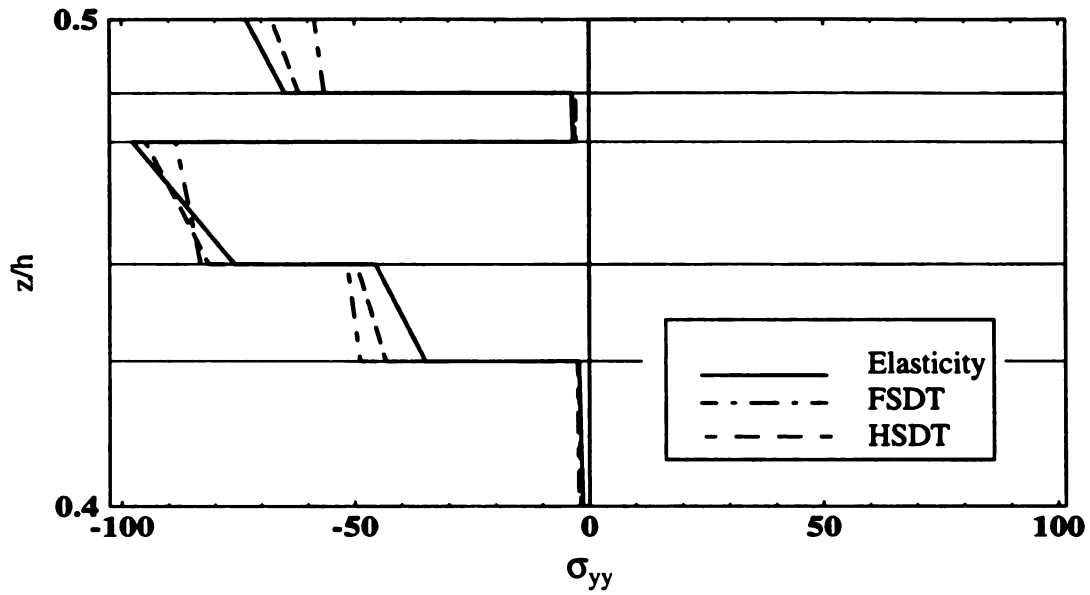


Figure (3.23) - Normal stress vs. normalized thickness for ESL theories,  $a/h=10$  layup 2.

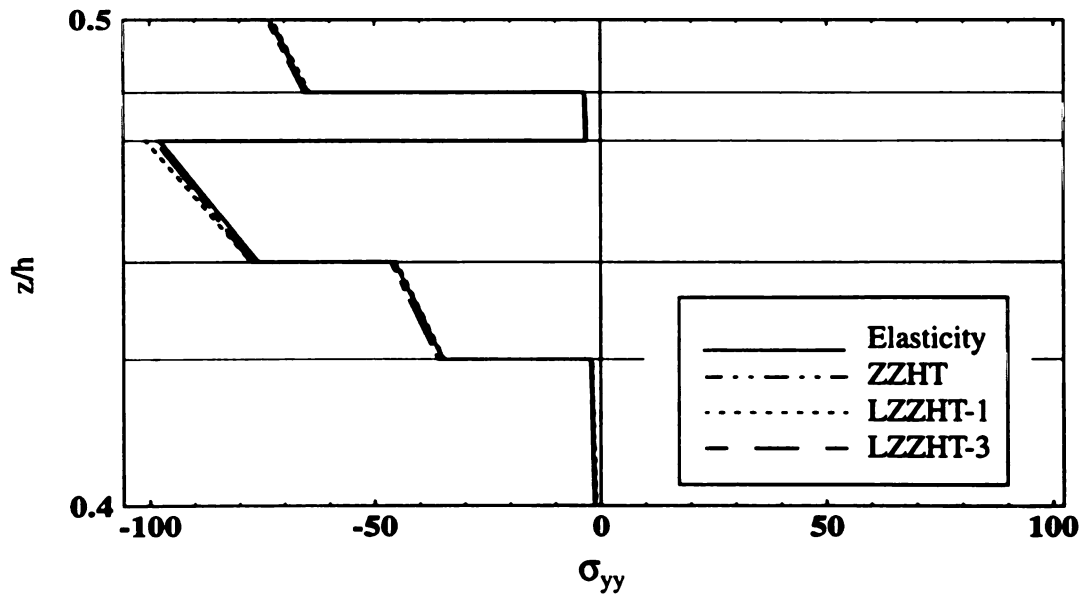


Figure (3.24) - Normal stress vs. normalized thickness for zig-zag theories,  $a/h=10$  layup 2.

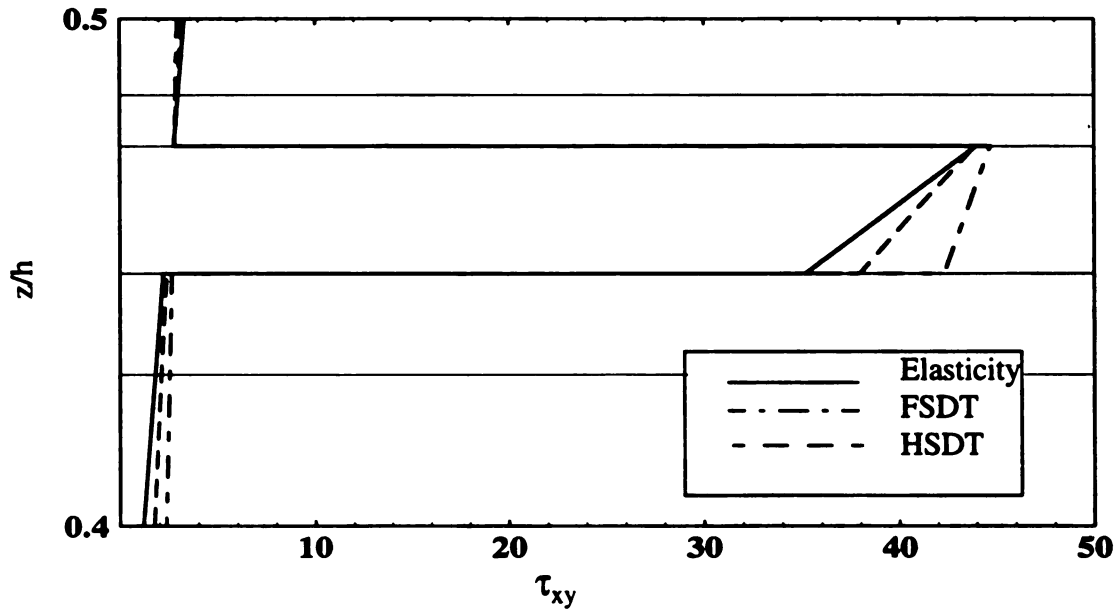


Figure (3.25) - Shear stress vs. normalized thickness for ESL theories,  $a/h=10$  layup 2.

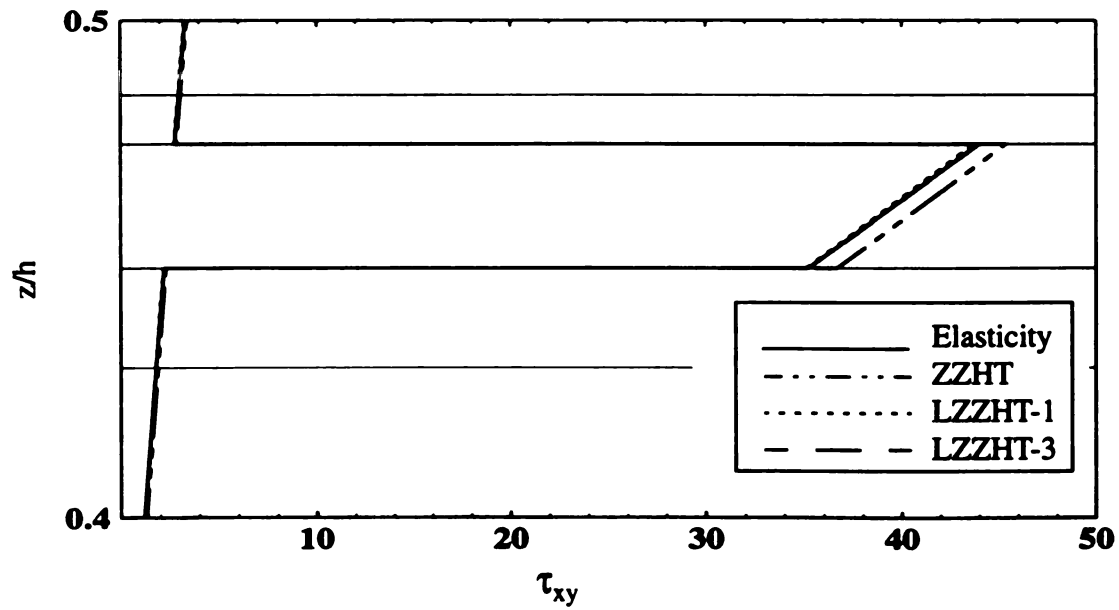


Figure (3.26) - Shear stress vs. normalized thickness for zig-zag theories,  $a/h=10$  layup 2.

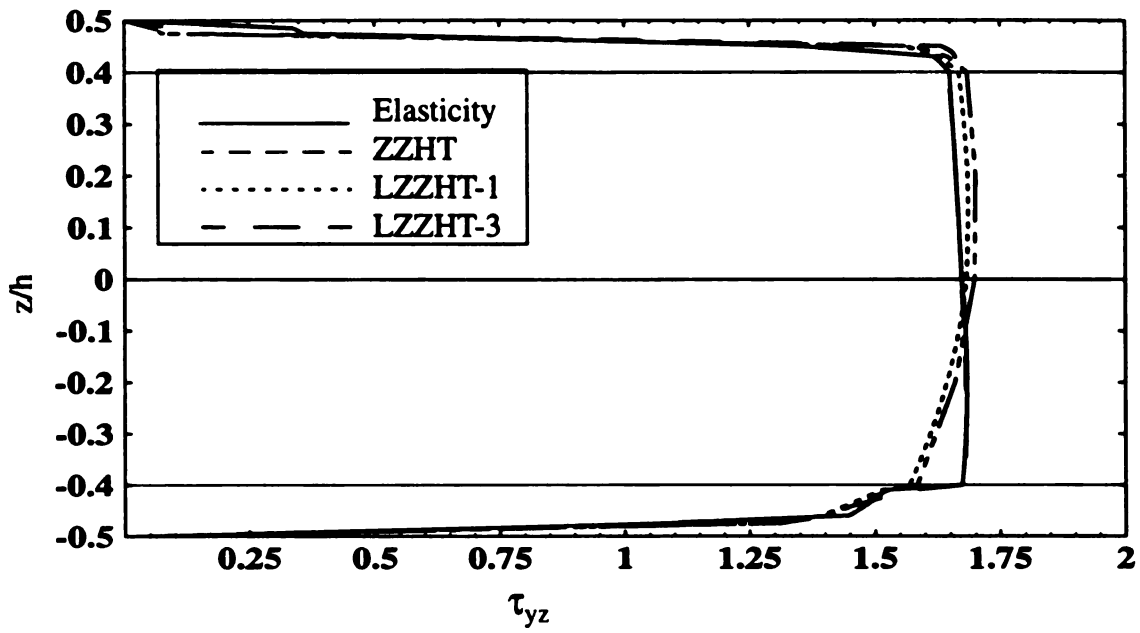


Figure (3.27) - Shear stress vs. normalized thickness for zig-zag theories,  $a/h=10$  layup 2.

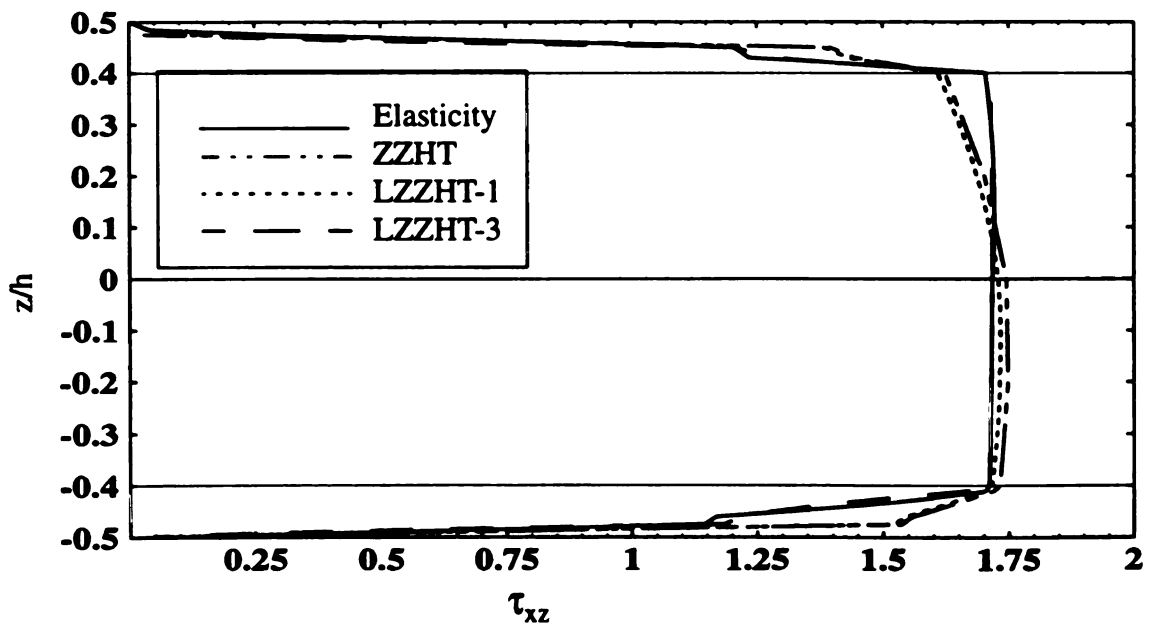


Figure (3.28) - Shear stress vs. normalized thickness for zig-zag theories,  $a/h=10$  layup 2.

## **Chapter 4**

# **Optimal Design Laminated Composite Sandwich Structures Using Genetic Algorithms.**

### **4.1 Introduction**

Laminated composite structure design lends itself quite openly to optimization techniques. Ply thickness and stacking sequence are two often optimized design variables when considering a laminate design. Numerous optimization techniques are available, one category of which is calculus-based or gradient-based methods. Gradient-based methods can be classified as either direct or indirect [16]. Both approaches rely on the gradient of the objective function providing necessary information to locate a local optimum. One obvious drawback of this method is the gradient of the function must exist and be obtainable. Also, these methods seek out local optima, which may or may not be the global optimum. Gradient based methods are clearly not well suited for finding singular optima common in optimization of laminated composite structures.

Various algorithms exist which search finite design spaces. Evaluating an objective function at all points in a given domain is obviously inefficient for large domains. Random search techniques perform a random search of the design space for optima, but are also inefficient. Directed random search techniques are a more effective means of searching a

design space. Such methods may, for example, mimic nature in their search for an optimum state. Genetic algorithms (GA) are guided random searches which utilize information obtained during the search for direction. This technique is relatively effective and robust by comparison to other methods.

Nature's means of dealing with existence and reproduction of all species is described as "survival of the fittest". Genetic algorithms draw from this phenomenon, employing a similar philosophy when searching a design space for global optima. GAs maintain one or more populations containing a number of possible designs, and perform operations of selection, reproduction, crossover, mutation, and permutation of the coded design variables.

Genetic algorithms differ intrinsically from traditional search and optimization techniques. As previously stated, traditional methods utilize derivatives whereas GAs make use of objective function data. Also, GAs work with a coded set of variables and not the actual variables as do traditional methods. Another important distinction is that GAs simultaneously search from numerous points in the design space while traditional methods search from a single point. Thus it is apparent traditional methods may locate a local maximum and not the global maximum, depending on the initiation point of the search. GAs can provide many "near optimal" designs which is advantageous to the designer. Finally, GAs are governed by stochastic rules, and traditional methods are governed by deterministic rules.

## 4.2 Previous Work

The design of composite laminates with design variables of ply thickness and fiber orientation is a common continuous optimization problem. With only these two design variables present the optimization is an integer problem which can be linearized. Branch and bound algorithms have been used to solve this type of problem once it has been linearized as done by Haftka et al. [33]. In their study results for optimization of stacking sequence obtained via branch and bound methods were found to be within 0.5% of those found using GAs. Genetic algorithms can optimize nonlinear problems without the need for linearization. Inclusion of frequency and strength constraints, such as in buckling load optimization problems, leads to a nonlinear problem.

Haftka et al. [24, 25, 27, 33, 39] have used GAs for determining an optimum laminate stacking sequence which minimizes laminate thickness or weight subject to strength, buckling, and ply contiguity constraints. In these studies, balanced, symmetric, simply supported laminates comprised of 0, +/-45, and 90 degree plies of equal thickness were subject to in-plane biaxial loading. To improve efficiency of the algorithm Haftka et al. [24, 25, 27] utilized a genetic algorithm with memory, storing useful information about past designs in a *binary tree*. Use of binary tree storage was shown to reduce the number of analyses required by 30-40%. Another attempt at improved efficiency was a procedure called local improvement which utilized information stored in the binary tree [24, 25].

GAs are gaining popularity and becoming more frequently used in a variety of optimization problems. Applications include minimizing the weight of a stiffened composite laminate with a hole [34], optimizing elastic support locations on a square plate to

maximize the first system eigenvalues [19], optimizing a simple truss structure capable of supporting given forces [28], optimizing the cross-section and minimizing the weight of an automobile bumper and minimizing the weight of an automobile body panel with stress and deflection constraints [46], and optimizing the placement of accouters on large space structures [13].

Previously work has been done by Punch et al. [39] on laminated composite beams. The objective was to design the beam for maximum energy absorption, such as is required for tank armor or automobile bumpers. This study reported work designing a 24-layer beam made of graphite-epoxy composite layers with clamped-clamped end conditions and an applied point load at midspan. A thin layer (about 5.5% of the nominal ply thickness) is placed at the top of each composite layer, so there are actually 48 layers in the model. Each thin layer may be assigned the same material properties as the layer immediately below it, or it may be assumed that the thin layer is compliant, with stiffness properties three orders of magnitude less than the composite layers. The length-to-thickness ratio of the beam is 50. The length of the beam is divided into 20 subsections (finite elements), so there are  $20 \times 48 = 960$  design elements. The GA must decide whether to place a 0 degree ply (henceforth called material 1) or a 90 degree ply (henceforth called material 2) in each of the 480 structural ply design elements, and whether or not to place a compliant material in each of the 480 thin layer design elements.

In this application, a number of representations were used but the focus was on a 480-bit-string version which fully represents one half of the beam, and which was then mirrored across the vertical centerline to create a full beam. Thus the search space examined by the GA was  $2^{480}$ , representing all possible combinations of material and compliant

material. The results of this work were quite promising. The GA generated a number of unique designs, including designs with “cantilever” beams of compliant layers.

In aerospace structures, the use of laminated composite materials offers many advantages over conventional materials such as aluminum. One particular advantage is the ability to tailor the lamination scheme (or ply stacking sequence) to achieve desired structural response to a given loading situation. For example, during certain maneuvers, an aircraft wing may be subjected to aerodynamic loadings which cause the wing to twist in an aerodynamically undesirable manner. By taking advantage of the stretching-bending-twisting coupling of laminated composite materials, more desirable responses to such loads are possible.

During flight, aircraft wings experience aerodynamic loadings which cause bending and twisting to occur. The twisting load is due to a pressure differential across the airfoil in which pressure is greater at the leading edge than at the trailing edge. Many aircraft are designed and built with up to five degrees of initial wing twist or washout. Washout means the plane of the wing twists forward as it extends from the fuselage. This helps compensate for gust loads the wing experiences causing the wing to twist up and back, adversely affecting lift. Washout is built into an aircraft to reshape the spanwise lift distribution to approximate an ellipse and to prevent tip stall [41]. At a given lift coefficient the lift distribution can be optimized by correct choice of initial wing twist. In this study, for a given load, a desired wing twist which is opposite in direction from that caused by aerodynamic loads is sought. This can be achieved using composite sandwich structures in which inherent bending-twisting coupling allows tailoring of the twisting response.

### 4.3 Model Description

The model used is a rectangular, cantilever sandwich panel, intended as an idealized aircraft wing, see Figure (4.1). So as not to detract attention from the main objective of the current research, no attempt was made to exactly model actual aircraft wing loadings or geometry.

#### 4.3.1 Loading

The intent was to choose a loading which produced a bending and twisting response in the rectangular sandwich panel roughly similar to that of an aircraft wing while in service. This type of loading allows illustration of the ability to achieve a desired twist in a rectangular sandwich plate by optimizing the plate configuration via use of genetic algorithms. In the spanwise direction an elliptic lift distribution was used with the maximum load being at the wing root as illustrated in Figure (4.1)c. This is considered a good approximation of actual loading [18, 40, 41, 45, 49] in the spanwise direction. In the chordwise direction the lift distribution depends on numerous factors such as airfoil shape and angle of attack. A load decreasing linearly from leading to trailing edge was used (see Figure (4.1) b) since this type of loading will produce a twisting response in the wing similar to the response produced by actual wing loading, as desired. The total lift distribution is given in Equation (4.1).

$$P(x, y) = q_1(x)q_2(y) = P_0 \left(1 - \frac{y}{c}\right) \left(1 - \frac{x^2}{a^2}\right)^{1/2} \quad (4.1)$$

$P_0$  was determined so as to give the desired total loading on the wing.

To determine the actual wing loading the aircraft weight was assumed to be 13,349 N (3,000 lbf) and a design factor of 3.5g was used, where g is the acceleration due to gravity. Thus the load each wing must carry is  $W_s=23,362$  N, which is 1/2 the total design weight.  $P_0$  can now be determined by integrating Equation (4.1) as follows:

$$W_s = \int_0^a \int_0^c P_0 \left(1 - \frac{y}{c}\right) \left(1 - \frac{x^2}{a^2}\right)^{1/2} dy dx \quad (4.2)$$

and since  $W_s$  is known,  $P_0$  is found to be:

$$P_0 = \frac{8W_s}{ca\pi} = 13,021 N \quad (4.3)$$

#### 4.3.2 Geometry

The intent was not to exactly model the geometry of an aircraft wing but to use as a gage the gross dimensions of typical aircraft wings. Dimensions of the sandwich panel were chosen based on historical data provided by Raymer [41]. Wing aspect ratio, as used in industry, is defined as the ratio of wing span (s) to chord length (c), with wing span being the total tip to tip dimension of the wing. Typical wing aspect ratios are 7.5 for jet transport aircraft, 7.6 for single engine aircraft, 7.8 for twin engine aircraft, and as high as 9.2 for twin turboprop aircraft. Tail aspect ratios range from 6-10 for sail planes, 3-4 for fighter aircraft, and 3-5 for other aircraft.

The wing dimensions used in this study were chosen to be similar to common,

non-commercial aircraft. The wingspan was considered to be 9.75 meters (32 ft) with an aspect ratio  $s/c=8$ , or for one wing an aspect ratio  $s/2c=4$ . Fuselage width, assumed to be 0.122 meters (4 ft), was subtracted from the wing span dimension thus making the dimensions of one wing  $a=4.27$  meters (14 ft) by  $c=1.07$  meters (3.51 ft), where  $a$  is the length of the single wing (see Figure (4.2)).

The National Advisory Committee for Aeronautics (NACA), which is the

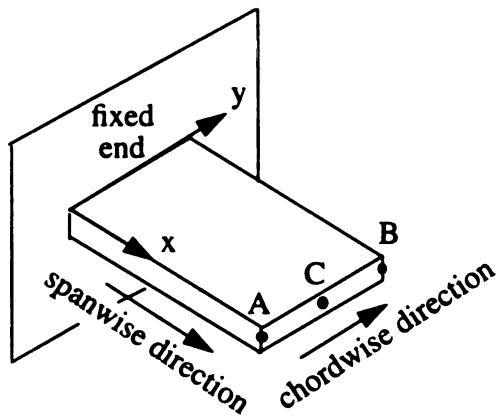


Figure (4.1) - (a) Elliptical spanwise load distribution approximation.

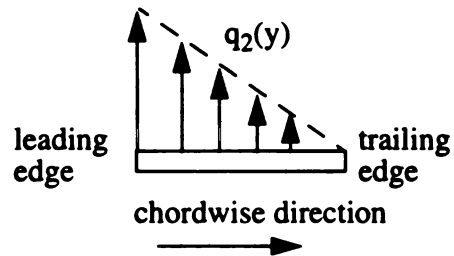


Figure (4.1) - (b) Linear chordwise load distribution approximation.

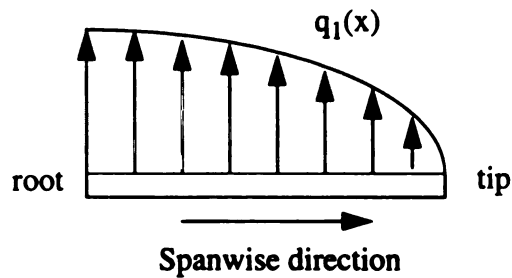


Figure (4.1) - (c) Elliptical spanwise load distribution approximation.

precursor to NASA, devised various numbering schemes for airfoil classification. The first was a four digit system which was developed around 1932 [18]. An example of an airfoil using this classification is the NACA2412. Five digit and other classification systems arose in the late 1930s for representation of more complicated airfoils. These numbering schemes contain information about an airfoil's shape such as thickness to chord ratio. The NACA65<sub>2</sub>-415 airfoil is of the same series first used for the P-51 Mustang aircraft [45]. As is indicated by the last two digits in the code, this airfoil has a thickness to chord ratio of 0.15. This is the ratio of thickness to chord used for the sandwich panel in this study, and for this thickness to chord ratio the corresponding actual thickness of the wing is  $t=0.1605\text{m}$ , see Figure (4.2).

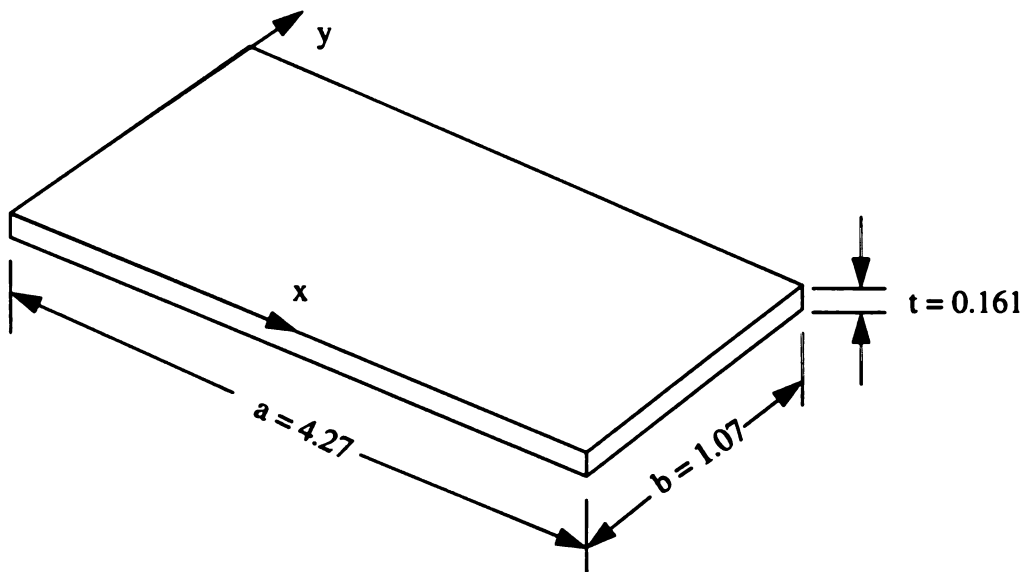


Figure (4.2) - Sandwich panel dimensions in meters.

### 4.3.3 Material Properties

The wing consists of a sandwich panel comprised of two materials. Material properties are contained in Table (4.1). The outer reinforcing layers have the properties of an orthotropic graphite/epoxy material and the core region exhibits the properties of an aluminum honeycomb material consistent with the theory of Gibson and Ashby [15].

**Table (4.1) Sandwich Panel Material Properties.**

Property	Material 1 (face sheets)	Material 2 (core)
$E_{11}$ (Pa)	0.1390E+12	0.1587E+06
$E_{22}$ (Pa)	0.9860E+10	0.1587E+06
$E_{33}$ (Pa)	0.9860E+10	0.6900E+09
$\nu_{12}$	0.300E+00	0.9900E+00
$\nu_{23}$	0.373E+00	0.000E+00
$\nu_{13}$	0.2128E-01	0.300e+00
$G_{12}$ (Pa)	0.5240E+10	0.3933E+05
$G_{23}$ (Pa)	0.3250E+10	0.1500E+09
$G_{13}$ (Pa)	0.5240E+10	0.1500E+09

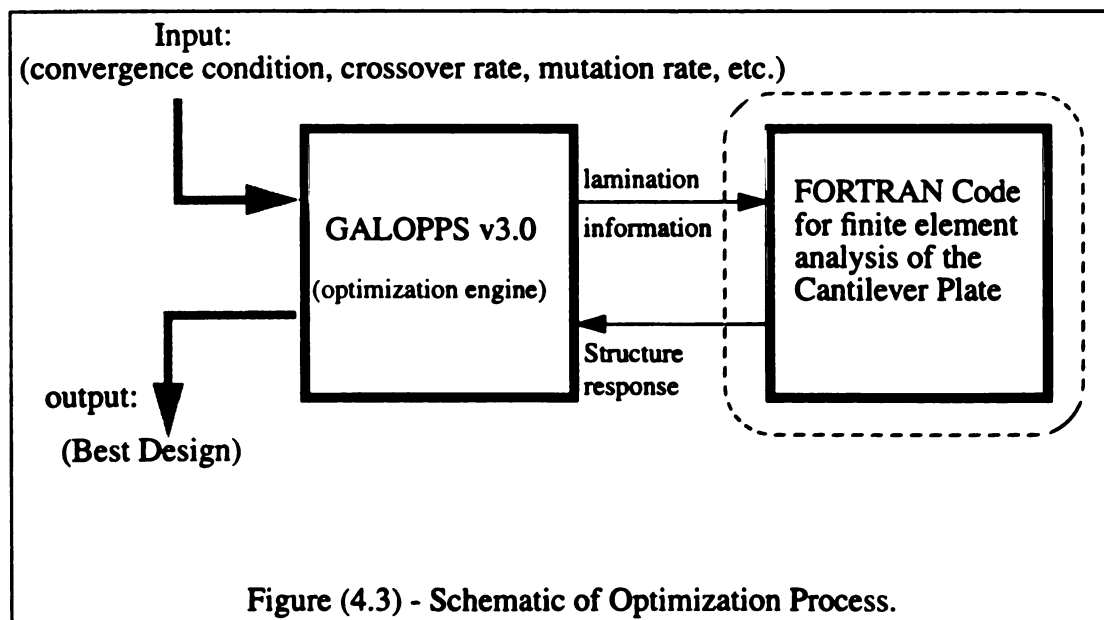
## 4.4 Optimization Problem

Structural optimization problems have been around for centuries. In aerospace applications the goal of structural optimization is to minimize structure weight while

maintaining sufficient structural integrity. Various works on optimization of laminated composite plates have been published (see for example [2, 3, 23, 25, 27, 34, 35, 50]). Nearly all these cases require the laminates to be symmetric. In the current research, no such restrictions are placed on the layup.

In the current research, a rectangular laminated composite sandwich panel (see Figure (4.1)) serves as an idealization of an aircraft wing and the lamination scheme is sought which minimizes weight, maximizes in-plane stiffness, and achieves a desired twisting response of the wing. To obtain an optimal design the genetic algorithm GALOPPS, developed by Eric Goodman at Michigan State University, is used in conjunction with the finite element code employing the ZZHT theory discussed in Chapters 2 and 3 (see Figure (4.3)). This finite element code provides the necessary displacements and stresses for each design.

This optimization problem is presented as a maximization. This is necessary for



problems optimized by genetic algorithms which seek the design having a maximum fitness. However, all optimization problems can be posed in both ways (as a maximization or minimization) [17]. The optimization problem in the current research is classified as a constrained multicriterion optimization problem which is posed as follows:

$$\begin{aligned}
 & \text{maximize} \left( f(\bar{x}) = 4000 - \sum_n^N c_n f_n(\bar{x}) - \sum_i^I P_i(\bar{x}) \right) \\
 & \text{subject to} \\
 & 0 \leq x_1 \leq 16, \quad 0 \leq x_2 \leq 16, \\
 & -\frac{\pi}{2} \leq x_3 \leq \frac{\pi}{2}, \quad 0.148m \leq x_4 \leq 0.169m, \\
 & \text{and} \\
 & \sigma_{1,max} < \sigma_1^{iu} = 1.24 \times 10^9 Pa \\
 & \sigma_{2,max} < \sigma_2^{iu} = 4.1 \times 10^7 Pa
 \end{aligned} \tag{4.4}$$

where  $f$  is the fitness,  $c_n$  are weighting coefficients,  $f_n$  are design objectives,  $x$  are the design variables,  $P_i$  are penalty functions,  $\sigma_{1,max}$  is the maximum stress in the fiber direction, and  $\sigma_{2,max}$  is the maximum stress in the transverse direction. Values for  $c_n$  are given in Table (4.2). The design variables in Equation (4.1) are as follows:  $x_1$  and  $x_2$  are the number of layers in the top and bottom face sheets, respectively,  $x_3$  is the fiber orientation angle, and  $x_4$  is the core thickness.

**Table (4.2) Weighting Coefficient Values.**

c1	c2	c3	d1	d2	d3	k2	k3
50	50	-1000	10	20	100	500	1000

The design objectives  $f_n$  in Equation (4.4) are comprised of wing twist, weight, and in-plane stiffness as follows:

$$f_1(\tilde{x}) = \left( \frac{W_{baseline}}{W(\tilde{x})} \right)^2 \quad (4.5)$$

$$f_2(\tilde{x}) = \left( \frac{a(\tilde{x})}{a_{baseline}} \right)^2 \quad (4.6)$$

$$f_3(\tilde{x}) = \left( \frac{t(\tilde{x}) - t_{desired}}{t_{desired}} \right)^2 \quad (4.7)$$

where  $W$  is the panel weight,  $a$  is the minimum of the two in-plane stiffness values,  $A_{11}$  and  $A_{22}$  from the extensional stiffness matrix, and  $t$  is the wing twist. These three quantities are normalized by values obtained from a baseline case. This normalization provides the same order of magnitude for each design objective. The baseline case consisted of a symmetric sandwich panel having face sheets oriented such to produce a specially orthotropic laminate. The lamination scheme for both the top and bottom face sheets was  $[0/90/+45/-45]_s$  and the core thickness was 0.158 meters.

The wing twist is defined as:

$$t(\tilde{x}) = (w_A - w_B) \quad (4.8)$$

where  $w_A$  and  $w_B$  are transverse deflections of the tip at the leading edge and trailing edge (see Figure (4.1)). The desired twist,  $t_{desired}$ , was chosen based on the twist of the baseline panel which was 0.007 meters. The intent was to achieve a twist of -4 times the baseline twist or  $t_{desired} = -0.028$  m, which gives an angle of  $-1.5^\circ$  with respect to the horizontal. Negative twist indicates the leading edge of the wing will deflect less vertically upward than the trailing edge indicating the wing is twisting in the direction opposite that caused by the aerodynamic loading.

The normalizing values used in Equations (4.5) and (4.6) are the weight and in-plane stiffness, respectively, of the baseline sandwich panel. For the baseline laminate  $W_{baseline} = 60.03$  kg, and  $a_{baseline} = A_{11} = A_{22} = 1.223E+08$  Pa.

Second-order polynomials were found to work best for representation of design objectives in the fitness function. To achieve the desired amount of twist a quadratic function was used to represent the normalized difference in twist. The vertex of the function is located at the desired twist value thus driving the twist toward the desired value by rewarding the fitness of the designs whose twist is near the desired value. As a matter of consistency, quadratic functions were used for the normalized weight and in-plane stiffness objectives of Equations (4.5) and (4.6), respectively.

Fitness is penalized when stress levels in a design exceed the material strengths in

the fiber and transverse directions. A penalty is also applied to the fitness for exceeding the given maximum deflection. The penalty functions,  $P_i$ , in Equation (4.4) are as follows:

$$P_1(\tilde{x}) = \begin{cases} 0.0 & (w_c \leq w_0) \\ d_1 \left[ \frac{w_c(\tilde{x}) - w_0}{w_0} \right]^2 & \textit{otherwise} \end{cases} \quad (4.9)$$

$$P_2(\tilde{x}) = \begin{cases} 0.0 & (\sigma_{1,max} \leq \sigma_1^{iu}) \\ k_2 + d_2 \left[ \frac{\sigma_{1,max}(\tilde{x}) - \sigma_1^{iu}}{\sigma_1^{iu}} \right]^2 & \textit{otherwise} \end{cases} \quad (4.10)$$

$$P_3(\tilde{x}) = \begin{cases} 0.0 & (\sigma_{2,max} \leq \sigma_2^{iu}) \\ k_3 + d_3 \left[ \frac{\sigma_{2,max}(\tilde{x}) - \sigma_2^{iu}}{\sigma_2^{iu}} \right]^2 & \textit{otherwise} \end{cases} \quad (4.11)$$

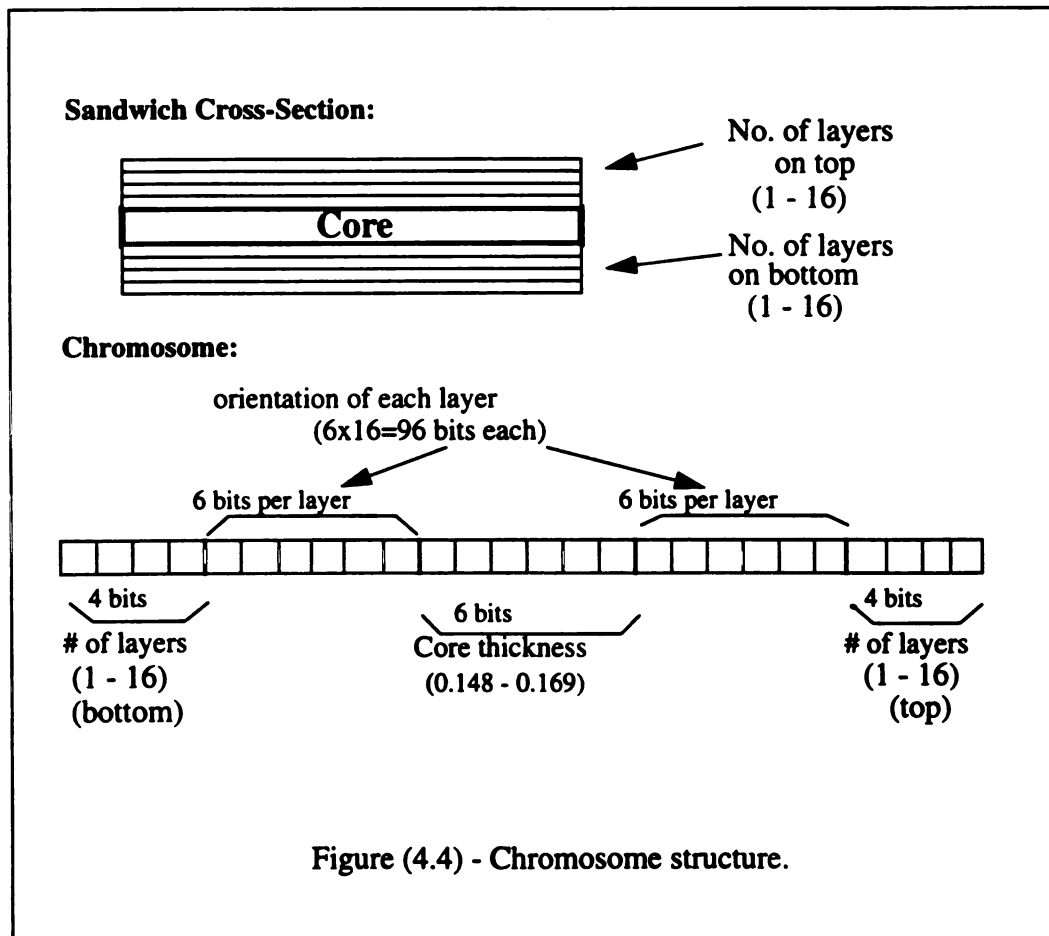
where  $w_c$  is the transverse deflection of the wing tip at mid-chord,  $w_0$  is the transverse tip deflection of the baseline case, and  $d_1$ ,  $d_2$ ,  $d_3$ ,  $k_2$ , and  $k_3$  are weighting coefficients whose values are listed in Table (4.2).

The weighting coefficient values in Table (4.2) were chosen in part based on the relative importance of each objective and penalty. Another factor influencing the choice of weighting factor values is the ease with which the constraint is violated. In this study the constraint on  $\sigma_2$  was most easily violated. This is an important constraint since designs in violation of this constraint are not valid. Consequently a large weighting factor was used for this function thus assessing a large penalty to discourage the GA from choosing

designs in violation of this constraint. After many iterations of fitness function revisions the values in Table (4.2) were chosen. These values enabled the GA to determine designs which produced the desired amount of twist, had the maximum in-plane stiffness and minimum weight, and not did not exceed maximum allowable stress values.

#### 4.4.1 Design Coding

Each design is represented by a coded string of binary numbers called a chromosome. The chromosome structure used in the current research is given in Figure (4.4). The chromosome consists of a string of binary numbers in which different portions represent



different physical characteristics of the design. The string contains 206 total bits giving a design space of  $2^{206}$ . The first and last four bits of the chromosome represent the number of layers on the bottom and top of the laminate, respectively, providing a range of 1 to  $2^4 = 16$  layers.

The next 96 bits inward represents the fiber orientation angle of each ply in the top and bottom face sheets. Fiber orientation angles are given a range of  $180^\circ$  ( $-90^\circ$  to  $90^\circ$ ). Each angle is represented by a 6-bit portion of the total 96 bits allotted for the top or bottom face sheets. With six bits representing each angle the  $180^\circ$  increment is divided into  $2^6 = 64$  divisions, thus producing an angular resolution of  $2.8125^\circ$ .

The middle six bits in the chromosome structure determine the core thickness which is confined to a range of 0.148 to 0.169 meters. This range was chosen to maintain the thickness to chord ratio of the panel near 0.15 as discussed previously.

#### **4.5 Genetic Algorithm Topologies**

A comparison is made between four different GA topologies or structures. The four different topologies are the single node, ring, injection, and hybrid architectures. In all four cases results were obtained for five runs of each topology. Each of the five runs contained a different random seed to generate a different initial population. The total population size for each case was 140 and each run terminated after 150 generations which provided sufficient time for results to converge. A *generation* is defined as the completion of a cycle in which two “parent” strings are selected from the population to be mated. They then reproduce, thus producing two offspring who are now a part of the population.

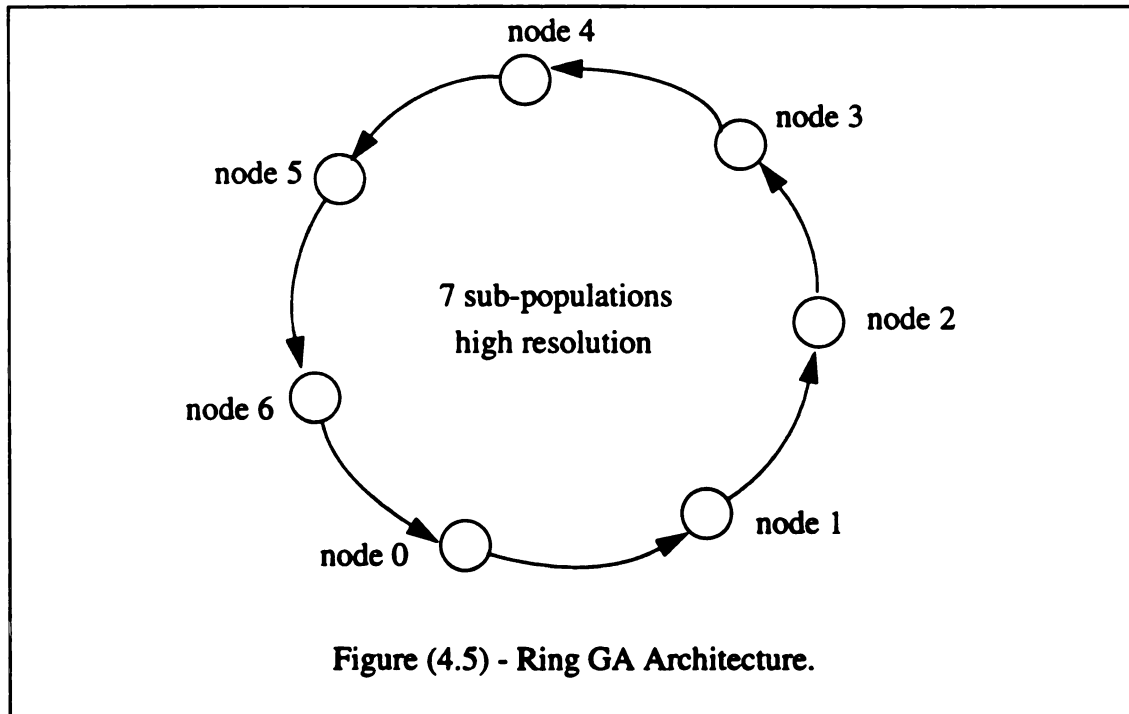
The GA uses a tournament selection method in which individuals compete (as the name *tournament* suggests) for the chance to mate. All four GA topologies use a two point crossover with a probability of 0.75. Mutation rate was 0.001. A description of the different topologies follows.

#### 4.5.1 Single Node Architecture GA

The least complicated GA structure is the single node. While this structure is simple in appearance it is no less robust than the other structures. The single node GA contains the entire population at a single node where all genetic operations are performed.

#### 4.5.2 Ring Architecture GA

The ring structure GA contains seven nodes arranged in a ring configuration as

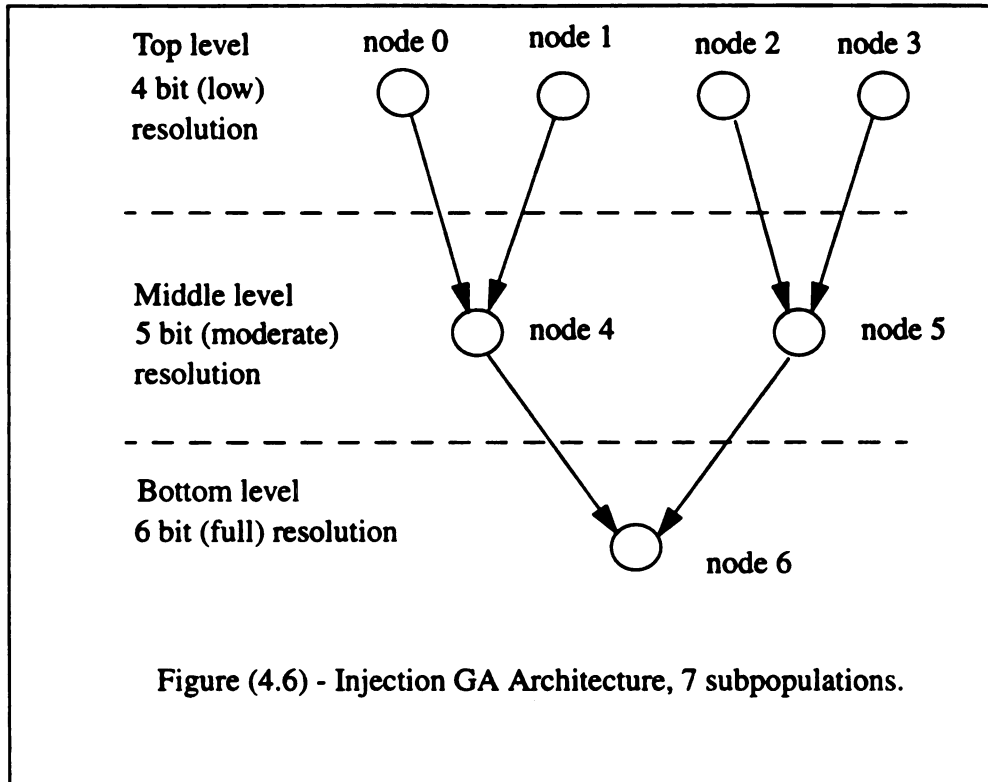


shown in Figure (4.5). Each node is an individual, self sufficient, sub-population similar to the single node case. A population size of 20 individuals at each of the seven nodes gives the same total population size as the other cases of 140. With the same population size for all topologies a direct comparison between structures can be made. The same total number of generations (150) is used for the ring structure with 5 generations per cycle and 30 cycles totaling 150 generations.

On the node level, the ring structure works similar to the single node case since each node simultaneously searches for the best fit individual, performing all the genetic operations of selection, reproduction, crossover, and mutation. The difference lies in the fact that each subpopulation performs 5 generations after which the best fit individual (chromosome) is copied to the adjacent subpopulation. This chain of events constitutes one cycle. This continues for 30 cycles for a total of 150 generations. The chromosome exchange occurs in one direction only, in this case from node 0 to 1, node 1 to 2, node 2 to 3, etc., as indicated by the arrows in Figure (4.5). This structure was devised to improve GA performance by accelerating convergence. One inherent characteristic of this structure is the tendency of a single design with high fitness to dominate the entire population in later generations.

#### 4.5.3 Injection Architecture GA

In previous work with parallel genetic algorithms for design, Punch, et al. [39] examined a number of exchange topologies in attempts to discover the most appropriate topologies for the laminated composite beam design example. In so doing, a new topology called injection island parallelism, or iiGA, was created. A similar injection structure is used in



the current research.

Two interesting aspects of an iiGA are its migration rules and the heterogeneous nature of its populations. In most GA parallel processing approaches, multiple subpopulations are used to generate solutions, and these solutions are exchanged between subpopulations in hopes of acquiring better solutions. Two common properties of most such approaches are first all subpopulations use the same GA representation of the problem, and second the exchanges are typically two-way meaning each subpopulation gives and receives solutions from other subpopulations.

The iiGA used in [39] as well as in the current research differs from both of these situations. First, the subpopulations are organized in a hierarchical exchange which is one way

and tree-like; that is, solutions are passed from children to parent subpopulations, but no exchanges occur between subpopulations on the same level (see Figure (4.6)). Second, various subpopulations are allowed to work with different representations of the same problem. The form of the representation typically follows the hierarchical exchange topology, with “child” subpopulations using a less refined or more abstract representation of the problem, which is then passed to a more detailed representation in the parent for refinement. This allows subpopulations to search smaller, but more abstract, search spaces for areas of possible interest, which can then be refined by parent subpopulations using a more detailed and more focused search. The top level or leaf nodes are autonomous, so their search experiences no influence from local optima discovered in other nodes on the way to the global optimum.

In previous work, the iiGA approach was applied to a laminated composite beam design problem [39]. The result of the iiGA approach to this problem showed dramatic improvement both in the energy absorption characteristics of the beams and the computational time required to find these solutions. Lessons learned from using iiGAs for the beam design in [39] are extended to the more complicated domain of composite sandwich panel design in the current study.

The 7-subpopulation tree shown in Figure (4.6) illustrates the topology of the iiGA used in the current research. The injection structure is capable of representing a design with different levels of refinement to decrease computational costs and improve efficiency. Three levels of refinement are used for representation of the fiber orientation angle. As mentioned previously, 6 bits are allotted for representation of the fiber orientation angle of each ply. In the top level of the injection structure (low resolution) orientation angles are

represented by only 4 bits, where in the middle level (moderate resolution) a 5 bit representation is used, and finally in the bottom level the full resolution of 6 bits is used.

The iiGA has the same population size of 140 as do the other structures which is obtained from a population size of 20 per each of the seven nodes. Each subpopulation simultaneously performs all genetic operations, increasing the fitness of the best individual. As with the ring structure, the iiGA performs 30 cycles consisting of 5 generations each for a total of 150 generations. After each cycle the four subpopulations in the top level *inject* the best fit individual into the two middle subpopulations and the middle subpopulations inject the best fit individuals into the bottom level subpopulation where the designs are further refined. The top level designs receive no data from outside the population and the bottom level does not inject data into any other population. Sharing of data is one way as indicated by the arrows in Figure (4.6).

#### 4.5.4 Hybrid Architecture GA

The final GA structure used is a hybrid structure which combines the ring and injection topologies (see Figure (4.7)). This structure was developed in an attempt to achieve improved performance over the ring and injection GAs. In the injection structure the moderate and low resolution subpopulations very quickly converge to a low fitness and thereafter do not contribute to the performance of the GA. The intent is to take advantage of the initial rapid increase in fitness of the injection GA and then finish with the ring structure to achieve higher fitness.

This hybrid approach uses the same 7 subpopulation injection structure shown in

Figure (4.6) for the first one half of the total generations with the orientation angle resolutions exactly the same as the iiGA discussed previously. For the last half of the generations the GA structure is converted into the same ring structure discussed previously with each node having full resolution.

#### 4.6 Finite Element Model

The wing was modeled as a rectangular sandwich panel which was fixed at one end and free on all other edges. The rectangular domain was discretized into a mesh of elements, the size of which was chosen based on a convergence study. The convergence study determined the coarsest mesh possible which gives sufficiently converged results (see

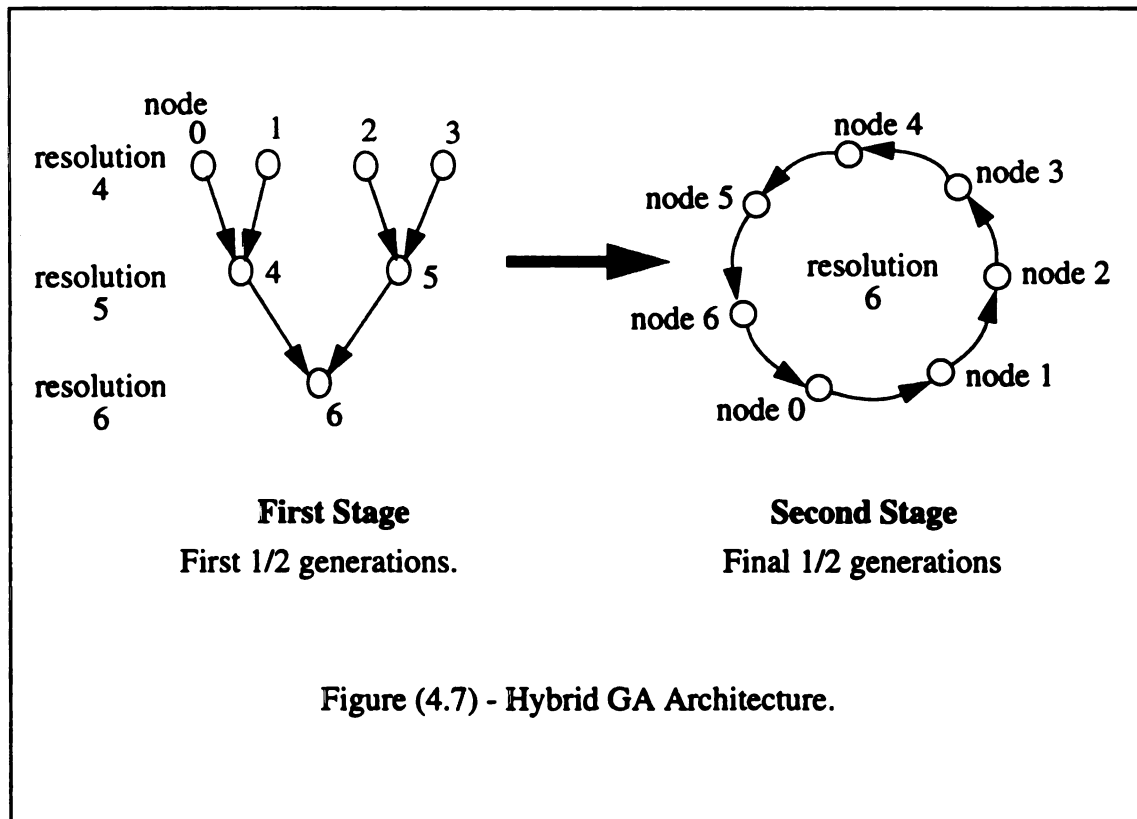


Table (4.3)). It is imperative to use a mesh with the fewest number of elements since computational expense is directly affected by the number of elements. In an optimization problem tens of thousands of calculations are performed so even a seemingly small savings in computational time can amount to a large savings over the course of an optimization run. The quantities  $w_C$  and  $w_B$  in Table (4.3) are the transverse deflections of the free end (or tip) of the plate at the leading edge and mid-chord respectively.

**Table (4.3) Mesh Convergence Data.**

Mesh	$\sigma_{xx}$ ( $\times 10^{-9}$ )	$\sigma_{yy}$ ( $\times 10^{-8}$ )	$\sigma_{xy}$ ( $\times 10^{-7}$ )	$w_C$	$w_B$
2x4	0.5291	0.0980	-0.1906	0.2280	0.2314
2x8	0.5774	0.1105	-0.1370	0.2335	0.2300
2x12	0.5737	0.1165	-0.1343	0.2341	0.2306

A mesh containing two 4-noded plate elements in the chordwise direction (the short dimension of the wing) and eight elements in the spanwise direction was found to be sufficient. This mesh provided in-plane stresses which were converged to within 5% and transverse tip displacement which were converged to within 3%.

The displacements and stresses used by the optimization algorithm were determined by the FORTRAN finite element code employing the ZZHT model discussed in Chapters 2 and 3.

## 4.7 Results and Discussion

### 4.7.1 GA Results

Five runs of each GA topology were performed and results compared. Table (4.5) contains results for each run of each structure. To obtain different results for each run the different random seed was changed in the input file. Changing the random seed assures a different initial population is generated for each run. Table (4.5) contains the fitness of the best fit individual (design) from each run of each structure, the subpopulation number from which this individual came, and the average of the best fitness values.

Each structure achieved nearly the same level of fitness with the maximum difference in average fitness being 0.3%. This indicates the ability of all structures to solve the optimization problem sufficiently. The individual with the highest absolute fitness of 4,140.25 came from node 6 of run 4 of the ring structure. The ring and hybrid structures produced the same average fitness of 4,130.80 indicating the performance of these two structures is superior to the injection and single node structures. The injection structure gave the lowest performance which is due to the application specific nature of the injection structure. For problems with much larger design spaces the injection structure should out-perform at least the single node structure and likely would out-perform the ring structure as well. While one GA topology can be termed the best for this study, all structures performed sufficiently well.

Figures (4.8) through (4.11) contain results of fitness versus generation number for each of the topologies. In all cases results are converged long before the maximum number of generations (150) is reached. In the case of the single node structure the fitness is

converged to within 2% of the maximum by generation 10 and to within 1% by generation number 20. Figure (4.8) contains the single node results.

The ring structure results are given in Figure (4.9). Seven sets of data points are plotted, one for each of the seven subpopulations or nodes. Node 5 initially increases in fitness the most rapidly while node 1 increases the slowest. Node 4 produced the individual (design) with the highest absolute fitness. At node 4 fitness increases to within 4% of the maximum by generation 10 and to within 2% of the maximum by generation 20 which is a slightly slower convergence rate than the single node case but on the same order.

Figure (4.10) shows results from each of the seven nodes of the injection structure. As discussed previously nodes 0 through 3 use the lowest resolution representation of the design, nodes 4 and 5 use moderate resolution, and node 6 uses the full resolution (see Figure (4.6)). The design fitness from node 6 increases to within 4% of the maximum by generation 10 and to 0.7% by generation 20 making the injection structure the quickest of the four structures to converge.

The hybrid structure's convergence performance (see Figure (4.11)) is similar to the injection structure since for the first 75 generations the hybrid structure uses the injection structure (see Figure (4.7)). From generation 75 to 150 the hybrid structure uses the ring architecture. Once the structure changes from injection to ring at generation 75 the fitness of all the nodes converge quickly as can be seen in Figure (4.11). As expected the lower resolution nodes begin to converge to a low fitness value when the injection structure is used. This is evident for the hybrid structure (see Figure (4.11)) more so than for the injection structure results of Figure (4.10) which is due to a different initial population. In both the injection and hybrid structures the final fitness converges to similar maximum

values and the fitness convergence rate of node 6 is very similar. For the hybrid structure the fitness is within 7% of the maximum by generation 10 and within 1% by generation 20.

The various quantities in the fitness function (Equation (4.4)) are presented in Figures (4.12) through (4.15). These figures illustrate how the GA works to achieve maximum fitness while satisfying all constraints. Seven quantities are plotted for each GA structure. These quantities show how the design is evolving physically as the GA conducts its search of the design space.

Fitness is the first quantity plotted. The fitness is plotted for the subpopulation from which the best fit individual came (see Table (4.5)). This plot exhibits the increase in fitness as the generation number increases, which is shown in Figures (4.8) through (4.11).

The next quantity plotted, labeled  $wt^*$ , is the normalized weight objective multiplied by the weighting factor and is calculated as follows:

$$wt^* = c_1 \left( \frac{W_{baseline}}{W(\tilde{x})} \right)^2 \quad (4.12)$$

where  $c_1$ ,  $W_{baseline}$  and  $W$  are the previously defined quantities. These graphs show how the structure weight evolves during the optimization process with final weights for each structure given in Table (4.4). The single node structure determined the lightest weight design at 66.19 kg and the hybrid structure determined the heaviest design at 71.76 kg.

**Table (4.4) Results for Best Design of Each GA Structure.**

GA Structure	wt* (actual weight kg)	Stiff* ( $a_{11}, a_{22}, (*10^{-8})$ )	twist* (actual twist m)
single	45.35 (66.19)	86.49 (2.110,2.133)	-0.0044 (-0.0279)
ring	44.00 (68.22)	96.84 (2.363,2.390)	-0.0249 (-0.0273)
injection	45.04 (66.65)	82.58 (2.201,2.015)	-0.0380 (-0.0209)
hybrid	41.83 (71.76)	97.56 (2.427,2.380)	-0.0120 (-0.0277)

The next quantity  $stiff^*$  is the stiffness objective term in the fitness function, calculated from the following equation:

$$stiff^* = c_2 \left( \frac{a(\vec{x})}{a_{baseline}} \right)^2 \quad (4.13)$$

where all quantities are as previously defined. The in-plane stiffness of the wing structure is maximized to maximize the buckling strength of the structure. As these figures illustrate, stiffness is maximized as the generation number (and fitness) increases. In all cases in-plane stiffness converges to similar values. The hybrid structure determined the design having the highest in-plane stiffness and the injection structure determined the design with the lowest in-plane stiffness (see Table (4.4)). The difference in stiffness values for each

GA structure is due to the fact the total fitness is a weighted balance of all design objectives which allows a design with the similar fitness to have different values for each design objective.

The next quantity plotted,  $twist^*$ , is the relative difference in twist of the wing, where twist is defined in Equation (4.8). The  $twist^*$  quantity is calculated from the following equation:

$$twist^* = \left( \frac{t(\tilde{x}) - t_{desired}}{t_{desired}} \right) \quad (4.14)$$

As the graph of this quantity indicates  $twist^*$  converges to zero as the generation number (and fitness) increases indicating the wing structure has achieved the desired amount of twist. This was the most difficult objective to achieve so the largest weighting was given to it. The single node structure produced a design having the “best” twist, deviating only 0.4% from the desired twist. The largest deviation, 3.8%, from the desired twist was from the design produced by the injection structure.

The final three quantities plotted are the constraint or penalty terms:  $\delta^*$ ,  $\sigma_1^*$ , and  $\sigma_2^*$ . The  $\delta^*$  quantity is the transverse tip deflection penalty calculated from Equation (4.9). The plot of this quantity shows all best designs of each generation do not exceed the maximum allowable tip deflection. The stress constraints are plotted as the quantities  $\sigma_1^*$  and  $\sigma_2^*$  where  $\sigma_1^*$  is the stress constraint in the fiber direction calculated from Equation (4.10), and  $\sigma_2^*$  is the stress constraint in the transverse direction calculated from Equation (4.11). It should be noted that these three

constraints are satisfied for the best design of each generation throughout the 150 generations as indicated by the final three graphs of figures (4.12)-(4.15). Thus no penalty is assessed to the fitness for these designs. In the remainder of each population there may exist many designs which violate these constraints however their fitness is not high enough to make them the “best” individual of a generation. The design space does not exclude such designs and thus the population diversity is maintained.

To ensure the designs found were near global optima an optimization was performed with an initial population of 1,000. A larger initial population increases the number of designs from which the GA can choose which increases the chances of the best design being found by the GA. From this optimization run fitness changed less drastically in early generations and the fitness of the best individual was 4,123.94 which is on the same order as the results obtained from using a population size of 140 individuals. This validates the use of the smaller population which is preferable to use since it conserves computational resources.

#### 4.7.2 Stiffness Matrix Results

Fiber orientation angles, number of plies, and core thickness were design variables in this optimization project. Over the course of the optimization these variables are changed by the genetic algorithm in the search for the optimum design. Altering these variables affects the structure’s response since the overall laminate stiffness matrix, often referred to as the [ABD] matrix [9,20]. In preceding sections the evolution of the design was traced by examining the weight, stiffness, and twist for each generation. Another means of illustrating the evolution of the design is to examine the various terms of the

[ABD] stiffness matrix. Figures (4.16) through (4.18) display the behavior of the stiffness matrix as the genetic algorithm seeks out the optimum design. Results are given for run 4, node 6, of the ring ga structure which produced the individual (design) with the highest fitness.

The [ABD] matrix as well as each of the [A],  $[B]=[B]^T$ , and [D] matrices are symmetric so only the upper diagonal half of each matrix needs to be considered. In Figure (4.16) [A] matrix values are given for the best individual of each generation. This portion of the [ABD] matrix is called the extensional stiffness matrix and it relates in-plane stress resultants to in-plane mid-surface strains (shear and normal) [48]. One design objective was to maximize the in-plane stiffness or the  $A_{11}$  and  $A_{22}$  terms of the [A] matrix. These terms relate the in-plane normal stress resultants to in-plane normal strains. Maximizing these two terms increases the buckling strength of the wing (plate). As Figure (4.16) indicates these terms are maximized during the optimization, as desired, making these two terms the largest in the [A] matrix,  $A_{11}=2.363e+08$  and  $A_{22}=2.390e+08$ . The  $A_{12}$  and  $A_{66}$  terms exhibited similar behavior to each other during the optimization. Tension-shear coupling terms  $A_{16}$  and  $A_{26}$  are non-zero indicating coupling occurs between in-plane normal stress resultants and in-plane shear strain. Their final values are  $A_{16}=-7.007e+07$  and  $A_{26}=-2.276e+07$ .

The [B] matrix portion of the [ABD] stiffness matrix is called the bending-stretching coupling stiffness. Values for the [B] matrix are given in Figure (4.17). The [B] matrix, in part, determines the twisting response produced by the wing, which was the main objective of this optimization. Bending-shearing and extension-twist coupling is present since the  $B_{16}$  and  $B_{26}$  terms are non-zero [48],  $B_{16}=-8.873e+05$  and  $B_{26}=-2.159e+05$ . The  $B_{22}$

term had the largest absolute value at  $B_{22}=-7.317e+06$ .

The [D] matrix, called the flexural stiffness matrix, relates stress couples to curvatures [48]. The behavior of this matrix is very similar to the behavior of the [A] matrix with the  $D_{11}$  and  $D_{22}$  terms being the largest at  $1.321e+06$  and  $1.341e+06$ , respectively. Values for the coupling terms are  $D_{16}=-3.935e+05$  and  $D_{26}=-1.275e+05$ . These terms determine the bending-twisting coupling in the wing making them instrumental in achieving the desired amount of wing twist since a bending load was applied to the wing and a predetermined twist response was sought. As was the case with the [A] matrix, the  $D_{12}$  and  $D_{66}$  terms behaved similarly throughout the optimization, achieving final values of  $2.294e+05$  and  $2.725e+05$  respectively.

#### 4.7.3 Layups

The lamination schemes corresponding to the best design (the design with the highest fitness) as determined by each of the GA structures are contained in Tables (4.6) through (4.9). As indicated by Table (4.5) the ring structure produced the design with the highest fitness at 4,140.25 and the injection structure the lowest at 4,096.00. The design produced by the single node was the lightest of the four cases weighing 66.19 kg while the heaviest design came from the hybrid GA weighing 71.76 kg. The hybrid GA also produced the design having the highest in-plane stiffness value with  $A_{11}$  being  $2.4273e+08$  Pa.

The layups produced by each GA structure are quite different. Genetic algorithms typically locate several optimal solutions to a design problem which is a desirable situation in many instances. This allows the designer many options to choose from since one

design may be more desirable for reasons not accounted for in the fitness function such as aesthetics. All layups produced have no more than two contiguous plies with the same fiber orientation. This helps to alleviate matrix cracking which is a concern when a laminate contains several adjacent plies with the same fiber orientation.

## 4.8 Conclusions

The goal of this optimization problem was to illustrate the ability of a laminated sandwich structure (an aircraft wing) to achieve a specific twisting response which was opposite the direction the loading was applied. This objective was obtained while structure weight was minimized and in-plane stiffness maximized, subject to constraints on tip deflection and maximum stress. Optimum designs were determined satisfying all desired design criteria using genetic algorithms.

Four different GA structures were used to determine the best design: single node, ring, injection, and hybrid structures. Five runs were performed for each structure for determination of the maximum fitness and for evaluation of the average performance of each structure so the four structures could be compared. The maximum fitness of 4,140.25 was produced by run 4, node 6, of the ring structure and the lowest fitness of 4,096.00 came from the injection structure. Both the ring and hybrid architectures produced the highest average fitness of 4,130.8 and the lowest average fitness came from the injection structure. The maximum difference in average fitness was only 0.3%, thus all architectures performed comparably in regards to average fitness. Another measure of performance was the convergence rate of each structure. The injection GA converged the most rapidly of the

four structures and the ring GA the slowest. Again, the four structures exhibited a very small difference in convergence rates with the injection converging to 0.7% of the maximum fitness by generation 20, the hybrid and single node structures converging to within 1% and the ring structure within 2% by generation 20.

The single node structure produced the design with the lowest weight of 66.19 kg as well as the design having the “best” twist, -0.0279 m, which is only 0.4% less than the desired twist of -0.028 m. The design having the maximum in-plane stiffness,  $A_{11}=2.427e+08$  Pa, was produced by the hybrid structure.

The population size of 140 used in all cases was found to be sufficient by comparing results with a case using a population size of 1,000. Maximum fitness from the case using the larger population size was 4,123.94 which is 0.4% less than the results obtained by the ring structure using a population size of 140. This indicates the designs found are near the global optima.

The lamination sequence of the best design from each GA structure was included in the results section. The four lamination schemes are quite different from each other, however, they are all valid designs which satisfy all conditions and constraints of the problem. Each design provides a compromise between stiffness and weight. Equal weighting was given to both objectives. If maximum stiffness was more important than minimum weight, a larger weighting could be given to the stiffness objective to drive the design toward higher stiffness. The converse is also possible. Having a variety of optimal designs to choose from allows the designer greater flexibility. Genetic algorithms, in many cases, can provide several near optimal solutions to an optimal design problem, provided the problem lends itself accordingly.

The various terms in the [ABD] stiffness matrix were examined over the course of the optimization. The A and D matrices behaved similarly with  $A_{11}$ ,  $D_{11}$ ,  $A_{22}$ , and  $D_{22}$  terms having maximum values. The presence of extension-shear coupling was illustrated by non-zero  $A_{16}$  and  $A_{26}$  terms and bending-twisting coupling was present since the  $D_{16}$  and  $D_{26}$  terms were non-zero. Twisting-stretching and bending-shear coupling is indicated by non-zero  $B_{16}$  and  $B_{26}$  terms. The  $B_{22}$  term had the largest absolute value in the B matrix. The 16 and 26 terms of the D matrix were instrumental in achieving the desired "opposite" twisting response in the wing.

One concern which was not directly addressed in this problem is design manufacturability. Due to the highly unsymmetric lamination scheme necessary to achieve the desired twisting response in the wing, warping will occur in the manufacturing process as the laminate cures. Manufacturing of this structure will need to be done in such a way to minimize (or eliminate) the warping due to curing. The shape of the wing after curing can be determined by applying the appropriate thermal loading which will produce the same response in the wing. With the post-cured shape known it should be possible to manufacture the laminate in a shape which will correct for the warping by using an appropriately shaped mandrel.

## **4.9 Recommendations**

The motivation for this design problem came from the desire for aircraft wings to adjust their angle of attack when experiencing gust loads. Gust loading causes the wing to twist up and back which is detrimental to the wings lift. The desired response to such

loadings is for the wing to twist in the opposite direction. This research shows such a response is possible with laminated sandwich structures. Specific design data was idealized, i.e. wing shape, sweep back, aircraft size and weight, actual wing loadings, desired wing twist, etc., to devise a general case which illustrates the ability to solve such a problem using an experimental finite element plate model with genetic algorithms. This problem can be extended and refined as desired to account for more realistic designs when specific design information is known. Also a more refined failure criteria could be incorporated such as the Tsai-Hill, Tsai-Wu, Chamis, and Hoffman interactive failure criteria [48]. Design manufacturability and cost constraints could also be included in the fitness function.

**Table (4.5) Optimization Result From Various GA Structures.**

Run Number	Best Fitness	Subpopulation number	Average Best Fitness
Single Node Structure (popsize 140, 150 generations)	1	4.121654e+03	4.1215e+3
	2	4.121087e+03	
	3	4.131813e+03	
	4	4.114829e+03	
	5	4.118105e+03	
Ring Structure (7 nodes, popsize 20, 150 generations)	1	4.132970e+03	4.1308e+3
	2	4.119689e+03	
	3	4.138185e+03	
	4	4.140251e+03	
	5	4.123152e+03	
Injection Structure (7 nodes, popsize 20 150 generations)	1	4.126204e+03	4.1165e+3
	2	4.096004e+03	
	3	4.126848e+03	
	4	4.107464e+03	
	5	4.125922e+03	
Hybrid Structure (7 nodes, popsize 20 150 generations)	1	4.118339e+03	4.1308e+3
	2	4.121376e+03	
	3	4.137914e+03	
	4	4.136995e+03	
	5	4.139252e+03	

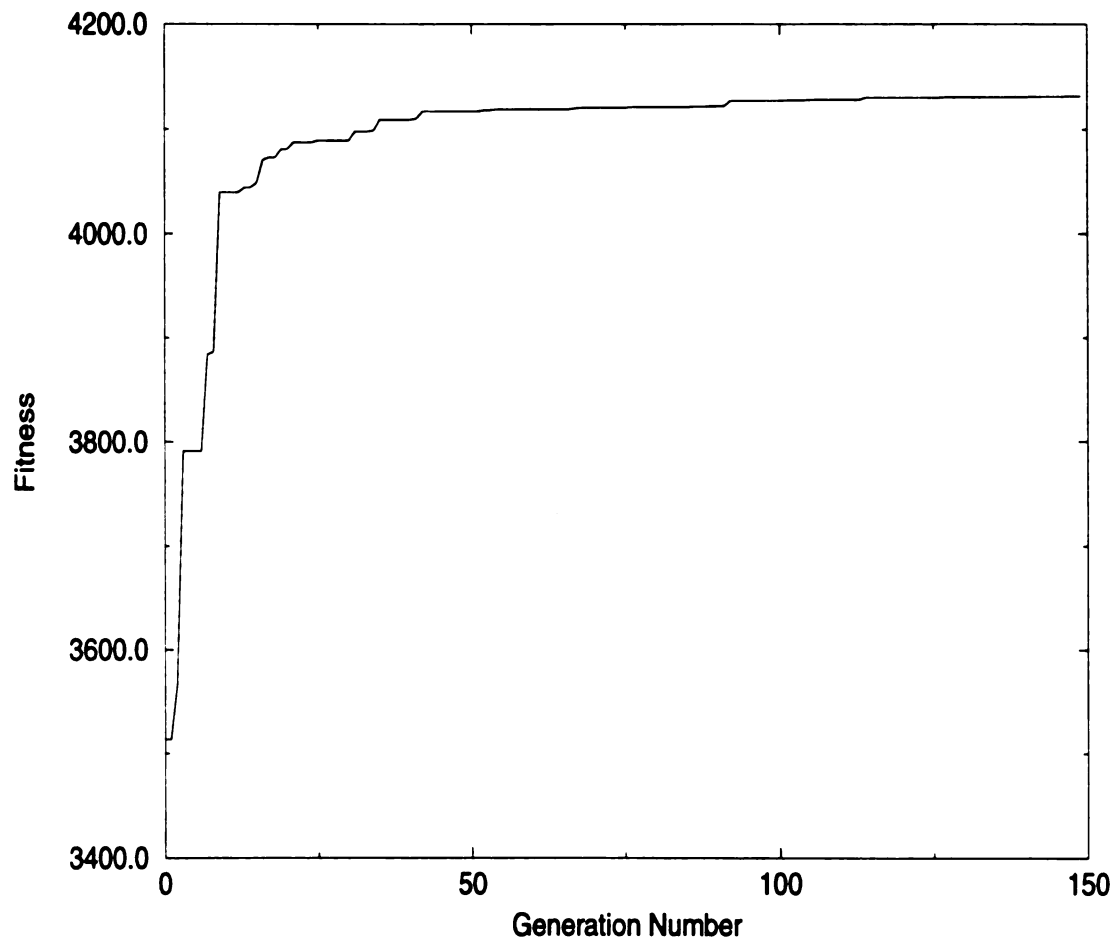


Figure (4.8) - Fitness versus generation number for single node GA structure.

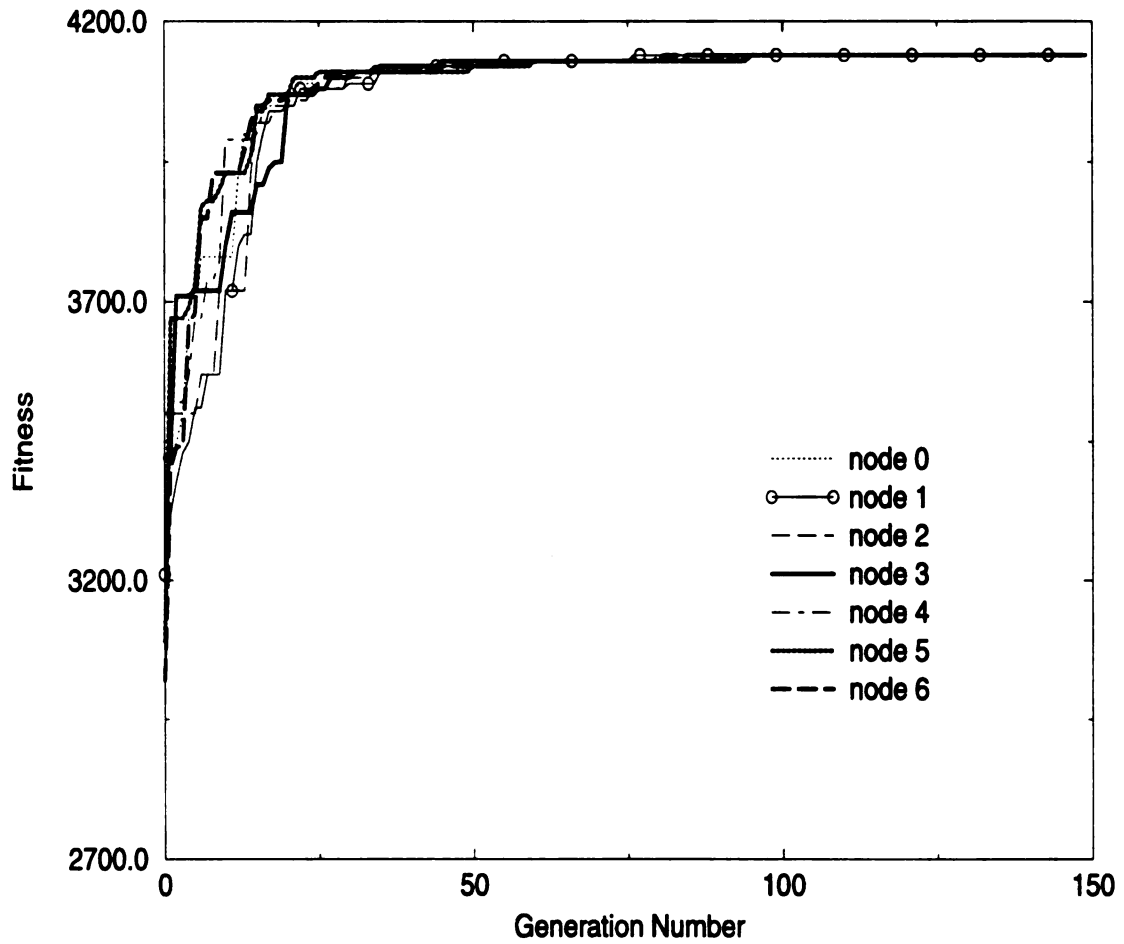


Figure (4.9) - Fitness versus generation number for ring GA structure.

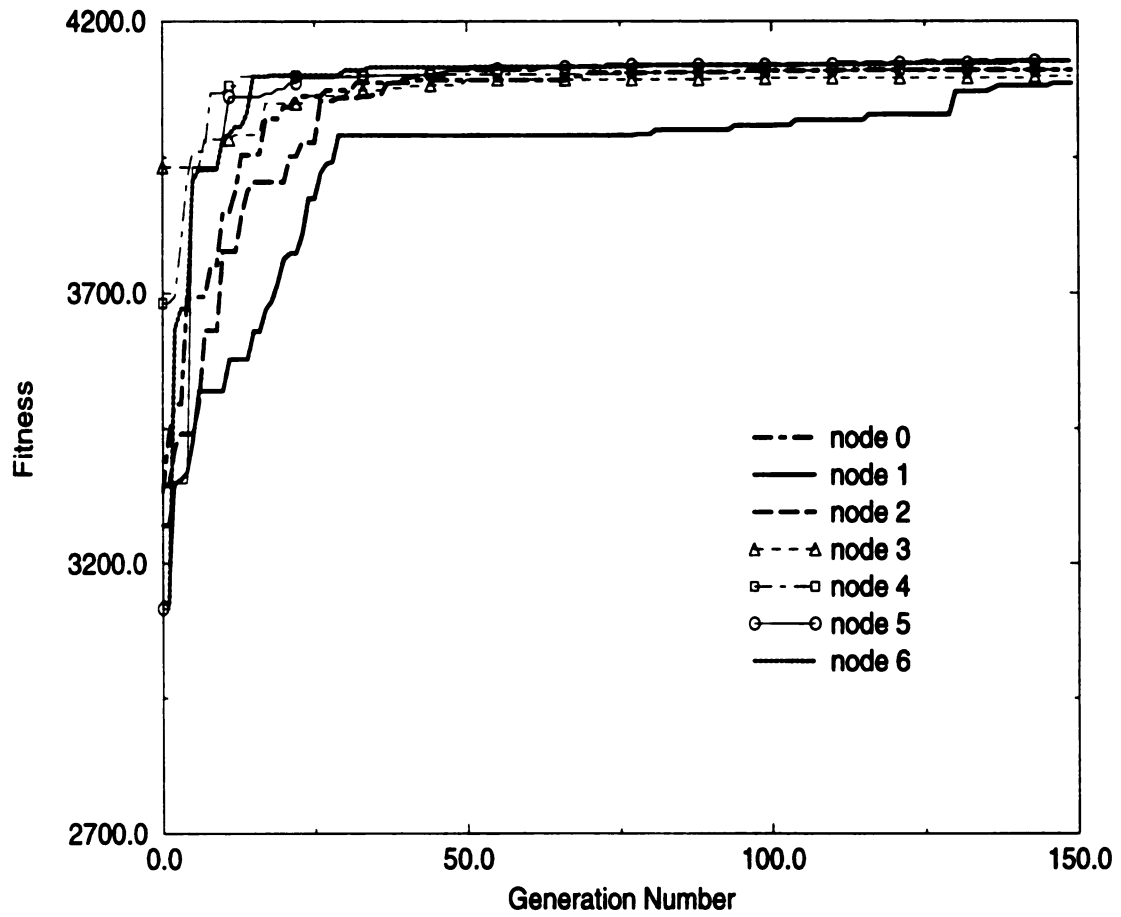


Figure (4.10) - Fitness versus generation number for injection GA structure.

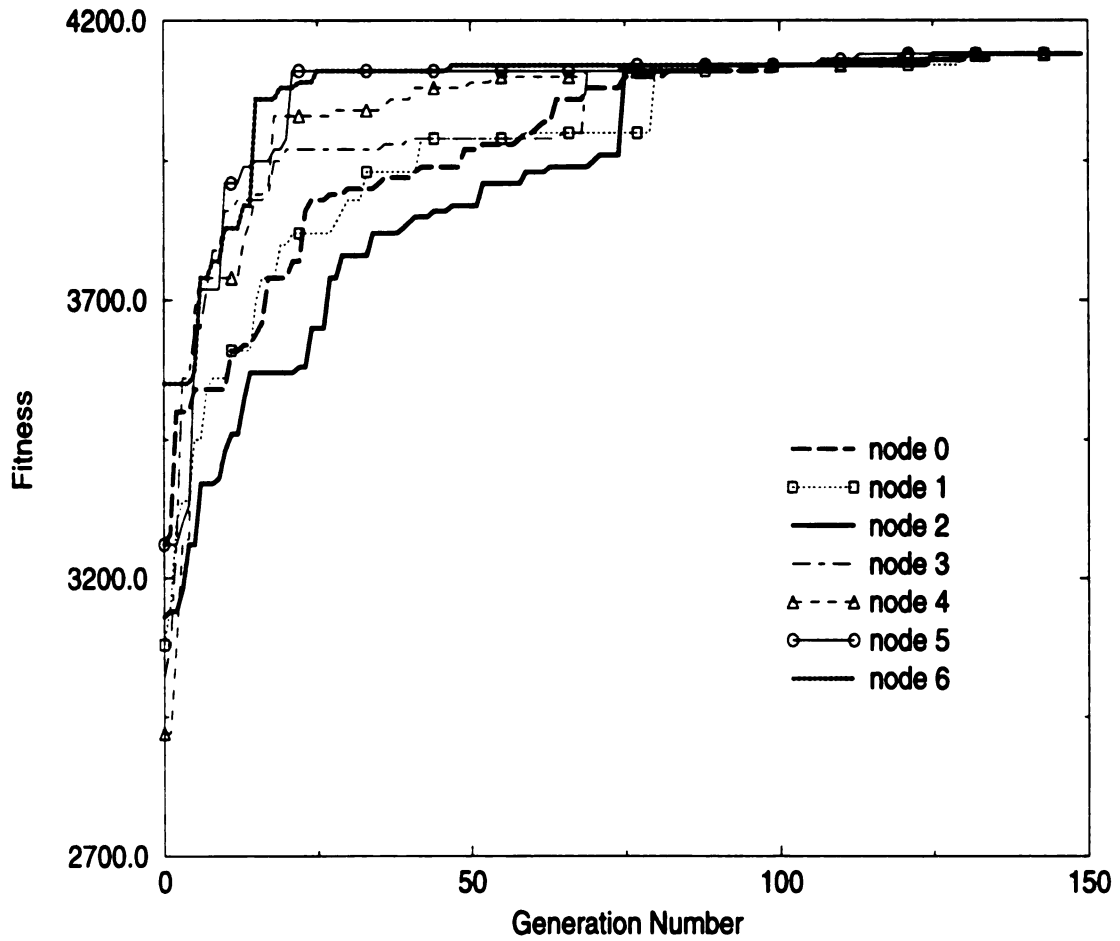


Figure (4.11) - Fitness versus generation number for hybrid GA structure.

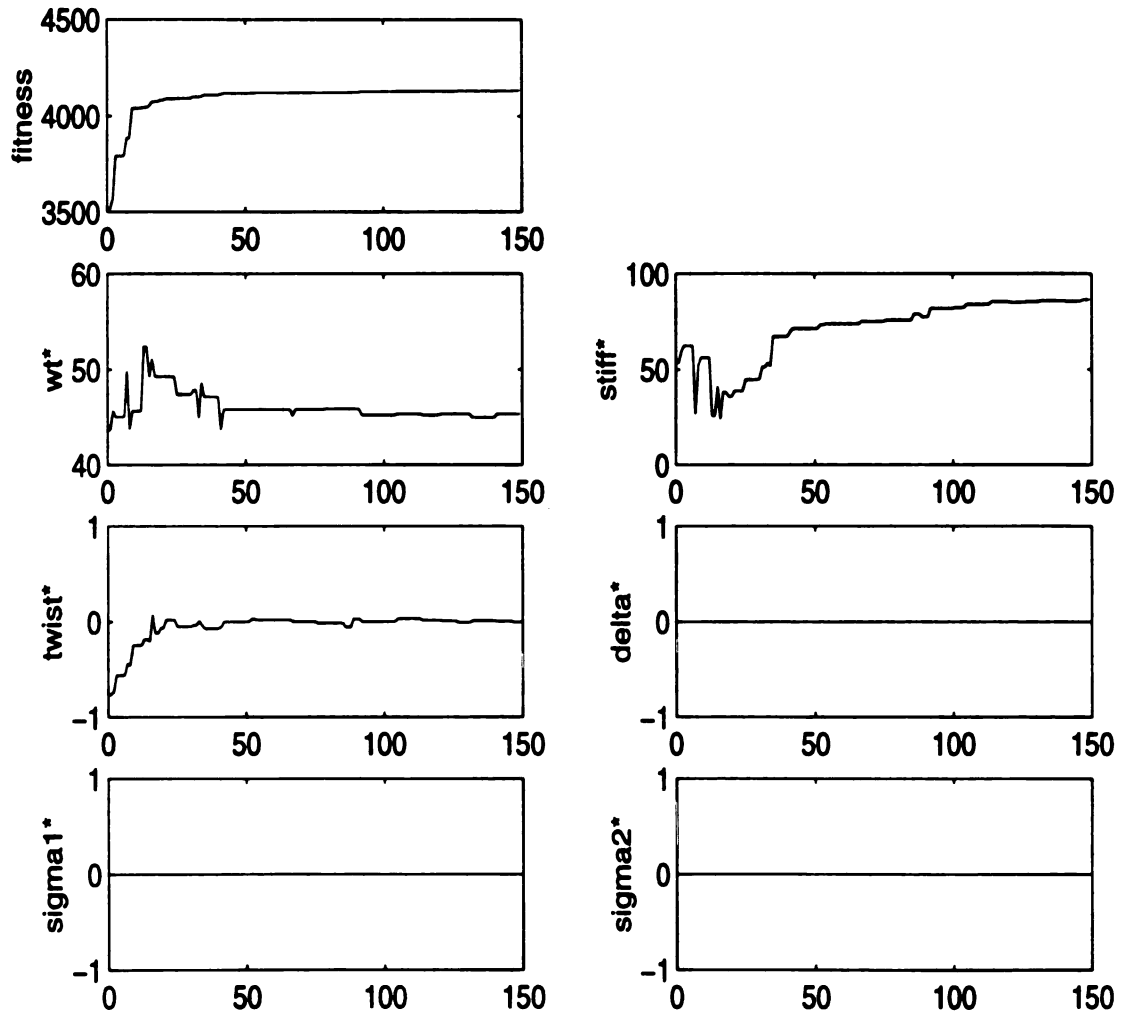


Figure (4.12) - Fitness function terms vs. generation number for single node topology GA.

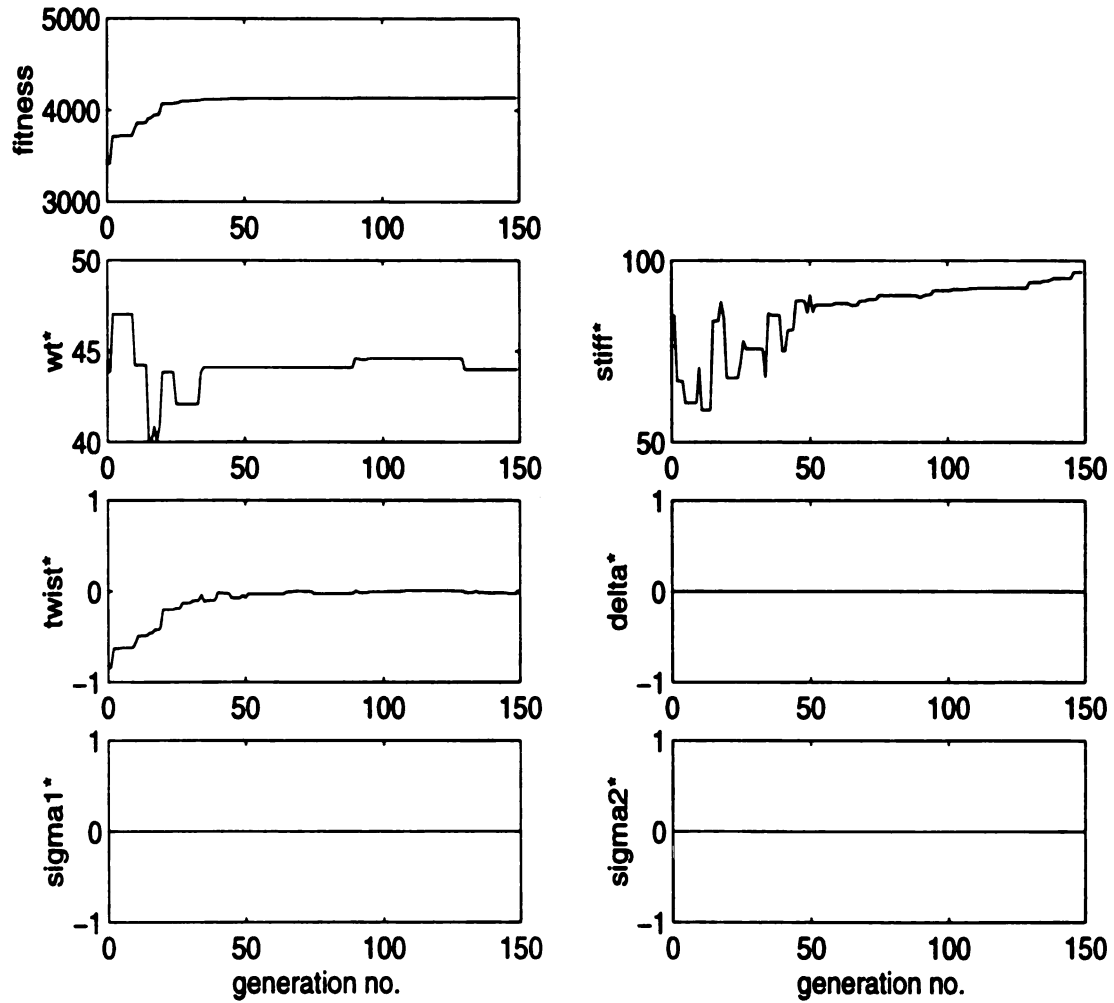


Figure (4.13) - Fitness function terms vs. generation number for ring structure GA.

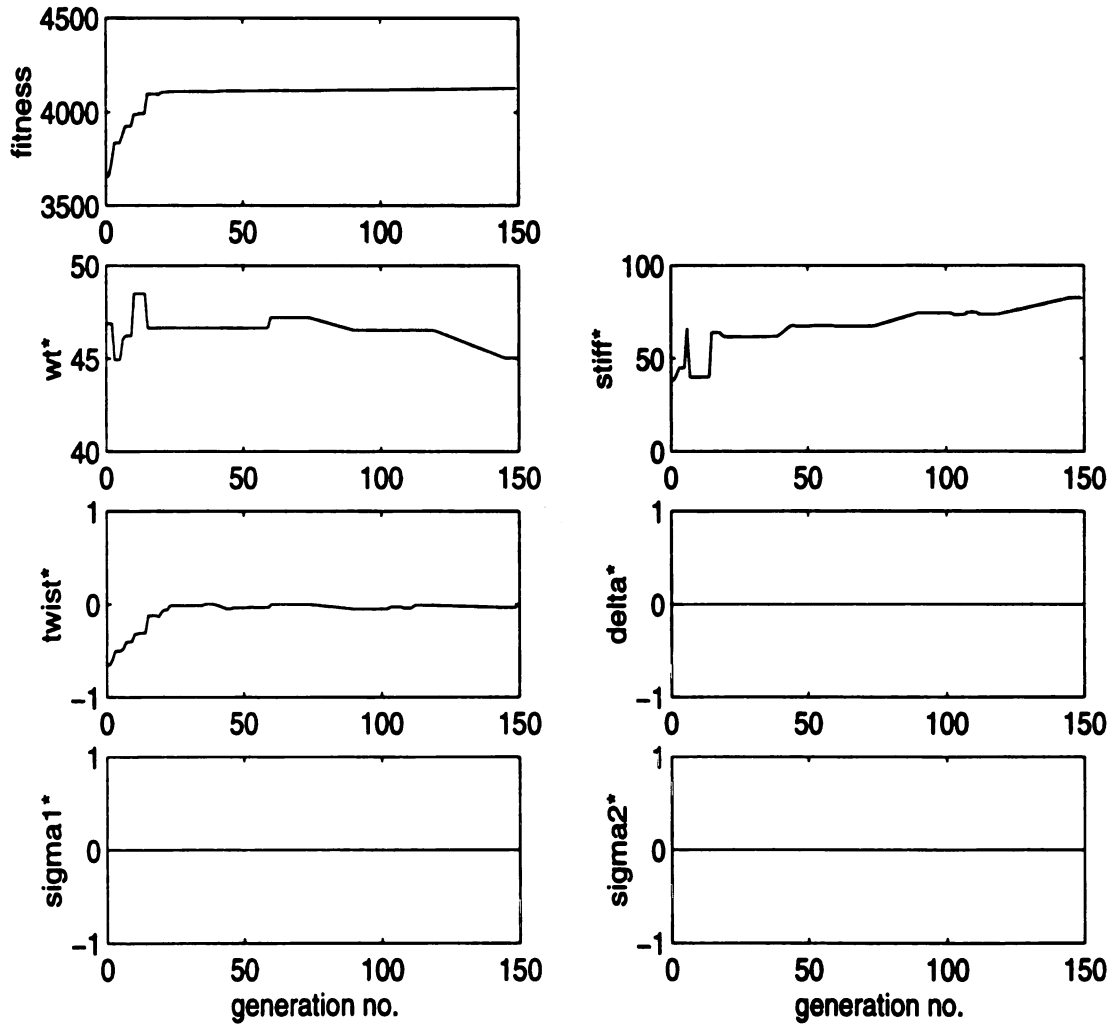


Figure (4.14) - Fitness function terms vs. generation number for Injection structure GA.

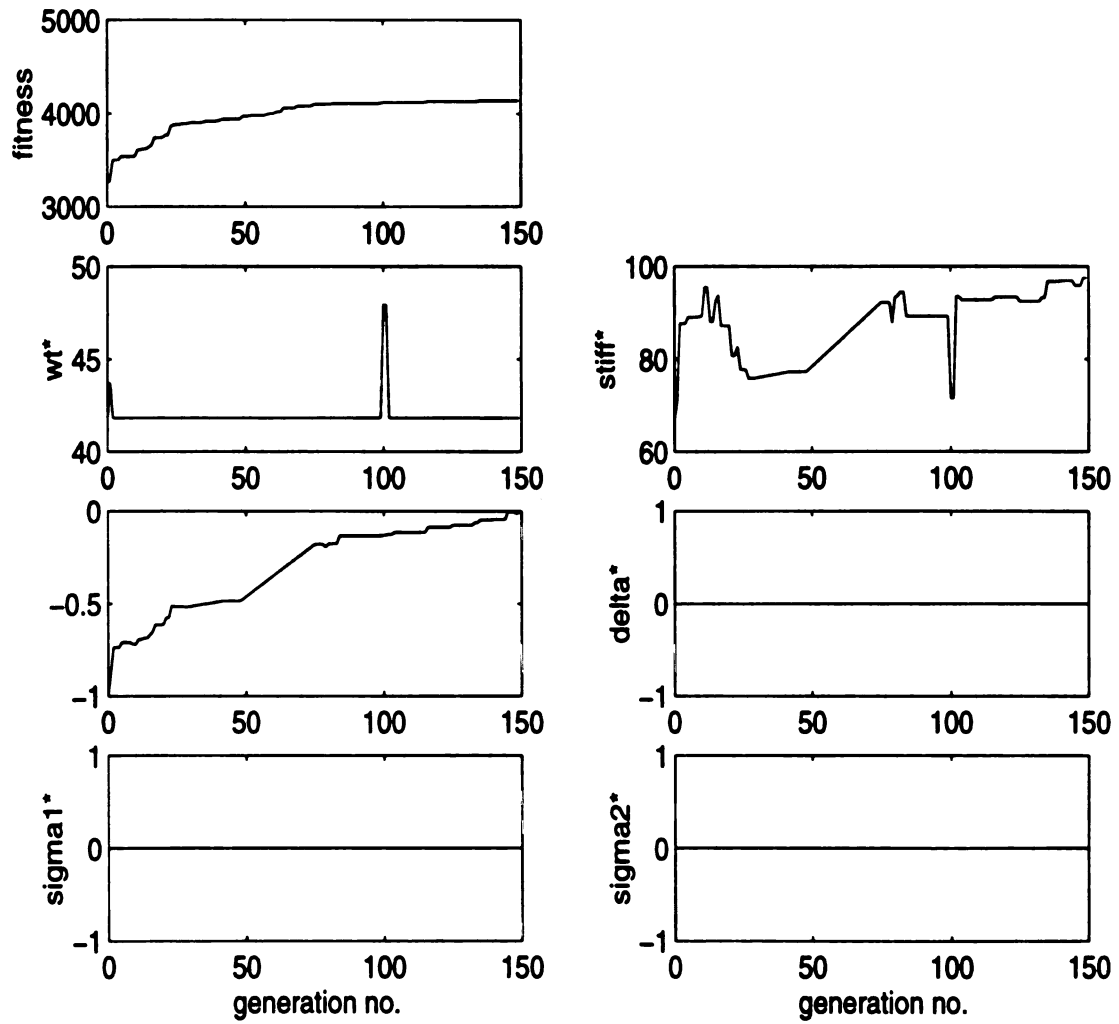


Figure (4.15) - Fitness function terms vs. generation number for hybrid structure GA.

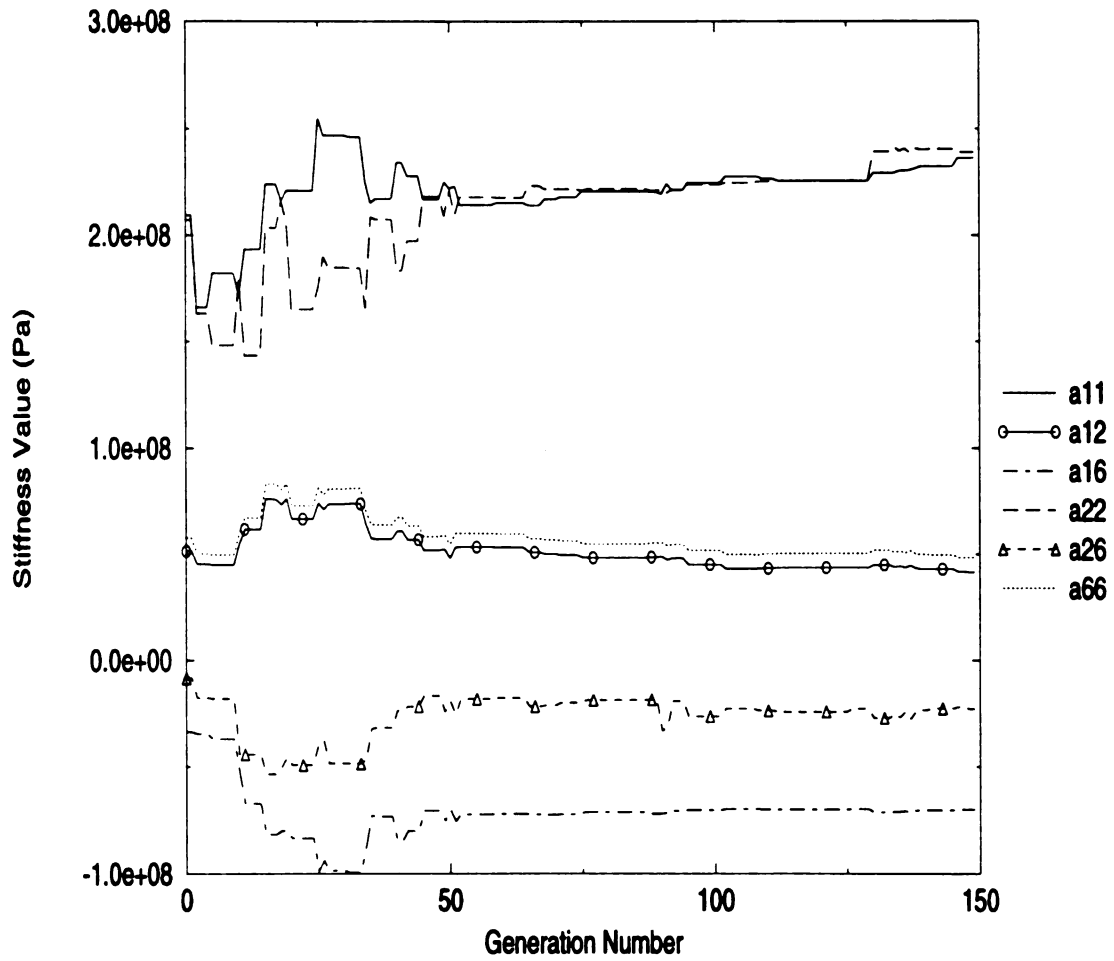


Figure (4.16) - Extensional stiffness matrix versus generation number.

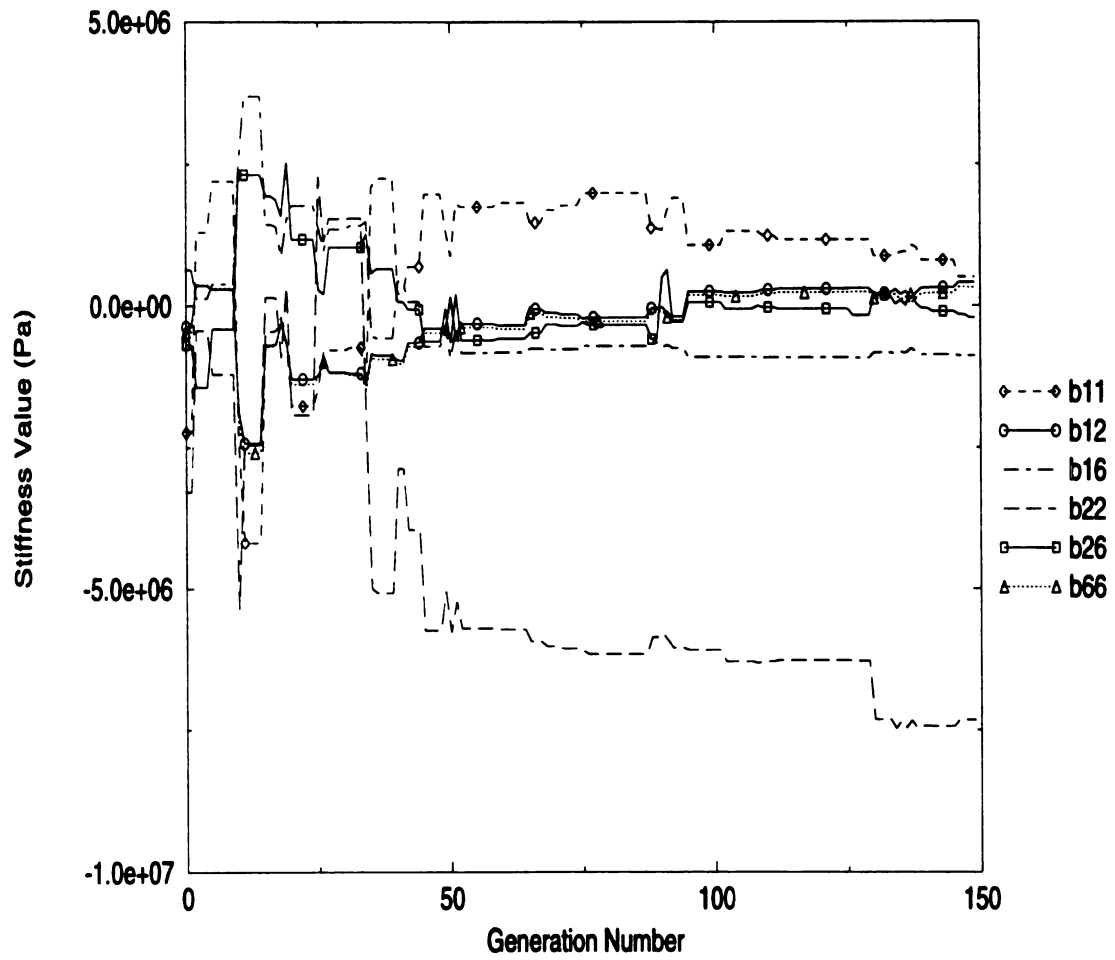


Figure (4.17) - Coupling stiffness matrix versus generation number.

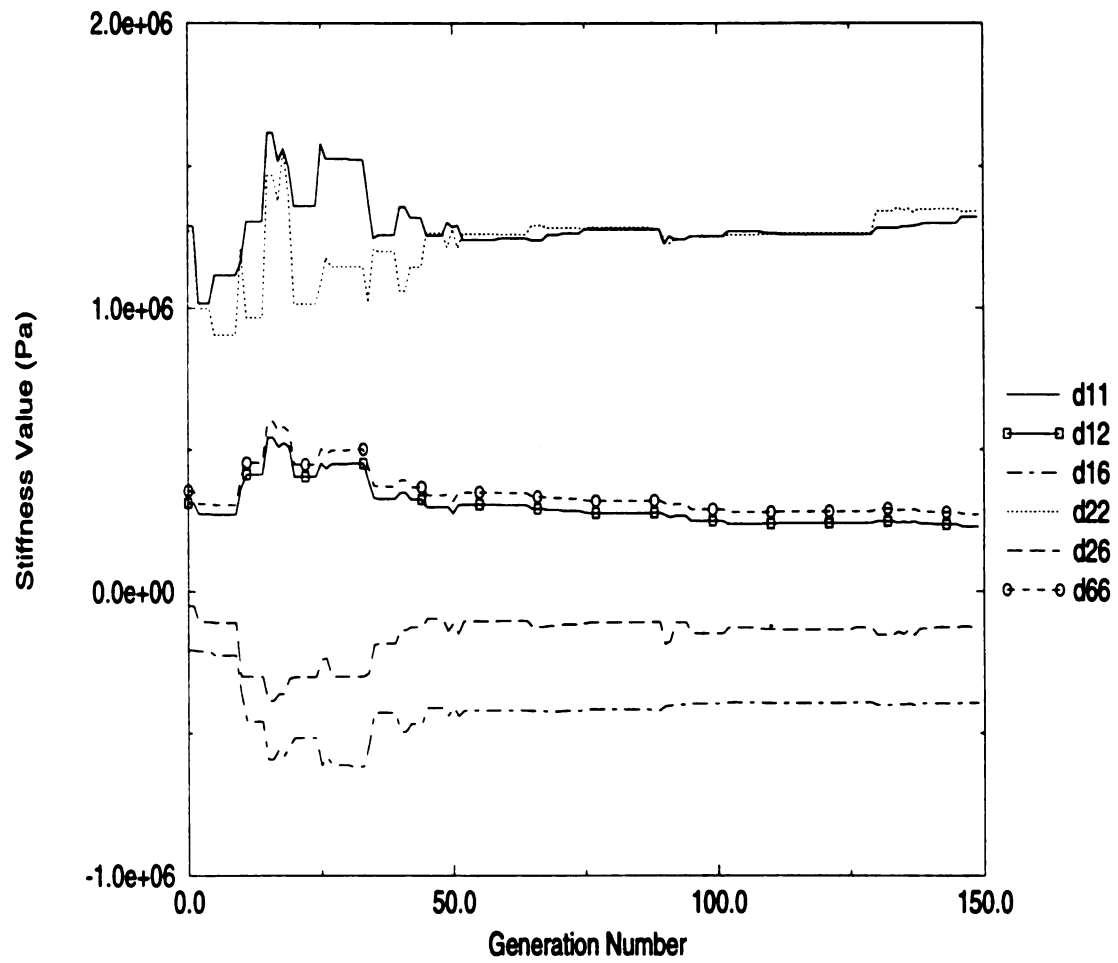


Figure (4.18) - Flexural stiffness matrix versus generation number.

**Table (4.6) Layup Determined by Single Node Structure.**

Ply No.	Mtl.	Orientation	Thickness
1	1	-1.406250e+01	1.27e-04
2	1	-1.968750e+01	1.27e-04
3	1	-2.250000e+01	1.27e-04
4	1	-2.531250e+01	1.27e-04
5	1	-2.812500e+01	1.27e-04
6	1	-2.531250e+01	1.27e-04
7	1	-1.687500e+01	1.27e-04
8	1	-1.406250e+01	1.27e-04
9	1	7.593750e+01	1.27e-04
10(core)	2	0.000000e+00	1.5076938e-01
11	1	8.156250e+01	1.27e-04
12	1	-3.656250e+01	1.27e-04
13	1	9.000000e+01	1.27e-04
14	1	-8.437500e+00	1.27e-04
15	1	8.718750e+01	1.27e-04
16	1	-2.812500e+01	1.27e-04
17	1	8.437500e+01	1.27e-04
18	1	-8.437500e+01	1.27e-04
19	1	8.718750e+01	1.27e-04
20	1	7.593750e+01	1.27e-04
21	1	-1.125000e+01	1.27e-04
22	1	7.875000e+01	1.27e-04
23	1	0.000000e+00	1.27e-04
24	1	-7.593750e+01	1.27e-04
25	1	-8.718750e+01	1.27e-04
26	1	-2.250000e+01	1.27e-04

**Table (4.7) Layup Determined by Ring Structure GA.**

Ply No.	Mtl.	Orientation	Thickness
1	1	-1.40625e+01	1.27e-04
2	1	-8.71875e+01	1.27e-04
3	1	8.15625e+01	1.27e-04
4	1	-2.53125e+01	1.27e-04
5	1	8.71875e+01	1.27e-04
6	1	-2.25000e+01	1.27e-04
7	1	-8.71875e+01	1.27e-04
8	1	-1.40625e+01	1.27e-04
9	1	-8.71875e+01	1.27e-04
10	1	-8.43750e+00	1.27e-04
11	1	-8.15625e+01	1.27e-04
12	1	8.71875e+01	1.27e-04
13	1	-7.87500e+01	1.27e-04
14	1	-1.96875e+01	1.27e-04
15	1	-8.43750e+01	1.27e-04
16	1	-2.25000e+01	1.27e-04
17(core)	2	0.00000e+00	1.4809438e-01
18	1	-5.62500e+00	1.27e-04
19	1	9.00000e+01	1.27e-04
20	1	-1.68750e+01	1.27e-04
21	1	-2.25000e+01	1.27e-04
22	1	-2.25000e+01	1.27e-04
23	1	-2.25000e+01	1.27e-04
24	1	-8.71875e+01	1.27e-04
25	1	-2.53125e+01	1.27e-04
26	1	-3.09375e+01	1.27e-04
27	1	-3.37500e+01	1.27e-04

**Table (4.7 (cont'd)).**

Ply No.	Mtl	Orientation	Thickness
28	1	-2.53125e+01	1.27e-04
29	1	-8.43750e+01	1.27e-04

**Table (4.8) Layup Determined by Injection Structure GA.**

Ply No.	Mtl.	Orientation	Thickness
1	1	-2.812500e+01	1.27e-04
2	1	7.312500e+01	1.27e-04
3	1	-7.875000e+01	1.27e-04
4	1	8.437500e+01	1.27e-04
5	1	-3.375000e+01	1.27e-04
6	1	-2.531250e+01	1.27e-04
7	1	-8.156250e+01	1.27e-04
8	1	-1.406250e+01	1.27e-04
9	1	-4.500000e+01	1.27e-04
10	1	8.437500e+01	1.27e-04
11	1	-2.250000e+01	1.27e-04
12	1	-1.968750e+01	1.27e-04
13	1	-3.656250e+01	1.27e-04
14	1	-1.125000e+01	1.27e-04
15(core)	2	0.000000e+00	1.490975e-01
16	1	-1.968750e+01	1.27e-04
17	1	-1.968750e+01	1.27e-04
18	1	-7.031250e+01	1.27e-04
19	1	-2.250000e+01	1.27e-04
20	1	-2.250000e+01	1.27e-04

**Table (4.8) Layup Determined by Injection Structure GA.**

Ply No.	Mtl.	Orientation	Thickness
21	1	-1.406250e+01	1.27e-04
22	1	-3.093750e+01	1.27e-04
23	1	-7.875000e+01	1.27e-04
24	1	-8.437500e+01	1.27e-04
25	1	-1.125000e+01	1.27e-04
26	1	7.875000e+01	1.27e-04
27	1	-8.437500e+01	1.27e-04

**Table (4.9) Layup Determined by Hybrid Structure GA.**

Ply No.	Mtl..	Orientation	Thickness
1	1	-1.968750e+01	1.27e-04
2	1	-3.375000e+01	1.27e-04
3	1	8.718750e+01	1.27e-04
4	1	8.156250e+01	1.27e-04
5	1	-2.250000e+01	1.27e-04
6	1	-8.718750e+01	1.27e-04
7	1	-6.187500e+01	1.27e-04
8	1	-3.656250e+01	1.27e-04
9	1	-2.812500e+01	1.27e-04
10	1	-8.437500e+01	1.27e-04
11	1	-1.687500e+01	1.27e-04
12	1	7.875000e+01	1.27e-04
13	1	-3.375000e+01	1.27e-04
14	1	-2.250000e+01	1.27e-04

**Table (4.9) (cont'd)**

Ply No.	Mtl.	Orientation	Thickness
15	1	-2.531250e+01	1.27e-04
16	1	-8.718750e+01	1.27e-04
17(core)	2	0.000000e+00	1.5076938e-01
18	1	8.437500e+01	1.27e-04
19	1	-3.375000e+01	1.27e-04
20	1	-4.781250e+01	1.27e-04
21	1	-3.656250e+01	1.27e-04
22	1	-2.531250e+01	1.27e-04
23	1	-2.812500e+01	1.27e-04
24	1	-1.125000e+01	1.27e-04
25	1	-3.375000e+01	1.27e-04
26	1	-8.437500e+01	1.27e-04
27	1	-8.156250e+01	1.27e-04
28	1	-3.656250e+01	1.27e-04
29	1	-8.437500e+00	1.27e-04
30	1	-2.531250e+01	1.27e-04
31	1	-8.718750e+01	1.27e-04
32	1	-3.375000e+01	1.27e-04

## Chapter 5

### Summary and Conclusions.

This document consists of three major parts dealing with the research performed. The first section, discussed in Chapter 2, dealt with describing different theories available for analyzing laminated composite plates. Classical laminated plate theory, first order shear deformation theory, a third order shear deformation theory, and two zig-zag theories were described and their details discussed along with the associated finite element models. Finite element models associated with the first order shear deformation theory (FSDT), third order shear deformation theory (HSDT), and two third-order zig-zag theories, ZZHT and LZZHT, were used to analyze symmetric and unsymmetric square sandwich panels subject to sinusoidally varying transverse surface loadings. Results from this comparison are contained in Chapter 3.

The FSDT theory proved the least accurate and only slight improvement was gained from using the third order shear deformation theory. As plate thickness became small in comparison to the other dimensions, accuracy of these theories improved, however the zig-zag theories were far superior in all cases analyzed. The third order zig-zag theories used two different displacement fields and different finite element models. The ZZHT theory used a four-noded plate element and the LZZHT theory an eight-noded brick element, both had 7 degrees of freedom per node. A sublaminar approach was possible with the LZZHT model because the element was formulated in such a way as to

allow elements to be stacked in the thickness direction. This was achieved by including transverse shear stress degrees of freedom in the element. The elements in the ZZHT theory cannot be stacked. The ability of the LZZHT model to be refined through the thickness of the plate (by stacking elements) makes this by far the most accurate plate theory analyzed. Results from this theory were shown to be nearly identical to the elasticity solutions. Even transverse shear stresses were in very close agreement with the elasticity solution when using only three sublaminae through the thickness. Results from the ZZHT theory were comparable in accuracy to the LZZHT model when only one sublaminate was used. Computational efficiency of the ZZHT model was far greater than the LZZHT model for the same number of elements since the LZZHT elements have eight nodes per element and the ZZHT elements have 4. The best combination of solution accuracy and computational efficiency belongs to the ZZHT model and thus it was chosen to be used in the design optimization portion of this research which is discussed in Chapter 4. Computational efficiency is very important in an optimization problem because many calculations must be performed. Any savings in computation time can amount to a large savings over the course of an optimization.

Chapter 4 discusses the results of a design optimization. The motivation for this design problem came from the desire for aircraft wings to adjust their angle of attack when experiencing gust loads. Gust loading causes the wing to twist up and back which is detrimental to the wing's lift. The wing needs to respond to such loadings by twisting in the opposite direction. This research shows such a response is possible with laminated sandwich structures. The ZZHT finite element model was used with the genetic algorithm, GALOPPS v3.0.

The desired amount of twist was achieved while maximizing in-plane stiffness and minimizing structure weight. To do this the number of plies in the top and bottom face sheets, the fiber orientation of each ply, and the core thickness were treated as design variables. Maximum tip deflection was constrained by penalizing the design fitness for exceeding a specified maximum value. The maximum stress in the fiber and matrix directions were constrained to be less than the strength of the face sheet material. This was achieved by applying a strong penalty to the fitness of designs exceeding the maximum allowable stresses.

Also in Chapter 4 four different GA architectures were used to solve the optimization problem and the performance of each compared. The ring structure generated the design with the highest fitness (4,140.25) and the injection structure generated the design with the lowest fitness (4,096.00). The average fitness of four runs for each of the four structures was compared with the ring and hybrid structures having the highest average fitness (4,130.8) and the injection structure the lowest at 4,116.5. This is a 0.3% difference which indicates all GA structures performed sufficiently well for this design problem. The injection structure seemed to converge the fastest followed by the hybrid, single, and ring structures.

The single node structure produced the design with the lowest weight of 66.19 kg as well as the design having the “best” twist, -0.0279 m, which is only 0.44% less than the desired twist. The design having the maximum in-plane stiffness,  $A_{11}=2.427e8$  Pa, was produced by the hybrid structure.

The designs generated by the four structures are valid designs, however they are slightly conservative because the ZZHT finite element model slightly overpredicts

maximum in-plane stresses. The LZZHT model is far too computationally expensive for large optimization problems so the ZZHT model was the best choice of the theories available.

As mentioned in Chapter 4, the wing design data, i.e. wing shape, sweep back, aircraft size and weight, actual wing loadings, desired wing twist, etc., was idealized to devise a general case which illustrates the ability to solve such a problem using an experimental finite element plate model with genetic algorithms. This problem can be extended and refined as desired to account for more realistic designs once specific design information is known. Also interactive failure criteria could be incorporated into the problem in lieu of the maximum stress failure criteria used here.

One concern which was not directly addressed by this research is design manufacturability. Due to the unsymmetric lamination sequence necessary to obtain the desired response, the wing will warp during curing. This could be corrected by manufacturing techniques. Alternatively, the  $B_{ij}$ ,  $A_{16}$ , and  $A_{26}$  terms could be forced to be zero using constraint or penalty methods. This would reduce coupling effects which cause warping during curing. Cost constraints could be incorporated into the design process as well.

## **LIST OF REFERENCES**

## List of References

1. Adali, S., Richter, S., Verijenko, V. E., and Summers, E. B., 1995, "Optimal Design of Laminates with Discreet Ply Angles for Maximum Buckling Load and Minimum Cost", *Composite Structures*, Vol. 32, pp. 409-415.
2. Arbate, S., 1994, "Optimal Design of Laminated Plates and Shells", *Composite Structures*, Vol. 29, pp. 269-286.
3. Avalle, M., and Belingardi, G., 1995, "A Theoretical Approach to the Optimization of Flexural Stiffness of Symmetric Laminates", *Composite Structures*, Vol. 31, pp. 75-86.
4. Averill, R.C., and Reddy, J. N., 1992, "An Assessment of Four-Noded Plate Finite Elements Based on a Generalized Third-Order Theory", *Int. Journal for Numerical Methods in Engineering*, Vol. 33, pp. 1553-1572.
5. Averill, R. C., 1994, "Static and Dynamic Response of Moderately Thick Laminated Beams With Damage", *Composites Engineering*, Vol. 4, no. 4. pp. 381-395.
6. Averill, R. C., and Yip, Y. C., 1996, "An Efficient Thick Beam Theory and Finite Element Model with Zig-Zag Sublaminates Approximations", to be published in *AIAA journal*.
7. Burton, W. S., and Noor, A. K., 1994, "Three-Dimensional Solutions for Thermo-mechanical Stresses in Sandwich Panels and Shells", *Journal of Engineering Mechanics*, Vol. 120, pp. 2044-2071.
8. Chattopadhyay, A., McCarthy, T. R., and Pagaldipti, N., 1995, "Multilevel Decomposition Procedure for Efficient Design Optimization of Helicopter Rotor Blades", *AIAA Journal*, Vol. 33, No. 2, pp. 223-230.
9. Chawla, K.K., 1987, "*Composite Materials, Science and Engineering*", Springer-Verlag, New York.

10. Cho, W-M., Youn, S-K, and Lee, Y-S., 1995, "A Numerical And Experimental Study on The Nonlinear Behaviour of Laminated Composite Structural Components", *Computers and Structures*, Vol. 57, No. 6, pp. 1071-1077.
11. Fukunaga, H., and Vanderplaats, G.N., 1991, "Strength Optimization of Laminated Composites With Respect to Layer Thickness and/or Layer Orientation Angle", *Computers and Structures*, Vol. 40, No. 6, pp. 1429-1439.
12. Fukunaga, H., and Vanderplaats, G.N., 1991, "Stiffness Optimization of Orthotropic Laminated Composites Using Lamination Parameters", *AIAA Journal*, Vol. 29, No. 4, pp. 641-646.
13. Furura, H., Haftka, R.T., 1993, "Locating Actuators for Vibration Suppression on Space Trusses by Genetic Algorithms", *Structures and Controls Optimization*, ASME, AD Col. 38, pp. 1-11.
14. Graesser, D.L., Zabinsky, Z. B., Tuttle, M.E., and Kim, G.I., 1993, "Optimal Design of a Composite Structure", *Composite Structures*, Vol. 24, pp273-281.
15. Gibson, L. J., and Ashby, M. F., 1988 *Cellular Solids, Structure and Properties*, Pergamon Press, New York.
16. Goldberg, D.E., 1989, "*Genetic Algorithms in Search, Optimization, and Machine Learning*", Addison-Wesley Publishing Company Inc., New York.
17. Haftka, R. T, and Gurdal, Z., 1992, "*Elements of Structural Optimization*", third edition, Kluwer Academic Publishers, Boston.
18. Houghton, E. L., and Carpenter, P. W., 1993, "Aerodynamics for Engineering students", 4th ed., John Wiley & Sons, inc., New York.
19. Johnson, E.A., 1994, "The Implementation of Continuously Updated Sharing in The Simple Genetic Algorithm Code, and it's Application to the Optimal Placement of Elastic Supports on a Simply Supported Plate", *Proceedings of the AIAA/ASME/ASCE/AHS Structures, Structural Dynamics, and Materials Conference*,

AIAA, New York, Vol. 4, pp. 2276-2286.

20. Jones, R.M., 1975, "*Mechanics of Composite Materials*", Hemisphere Publishing Corporation, New York.
21. Kam, T.Y., and Lai, M.D., 1989, "Multilevel Optimal Design of Laminated Composite Plate Structures", *Computers and Structures*, Vol. 31, No. 2, pp. 197-202.
22. Kam, T.Y., and Snyman, J.A., 1991, "Optimal Design of Laminated Composite Plates Using a Global Optimization Technique", *Composite Structures*, Vol. 19, pp. 351-370.
23. Kam, T. Y., and Lai, F. M., 1995, "Maximum Stiffness Design of Laminated Composite Plates via a Constrained global Optimization Approach", *Composite Structures*, Vol. 32, pp. 391-398.
24. Kogiso, N., Watson, L. T., Gurdal, Z., and Haftka, R. T., 1993, "Genetic Algorithms with Local Improvement for Composite Laminate Design", *Structures & Controls Optimization*, ASME, Aerospace Division, New York, Vol. 38, pp. 13-28.
25. Kogiso, N., Watson, L. T., Gurdal, Z., Haftka, R. T., and Nagendra, S., 1994, "Minimum Thickness Design of Composite Laminates Subject to Buckling and Strength Constraints By Genetic Algorithms", *Proceedings of the AIAA/ASME/ASCE/AHS/ASC Structures, Structural Dynamics, and Materials Conference*, AIAA, New York, Vol. 4, pp. 2257-2275.
26. Lake, R. C., Izadpanah, A. P., and Baucom, R. M., Jan 1993, "Experimental and Analytical Investigation of Dynamic Characteristics of Extension-Twist-Coupled Composite Tubular Spars", NASA TP-3225 ARL-TR-30.
27. Le Riche, T., and Haftka, R. T., 1993, "Optimization of Laminate Stacking Sequence for Buckling Load Maximization by Genetic Algorithm", *AIAA Journal*, Vol. 31, No. 5, pp. 951-956.
28. Leung, M., Nevill, G. E., 1994, "Genetic Algorithms for Preliminary 2-D Structural Design", *Proceedings of the AIAA/ASME/ASCE/AHS/ASC Structures, Structural Dynamics, and Materials Conference*, AIAA, New York, Vol. 4, pp. 2287-

2291.

29. Livine, E., 1994, "Equivalent Plate Structural Modeling for Wing Shape Optimization Including Transverse Shear", *AIAA Journal*, Vol. 32, No. 6, pp. 1278-1288.
30. Mase, G. E., and Mase, G. T., 1992, "*Continuum Mechanics for Engineers*", CRC Press, Ann Arbor.
31. Miki, M., 1985, "Design of Laminated Fibrous Composite Plates with Required Flexural Stiffness", *Recent Advances in Composites in the United States and Japan*, ASTM stp 864, pp. 387-400.
32. Miki M., and Sugiyama, Y., 1993, "Optimum Design of Laminated Composite Plates Using Lamination Parameters", *AIAA Journal*, Vol. 30, No. 5, pp. 921-922.
33. Nagendra, S., Haftka, R. T., and Gurdal, Z., 1992, "Stacking Sequence Optimization of Simply Supported Laminates With Stability and Strain Constraints", *AIAA Journal*, Vol. 30, No. 8, pp. 2132-2137.
34. Nagendra, S., Haftka, R.T., Gurdal, Z., 1993, "Design of a Blade Stiffened Composite Panel by a Genetic Algorithm", *Proceedings of The 34th Structures, Structural Dynamics and Materials Conference*, La Jolla, CA. pp. ??.
35. Nagendra, S., Jestin, D., Gurdal, Z., Haftka, R.T., and Watson, L.T., 1994, "Improved Genetic Algorithm for the Design of Stiffened Composite Panels", *Proceedings of the International Symposium on Mathematical Programming*.
36. Noor, A. K., 1992, "Mechanics of Anisotropic Plates and Shells-A New Look at an Old Subject" *Computers and Structures*, Vol. 44, No. 3, pp. 499-514.
37. Olhoff, N., Taylor, J.E., 1983, "On Structural Optimization", *Journal of Applied Mechanics*, Vol. 50, pp.1139-1151.
38. Punch, W. F., Goodman, E. D., Pei, M., Chia-Shun, L., Hovland, P., and Enbody, R., 1993, "Further Research on Feature Selection and Classification Using Genetic Algorithms", *Proceedings of the Fifth International Conference on Genetic*

*Algorithms, Urbana Champaign*, pp. 557-564.

39. Punch, W.F.III, Goodman, E.D., Lin, S.-C., Ding, Y., Averill, R.C., and Yip, Y.C., 1994, "Optimal Design of Laminated Composite Structures Using Course-Grain Parallel Genetic Algorithms", *Computing Systems in Engineering*, Vol. 5. pp. 415-423.
40. Rauscher, M., 1953, "Introduction to Aeronautical Dynamics", John Wiley & Sons, inc., New York.
41. Raymer, D. P., 1992, "Aircraft Design: A Conceptual Approach", AIAA Education Series, Published by AIAA Inc., Washington D.C.
42. Reddy, J. N., 1990, "A Review of Refined Theories of Laminated Composite Plates", *The Shock and Vibration Digest*, Vol. 22, no. 7, pp. 3-17.
43. Reddy, J. N., 1993, "An Introduction to the Finite Element Method, Second Ed.", McGraw-Hill, New York.
44. Reddy, J. N., and Robbins, D., H., 1994, "Theories and Computational Models for Composite Laminates", *Applied Mechanics Reviews*, Vol. 47, no 6, part 1, pp. 147-169.
45. Smith, H. C., 1992, "The illustrated guide to Aerodynamics" 2nd ed., TAB Books, inc., Blue Ridge Summit.
46. Sandgren, E., Jensen, E., Welton, J.W., 1990, "Topological Design of Structural Components Using Genetic Optimization Methods", *Sensitivity analysis and Optimization with Numerical methods*, ASME Advanced Materials Division, Vol. 115, pp. 31-43.
47. Stadler, W., and Dauer, J., 1992, "Multicriteria Optimization in Engineering: A Tutorial and Survey", *Structural Optimization: Status and Promise, Progress in Astronautics and Aeronautics*, Vol. 150, AIAA Inc., pp. 209-249.
48. Vinson, J. R., and Sierakowski, R. L., 1986, "The Behavior of Structures Com-

*posed of Composite Materials*", Martinus Nijhoff Publishers, Boston.

49. VonMises, R., 1945, "Theory of Flight", McGraw-Hill Book Co. inc., New York.
50. Wang, B.P., and Costin, D.P., 1991, "Optimum Design of a Composite Structure With Three Types of Manufacturing Constraints", *AIAA Journal*, Vol. 30, No. 6, pp. 1667-1669.
51. Whitney, J.M., 1973, "Shear Correction Factors for Orthotropic Laminates Under Static Load", *Journal of Applied Mechanics*, Vol. 40, pp. 302-304.
52. Yip, Y. C., 1996 "A 3-D Laminated Plate Finite Element With Zig-Zag Sublamine Approximations For Composite and Sandwich Panels", doctoral disseration, Department of Material Science and Mechanichs, Michigan State University.